Tomas Bata University in Zlín

Faculty of Technology

Tomas Bata University in Zlín

Faculty of Technology

Department of Polymer Engineering

Doctoral Thesis

Crystallization of polyolefin blends and nanocomposites

Krystalizace polyolefinových směsí a nanokompozitů

Krunal R Trivedi

April 2012

A Thesis Submitted for Fulfillment of PhD Degree

in:

Doctoral study programme: P2808 Chemistry and Materials Technology

Course: 2808V006 Technology of Macromolecular Compounds

Supervisor:

Assoc Prof. Ing. Petr Svoboda, Ph.D.

ABSTRACT

A profound scientific understanding of the crystallization behavior and the resulting semicrystalline structure in polymer blends and nanocomposites is necessary for effective manipulation and control of their properties. In this PhD work, the focus of the study was to understand various factors such as initial melting temperature, supercritical CO_2 affecting crystallization kinetics of polyolefin and its blends and nanocomposites with the help of current theories regarding crystallization kinetics. Different experimental methods like differential scanning calorimetry (DSC), hot-stage optical microscopy, transmission electron microscopy (TEM), x-ray diffraction (XRD) and Fourier transform infrared spectroscopy (FTIR) were employed to gain a general understanding of the crystallization growth behavior and kinetics of the polyolefin and its blend and nanocomposite systems. Finally a comparative study was conducted to study the effect of electron beam irradiation on crystallization ability of polypropylene (PP) and high-density polyethylene (HDPE).

ABSTRAKT

Hluboké vědecké porozumění krystalizačního chování a výsledných semikrystalických struktur u polymerních směsí a nanokompozitů je nutné pro účinné řízení a korigování jejich vlastností. Tato doktorská práce se soustředí na porozumění různých faktorů, jako například počáteční teploty tavení, superkritického CO_2 ovlivňujícího krystalizační kinetiku polyolefinů a jejich směsí a nanokompozitů, to všechno za pomoci současných teorií týkajících se krystalizační kinetiky. Různé experimentální metody, jako například diferenciální skenovací kalorimetrie (DSC), optická mikroskopie s vyhřívaným stolkem, transmisní elektronová mikroskopie (TEM), rentgenová difrakce (XRD) a infračervená spektroskopie (FTIR) byly použity k získání úplného porozumění krystalizačního růstu a kinetiky u polyolefinů, jejich směsí a nanokompozitních systémů. Nakonec byla provedena srovnávací studie vlivu ozáření elektronovými paprsky na schopnost krystalizace polypropylenu (PP) a vysokohustotního polyetylenu (HDPE).

Klíčová slova: polyolefin; nanokompozit; kinetika krystalizace; ozařování elektronovými paprsky; počáteční teplota tavení; supekritický CO_2

TABLE OF CONTENTS

INTRODUCTION

Many macromolecular species are structured as linear, long-chain molecules, for example, protein, DNA, cellulose and numerous synthetic polymers. These macromolecules consists thousands of repeating units and show characteristic behaviors. They are different from simple molecules during aggregation, degradation, and crystallization. One of the unique characteristic behavior is the formation of finely ordered structure from the entangled polymer chains during processes such as protein folding and polymer crystallization. These processes have attracted much interest since the idea of chain folding was first reported by Keller in 1957[1].

The science of polymer crystallization has a long history, but there is no unified theory that satisfactorily describes polymer crystallization; it remains a great academic challenge. Polymer crystallization arouses scientific interest in several fields, ranging from basic polymer science to polymer processing and application. Because crystallization occurs during the manufacture of polymeric materials, the understanding of its mechanism is necessary for macroscopic structure design and final product properties control. Besides macroscopic structure design, imminent nanometer-size composites and blends also open new possible application fields with improved thermal stability and mechanic properties.

In this context, the study of the crystallization behavior of polyolefins and its blends and nanocomposites has become a topic of foremost scientific importance. The present study is focused on the detail description of crystallization study of polyolefins with various blends and nanocomposites under diverse conditions. Crystallization of polyolefin blends and nanocomposites [2-7] have been of great interest to their potential applications to optimization for final product. Different compositions of polypropylene and ethylene-octene copolymer blend are an interesting area as this blend is certainly valuable in automotive industry. The use of supercritical carbon dioxide ($ScCO_2$) as a medium for polymer processing is another research area which has attracted much attention recently. This is because incorporation of $ScCO_2$ during processing of polymer has significant morphological implications due to the formation of crystallites [8-10]. Another important effect on the crystallization could be various initial melting temperatures which can alter its crystallization ability. Yet, in last few decades this issue was not explored at full extent, a limited number of researchers have worked on the melting temperature influence on crystallization [11-14]. Lastly, polypropylene [15-19] and high-density polyethylene [20-24] were studied several times after being treated with different irradiation sources to understand their crystallization properties, nevertheless still more research is needed to entirely explore its affects.

1. THEORETICAL BACKGROUND

1.1 Polyolefins

Polyolefins are high molecular weight hydrocarbons. They include: low-density; linear low-density and high-density polyethylene; polypropylene copolymer; polypropylene; and polymethylpentene. All are break-resistant, non-toxic, and non-contaminating. These are the only plastics lighter than water. They easily withstand exposure to nearly all chemicals at room temperature for up to 24 hours. Strong oxidizing agents eventually cause embrittlement. All polyolefins can be damaged by long exposure to light.

Polyolefins are the largest class of synthetic polymers. These materials have enjoyed great success because of their combination of useful properties such as light weight, low cost, high chemical resistance, low dielectric constant and losses. Polyolefins have the simplest chemical structure of all polymers, yet they vary due to branch concentration and distribution which provides a diversity of chain structure, and this is reflected in their morphology and miscibility.

Polyolefin technology may be divided into low-pressure or high-pressure processes. Resin properties, molecular weight (M_w), molecular weight distributions (MWD), density and others are dictated by the type of catalyst and reactor conditions employed. The manufacturing process is based on free radical polymerization at 200-300°C, and pressures between 0.1 and 0.3 GN/m^2, in tubular or stirred autoclave type reactors. Commercially, end products are used for film and packaging, industrial liners, heavy duty bags, lamination films, and cable and wire.

Ethylene-based polyolefins are normally produced either under low pressure conditions using transition metal catalysts resulting in predominantly linear chain structure or under high pressure conditions using oxygen or peroxide initiators resulting in predominantly branched chain structures of various densities and crystallinity levels. Propylene-based polyolefins are normally produced with transition metal catalysts resulting in linear chain structures with stereospecific arrangement of the propylene units or special stereoblock structures from a single-site catalyst. Higher polyolefins are normally produced using transition metal catalysts resulting in linear and stereospecific chain structures. Polyolefin elastomers are based mainly on a combination of ethylene and propylene. It may be produced by using metal or single-site catalysts with or without the inclusion of dienes (for cross-linking). They are mostly amorphous with high molecular weight and heterogeneous in phase structure. One may conclude that a given polyolefin may be a homopolymer, copolymer,

or terpolymer depending on the number of monomers used in making the polyolefin. It could be described as crystalline or amorphous depending on their chain conformation, configuration, and processing conditions.

1.1.1 Polypropylene (PP)

Polypropylene was discovered in the early 1950s. Since then PP has grown into a commodity polymer with numerous grades for specific end uses. By controlling the polymer chemistry it is now feasible to generate rather versatile polypropylene materials. It is translucent, autoclavable, and has no known solvent at room temperature. It is slightly more susceptible to strong oxidizing agents than polyethylene. It offers the best stress-crack resistance of the polyolefins. Products made of polypropylene are brittle at 0°C and may crack or break if dropped from benchtop height. Due to all these properties, it serves double duty, both as a plastic and as a fiber. As a plastic it is used to make molded articles, packaging films etc. As a fiber, polypropylene is used to make indoor-outdoor carpeting; it works well for outdoor carpet because it is easy to make colored polypropylene and it doesn't absorb water. Structurally, polypropylene is a vinyl polymer, with the repeating unit: $-[CH_2 - CH(CH_3)]_n -$, made by the polymerization of high-purity propylene gas in the presence of an organometallic catalyst. Classical Ziegler Natta or more recent metallocene catalysts are used for polymerization. A Ziegler-Natta catalyst is a reagent or a mixture of reagents used in the production of polymers of 1-alkenes (α-olefins).

Although PP has seen widespread application, its limited impact strength, especially at lower temperature due to its relatively high T_g is an obstacle to broader utilization as an engineering plastic. The impact properties of PP can be considerably improved by incorporation of a rubbery phase. Accordingly, rubber-toughened PP blends with various impact modifiers have been studied, including ethylene-propylene rubber (EPR), ethylene-propylene-diene rubber (EPDM), and ethylene-propylene-styrene rubber (SEBS). Recently, impact modification of PP, using metallocene-catalyzed ethylene-octene copolymer (EOC) has attracted attention. EOC provides better efficiency of impact modification than EPR, and is more cost effective than EPDM.

Polypropylene grafted by maleic anhydride (PP-g-MA)

In general polypropylene graft maleic anhydride (PP-g-MA) is prepared by reactive extrusion. It is introduction of polar side groups to the non-polar main chain molecules. It has improved affinity and dispersion of filler in the copolymer, hence the copolymer has better the tensile and impact strength compare to polypropylene.

On Fig 1.1, there is an example of polypropylene grafted by maleic anhydride (PP-*g*-MA) that is produced e.g. by Uniroyal Chemicals with trade name PB3150.
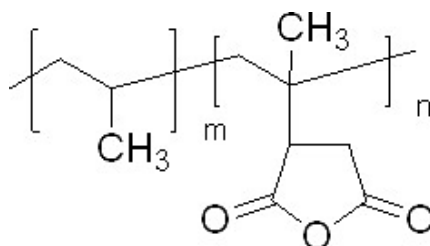

Figure 1.1 *General chemical structure of Maleic anhydride grafted polypropylene*

1.1.2 Polyethylene (PE)

The polymerization of ethylene results in an essentially straight chain, high molecular weight hydrocarbon. The polyethylenes ($-[CH_2 - CH_2]_n -$) are classified according to the relative degree of branching (side chain formation) in their molecular structures, which can be controlled with selective catalysts. It can be classified as HDPE, LDPE and LLDPE. Like other polyolefins, the polyethylenes are chemically inert but strong oxidizing agents will eventually cause oxidation and embrittlement. They have no known solvent at room temperature. Aggressive solvents will cause softening or swelling, but these effects are normally reversible.

PE had an extremely high crystallization rate, arising from its high chain flexibility, mostly from a perfect chain structure. This is particularly true in the case of HDPE. For this reason PE is not commonly available in a completely amorphous state, and therefore many characteristics of amorphous PE are derived via extrapolation of semi-crystalline samples.

Polyethylene generally has the advantageous properties of toughness, high tensile strength, and good barrier properties to moisture. A particularly important property of PE, which is due to their relatively low melting point ranges, is the ease with which PE packaging can be heat-sealed.

1.1.3 Ethylene-octene copolymer (EOC)

Thermoplastic elastomer (TPE) is a type of polyolefin, which, due to its structure, molecular weight and chemistry, can be molded into autoclavable parts, which are rubber-like in application and performance. It is used for several small caps and plugs on filtration and ultracentrifuge ware products. In 1993, DuPont Dow Elastomers has introduced POEs under the brand name ENGAGE®. They are ethylene-octene copolymers produced via advanced INSITE™ catalyst and process technolo-

gy designed to be processed like thermoplastic but can be also compounded like elastomers. The exceptional performance of ENGAGE® is attributed to extraordinary control over polymer structure, molecular weight distribution, uniform comonomer composition and rheology. They are being considered for use in diverse applications such as cushioning agents, gaskets, and particularly good alternative for sealing application due to their structural regularity and non-toxic composition.

1.2   Nanoclay

Nanoclays or organically modified layered-silicates have become an attractive class of organic–inorganic hybrid materials because of their potential use in wide range of applications such as in polymer nanocomposites, rheological modifier in paints, inks, greases and cosmetics, adsorbent for toxic gases, effluent treatment and drug delivery carrier. The generic term, layered silicates, refers to natural clays as well as synthesized layered silicates such as montmorillonite, laponite and hectorite.

The term polymer layered silicate nanocomposites describes a class where the reinforcing phase, in the shape of platelets, has only nanolevel dimensions. There is substantial improvement in mechanical and physical properties of nanocomposites and this too at a very low silicate content (3–6 wt %). Improved mechanical and thermal properties are of interest for under-the-hood applications in the automotive industry. Excellent barrier properties combined with good transparency make these materials ideal for packaging applications. The era of polymer nanocomposites received an impetus after the work of a researcher from Toyota in 1987 [25-27]. Toyota discovered the possibility of synthesizing polymer nanocomposites based on nylon-6/organophilic montmorillonite clay that showed dramatic improvements in mechanical and physical properties and heat distortion temperature at very low content of layered silicate.

1.3   Blends and nanocomposites
1.3.1 Blends

Polymer blending is a useful and economical way to produce new materials with a variety of properties. Many high-performance thermoplastics are prepared by the crystallization of polymer blends. The polymer-polymer interactions during crystallization can alter crystal structure, thermal stability, and mechanical properties such as rigidity and toughness. Understanding how adding a polymer component affects the morphology, crystallization, and mechanical and thermal properties of the

polymer blend is a significant scientific challenge. During past 15 years because of intensified technological interest study of the processing-morphology-property relations of polymer blends has become a topic of major scientific importance. The science and technology of polymer blends has now acquired an important position in the area of development of new polymeric materials. Moreover, the application of polymer blends has increased significantly and is expected to grow continuously. Of the total consumption of engineering polymers, more than 20% is currently thought to be composed of blends with important and various applications in the automotive, electrical and electronic industry, in computer and business equipment housings, in medical components, etc. About 65% of polymer alloys and blends are produced by polymer manufacturers, 25% by compounding companies and the remaining 10% by the transformers [28].

For a blend to be classified as a polyolefin blend, it is presumed that the polyolefin component is of significant composition in the blend. In terms of miscibility, polyolefin blends may also be classified as miscible and immiscible blends. Polyolefin blending requires knowledge of the miscibility and crystallinity of the blend, in addition to the contributions of the components of the blend. Miscibility depends on molecular structure, blend composition, and mixing temperature. To characterize miscibility, a phase diagram is needed.

Benefits of Blending – The following material-related benefits can be cited:
  I.   Providing materials with full set of desired properties at the lowest price,
  II.   Extending the engineering resins' performance,
  III. Improving specific properties, e.g. impact strength or solvent resistance,
  IV.   Offering the means for industrial and/or municipal plastics waste recycling.

Blending also benefits the manufacturer by offering:
  I.   Improved processability, product uniformity, and scrap reduction,
  II.   Quick formulation changes,
  III. Plant flexibility and high productivity,
  IV.   Reduction of the number of grades that need to be manufactured and stored,
  V.   Inherent recyclability, etc. [29, 30]

1.3.2 Nanocomposites

Nanocomposites are modified organic polymers. The structures are having nano-scale material (less than 100 nm) repeat distances between the different phases that incorporation of additives yields, with few exceptions, multiphase systems con-

taining the additive embedded in a continuous polymeric matrix [31]. The resulting mixtures are characterized by unique micro structures or macrostructures that are responsible for their properties. The primary reasons for using additives are [32]:

✓ Property modification or enhancement;
✓ Overall cost reduction;
✓ Improving and controlling of processing characteristics.

In general, composites are materials in which a second component with very different properties is added to the polymer so that both components contribute to the properties of the product. The second component often increases the strength or stiffness of the product and is said to reinforce it. Particulate materials such as carbon black are often used to reinforce elastomers, for instance in car tyres, but fibers are usually used for reinforcing other types of polymer and are also used in tyres. Glass or carbon fibers are often used, but polymeric fibers are appropriate for some applications, as are metallic filaments, e.g. again in tyres. Such fibers are often aligned in one direction within a matrix of polymer, which gives the material anisotropic properties. Materials that are isotropic in one plane can be produced by using layers with the fibers aligned in different directions within the plane or by using mats of chopped fibers as the reinforcement. In these mats the fibers point randomly in all directions in a plane [33, 34].

Additives in composites may be classified according to their functions as modifiers (e.g., fillers, plasticizers, blowing agents, coupling agents, impact modifier, and nucleating/clarifying agents), property extenders (e.g., heat stabilizer, antioxidants, flame retardants, light stabilizers, antistatic agents, and biocides), and processing aids (e.g., lubricants, slip agents, and antiblocking agent). In terms of specific chemical names, additives used in polyolefin composites include, but not limited to, the following: glass fibers, hollow glass bubbles, clay minerals, carbon black, carbon nanotubes, carbon fibers, graphite, wollastonite, magnesium hydroxide, aluminum trihydroxide, attapulgite, titanium dioxide, hydroxyapatite, calcium carbonate, silica, and natural fibers.

In addition to the polyolefin and the additives, composites may contain other thermoplastics or thermosetting polymers. The characteristics of composites are determined by the properties of their components, compositions, structures, and interactions, as is case with any multicomponent material. Composites may be prepared by processes that involve mixing and/or melting the components of the composites in a batch or in continuous mixers (single and twin screw extruders), followed by

fabrication (molding, thermoforming) into the desired shape. The mixing process may be physical or accompanied by chemical reactions in situations where chemical or reactive modifiers are used.

2. POLYMER CRYSTALLIZATION STUDY

Polymer crystallization has been an important research area ever since the concept of chain folding was introduced by Storks in 1938 and later validated independently by Keller (1957) and Fisher (1957). Crystallization, one of the two first - order transitions encountered in the thermal analysis of polymers, is a process in which a material from the amorphous state is transformed into the crystalline state from either solution or the melt. Crystallization of macromolecules is different from the crystallization of low - molecular - mass materials. First, similar to the melting process, it takes place at conditions far from equilibrium. When compared to low - molecular - mass substances, the crystallization process of polymers is much slower because of the lower mobility of the polymer chain segments; therefore in noniso- thermal conditions this process takes place over much wider temperature ranges.
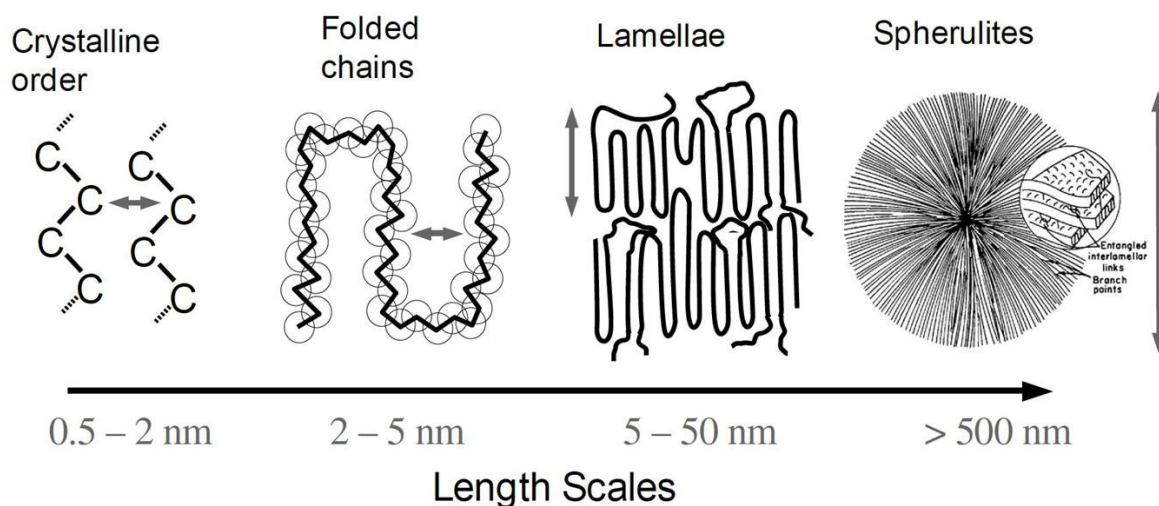

Figure 2.1 Length scales of polymer crystal

Crystallization of polymer chains follows the conventional habit whereby polymer chains fold back and forth into stems to form crystalline lamellae with a thickness of approximately 5 to 50 nanometers (see Fig 2.1). It is typical of crystalli- zation from the isotropic melt that the lamellae are organized in a spherulitic mor- phology. However, the processes of nucleation and growth that control the crystalli- zation kinetics can be profoundly affected by nanoscale confinement. The thickness of ultrathin polymer layers, usually a few tens of nanometers, is comparable to or a small multiple of the lamellar crystal thickness. Hence, the isotropic growth of la- mellar crystals is greatly hampered and crystallization under confinement can pro- duce a unique lamellar crystal orientation. Often, the preferred lamellar crystal ori- entation is vertical to the layer. However, at the other extreme, lamellar crystal ori-

entation parallel to the layer is observed. Although the mechanisms for the specific lamellar orientation during confined crystallization are still under investigation, it is believed that the confined crystals will show anisotropic properties.

Before considering the details of how the chains are arranged in the crystalline and non-crystalline regions of a polymer, it is useful to consider how the amount of material contained within the two types of region can be determined. It is important to realize also that the simple two-phase model, in which there are only two types of region, crystalline and non-crystalline, is an approximation that applies to some polymer samples better than it does to others. For the moment it will be assumed that it is a sufficiently good approximation. In principle, almost any property that is different in the crystalline and non-crystalline regions could be used as the basis for a method of determining the degree of crystallinity, *X*, or, as it is usually more simply put, the crystallinity, of a polymer sample. In practice the most commonly used methods involve density measurements, DSC measurements and X-ray diffraction measurements.

Studies by Keller and his group using electron diffraction showed that the chain axes were parallel to the thickness direction of these lamellar crystals and, once again, the only possibility was chain folding. Shortly afterwards (in 1957) Fischer showed by electron microscopy that the crystallites in melt-grown spherulites of polyethylene and nylon were most likely to be lamellar rather than fibrillar, as would be expected from the fringed-micelle model. It is now accepted that chain-folded lamellar crystallites play an important part in the structure of most ordinary crystalline polymers (see Fig 2.2).
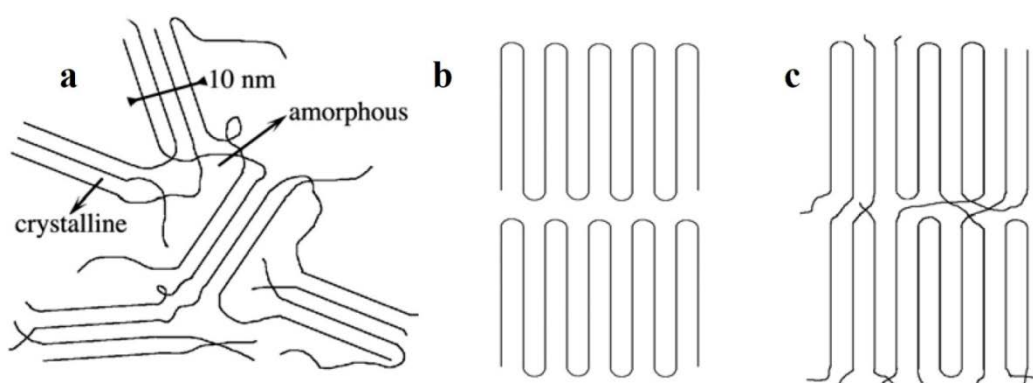

Figure 2.2 *Schematic illustrations of: (a) the fringed micelle model; (b) the folded chain crystal, showing adjacent re–entry; (c) the switchboard model.*

Melt crystallization, in which the crystal formation takes place from the polymer melt. Melt crystallization of polymers can be subdivided into (1) *isothermal*

crystallization, a crystallization process that takes place at a definite, constant temperature; and (2) *nonisothermal crystallization,* in which the polymer sample is melted and crystallization takes place during cooling at a constant rate. A special case of melt crystallization is what is called cold crystallization. This term describes the crystallization process of crystallizable polymers that had been quenched into the amorphous glassy state by extremely fast cooling of the polymer melt. Cold crystallization takes place above T_g and can be both isothermal and nonisothermal, the latter taking place during heating. Similar to low - molecular - mass materials, polymer crystals are unstable above the melting point, and the melt is stable, because at these temperatures the free energy of the melt is smaller than the free energy of the crystals. The curves of the free energy of the crystals and the melt intercept at the melting point, and crystallization takes place when the temperature is decreased. Crystallization itself is a three–step process, consisting of crystal nucleation, crystal growth, and impingement [35, 36].

Polymer crystallization is a mechanism of phase change in polymeric material. Starting with liquid polymer melt the temperature is gradually decreased below the melting point T_m of the material's crystal to appear and grow, which can be described by a stochastic process. As soon as spherulitic crystals hit each other, they abruptly stop the growth at the interface. These three parts – nucleation [37-40], crystal growth [41, 42] (Fig. 2.3a), and impingement [43] (Fig. 2.3b), constitute the process of spherulitic crystallization. The driving force behind the process is the temperature which effects both nucleation rate and growth speed. Vice versa, growing crystals influence the heat distribution by releasing energy in form of *latent heat* as a consequence of phase change.
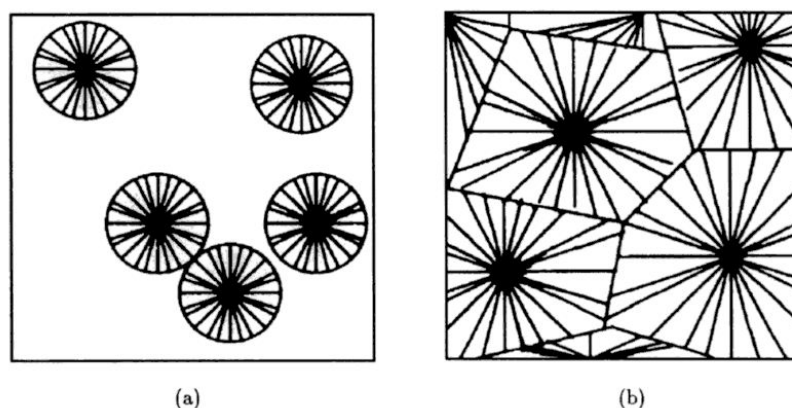

(a)   (b)

Figure 2.3 *Schematic representation of the development of spherulitic structure: (a) growth of spherulitic structure and (b) impingement of spherulitic structure*

At the beginning of the crystallization process there is a barrier in the free energy that needs to be overcome for nuclei to start growing. Density fluctuations help to overcome this barrier, and to proceed to a stage of stable, ordered regions of critical size. These are called *primary nuclei,* and the process of their formation is called *primary nucleation.* Thus, *nucleation* describes the formation of embryonic crystallites of critical dimensions that are stable at a given temperature and can initiate the growth of crystals. In this context "growth" means an increase of the crystallite size. When discussing nucleation, most chemists and physicists imply primary nucleation. The primary nuclei are the ones that initiate crystal growth in a polymer melt containing no crystals, provided that they have reached the critical size and are stable. In polymer physics, three other types of nucleation are important for the *primary nucleation* itself, or for the growth of crystals. The first one is molecular nucleation, in which the initial part of a polymer molecule is incorporated into a crystal. This may occur in the primary nucleation itself, or take place as part of a secondary or tertiary nucleation. This type of nucleation is especially important for formation of fringed micelles. *Secondary nucleation* refers to growth of a new layer of a polymer crystal on a smooth crystal surface, while *tertiary nucleation* characterizes attachment of macromolecular segments to edges of a growing crystal [44, 45].

Crystal growth is a process in which the dimensions of stable nuclei, and later the dimensions of polymeric crystallites, increase. The most important physical quantity used to characterize crystal growth is the linear growth rate, which is constant in time, but changes with temperature. This is the rate of crystal size increase in one dimension, and can be determined from polarization optical microscopy experiments. The kinetics of polymer crystallization is discussed in detailed in following sub-chapter.

2.1 Polymer crystallization kinetics

During crystallization from the bulk, polymers form lamellae, which in turn are organized into spherulites or their predecessor structures, hedrites. This section is concerned with the rates of crystallization under various conditions of temperature, molecular weight, chemical structure, and so on, and the theories that provide not only an insight into the molecular mechanisms but considerable predictive power [46-48].

Keller's early prepared of single crystals from dilute solutions. Since the crystals were only about 100 Å thick and the chains were oriented perpendicular to the flat faces, Keller postulated that the chains had to be folded back and forth. Similar

structures, called lamellae, exist in the bulk state. While their folding is now thought to be much less regular, their proposed molecular organization remains similar. In the bulk state, however, these crystals are organized into the larger structures known as spherulites.

The rate of radial growth of the spherulites is linear in time and the growth rate goes through a maximum as the temperature of crystallization is lowered. These several experimental findings form the basis for two theories of polymer crystallization kinetics. The first of these theories is based on the work of Avrami, which adapts formulations intended for metallurgy to the needs of polymer science. There is one intermediate model which was proposed by Hoffman-Weeks to understand the equilibrium melting temperature of polymeric mixture which later used in Hoffman-Lauritzen model to predict secondary nucleation growth during crystallization of polymer. The second theory was developed by Hoffman and Lauritzen who postulated the kinetic nucleation theory of chain folding, which provides an understanding of how lamellar structures form from the melt. This theory continues to be developed even as this thesis is being written. Together, these theories provide insight into the kinetics, not only about crystallization but also of the several molecular mechanisms taking part in it.

2.1.1 Avrami model (overall crystallization kinetics)

The Avrami approach is often used either to characterize crystallization under laboratory conditions or to predict crystallization during processing. The macroscopic study of the crystallization process is based in the evolution of the crystalline fraction of the material, α, as a function of the time in isothermal regime or of the temperature under dynamic constant rates. Whenever a polymer crystallizes, the extent of the phase transformation depends upon the crystallizing species and the experimental conditions. High molecular weight polymers do not crystallize completely because of topological constraints that lower crystallinity considerably. The classical isothermal transformation kinetics, initially formulated by Kolmogorov and Goler et al. were extended later by the Avrami theory that was initially formulated for metals and later modified, for example, by Evans and others, for polymers.

The crystallization kinetics of polymers is analyzed using a classical Avrami equation as given in Eq. (1) [49, 50]:

$$1 - X_t = exp(-kt^n) \qquad (1)$$

Where the k value is the Avrami rate constant and the n value is the Avrami exponent. Both k and n depend on the nucleation and growth mechanisms of spherulites. In order to deal conveniently with the operation, Eq. (1) is usually rewritten as the double logarithmic form as follows [51]:

$$ln\{-ln[1 - X_t]\} = \ln k + n \ln t \qquad (2)$$

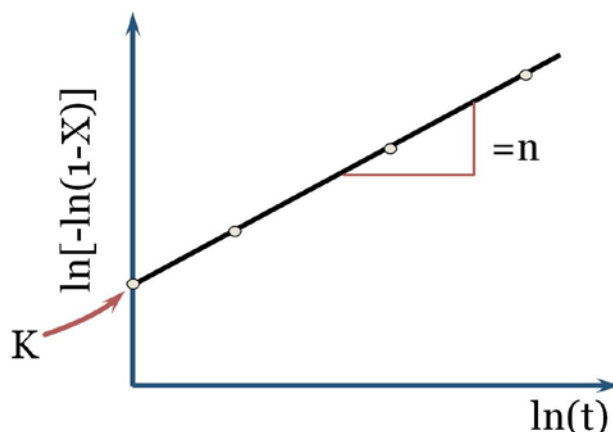The k and n values could be directly obtained using Eq. (3) from the slope and intercept of the best-fit line as shown fig. 2.4.

Figure 2.4 Schematic representation of the Avrami plot

kt^n is the volume of crystallization material, which should be determined by considering the following two cases (See Table 2.1): (a) the nuclei are predetermined, that is, they all develop at once on cooling the polymer to the preset temperature, which is termed heterogeneous nucleation, and (b) there is sporadic nucleation of spherical crystals, which is named homogeneous nucleation. Depending on whether preexisting nuclei are presented or not, nucleation can be classified into primary (homogeneous nucleation) and secondary nucleation (heterogeneous nucleation).

Table 2.1 – The Avrami parameters for crystallization of polymers [52-54]

Crystallization mechanism		Avrami Constants		Restrictions
		k	n	
Spheres	Sporadic	$2/3\pi g^3 l$	4.0	3 dimensions
	Predetermined	$4/3\pi g^3 l$	3.0	
Discs	Sporadic	$\pi/3 g^2 ld$	3.0	2 dimensions
	Predetermined	$\pi g^3 Ld$	2.0	
Rods	Sporadic	$\pi/4 gld^2$	2.0	1 dimensions
	Predetermined	$\frac{1}{2}\pi g Ld^2$	1.0	

2.1.2 Hoffman-Weeks model (the equilibrium melting temperature)

According to Hoffman and Weeks[55], the equilibrium melting temperature of a polymer, T_m^0, is defined as the melting point of an assembly of crystals, each of which is so large that surface effects are negligible and that each such large crystal is in equilibrium with the normal polymer liquid. Furthermore the crystals at the melting temperature must have the equilibrium degree of perfection consistent with the minimum free energy at T_m^0.

While this definition holds for most pure compounds, polymers as ordinarily crystallized tend to melt below T_m^0 because the crystals are small and all too imperfect. Thus the temperature of crystallization, usually still lower because of supercooling, has an important influence on the experimental observed melting point. Hoffman and Weeks found the following relation to hold:

$$T_m^0 - T_m = \phi'(T_m^0 - T_c) \qquad (3)$$

where ϕ' represents a stability parameter that depends on crystal size and perfection. The quantity ϕ' may assume all values between 0 and 1, where $\phi' = 0$ implies that $T_m = T_m^0$, whereas $\phi' = 1$ implies that $T_m = T_c$. Therefore crystals are most stable at $\phi' = 0$ and inherently unstable at $\phi' = 1$. Values of ϕ' near $\frac{1}{2}$ are common.
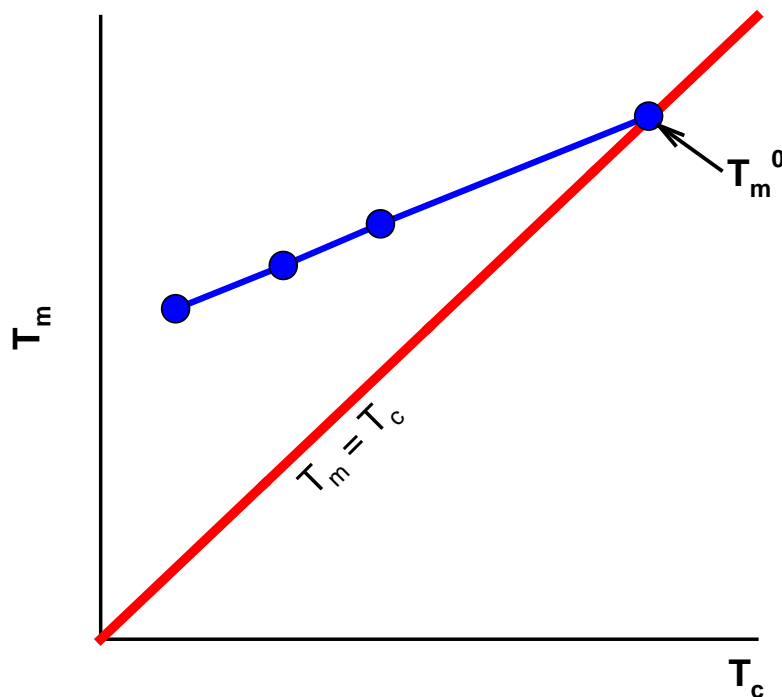

Figure 2.5 *Schematic representation of Hoffman-Weeks plot, showing the extrapolation to T_m^0.*

To determine T_m^0, a plot of T_c versus T_m is necessary to prepare (Fig. 2.5). A line is drawn where $T_c=T_m$. The experimental data are extrapolated to be intersection with the line. The temperature of intersection is T_m^0.

2.1.3 Hoffman–Lauritzen model (secondary nucleation growth)

According to the classical nucleation growth theory for polymers, developed by Lauritzen and Hoffman, a nucleus becomes stable, meaning that folded chain lamellae can spontaneously grow from its surface, when it reaches a critical size. It has been common practice, for modeling purposes, to derive an expression for the rate at which nuclei cross this size barrier, i.e. the nucleation rate.

The mechanism of polymer crystallization can be divided into two basic steps: nucleation and growth. The theory developed more than 40 years ago by Hoffman and Lauritzen (Hoffman and Lauritzen, 1961[56]; Hoffman *et al.*, 1964[57]; 1969[58]), provides a general formalism to treat the crystalline nucleation. During this process, the relaxation of a metastable under cooled melt toward the equilibrium state (which is rarely reached) is required to overcome a free-energy barrier, whose height depends on the degree of undercooling. In order to create a new phase in the metastable melt, interfaces must be introduced. If the resulting cluster, originated by the reactions of association and dissociation of chain segments, has a size smaller than a critical one, it is unstable, i.e. its probability of decrease is higher than its probability of growth. On the contrary, if a critical size is overstepped, the growth probability of the nucleus is greater than its probability of decrease. This kind of nuclei, called active, can continuously grow toward a stable crystalline phase. In general, if nucleation is initiated from a single phase, it is called homogeneous nucleation. Homogeneous nucleation generates primary nuclei without the help of any substrate or external nucleating particles. If the process is initiated from multiple phases, heterogeneous nucleation occurs. In this case the nuclei are formed on the surface of foreign bodies or crystals of the same material already present in the undercooled liquid.

In practice homogeneous nucleation is an unusual and unlikely event. In most cases heterogeneous nucleation takes place. According to the theory, the growth of polymer lamellar evolves through a front provided by an existing crystal with a defined crystallographic surface. Chain molecules deposit onto a growth plane and start crystallizing onto the lattice one stem at a time to form lamellae[59, 60]:

$$G = G_0\, exp\left[\frac{-U^*}{R(T_c - T_\infty)} - \frac{K_g}{T_c(\Delta T)f}\right] \qquad (4)$$

where G is the crystal growth rate, U^* is a constant characteristic of the activation energy for repetitive chain motion and is equal to 1500 cal mol^{-1}, R is the gas constant, T_c is the crystallization temperature (K), $T_\infty = T_g$-$30K$ and (for PP the glass transition temperature T_g=270 K, $\Delta T = T_m^0$-T_c, T_m^0 is the equilibrium melting temperature of an infinitely thick crystal[61], K_g is the nucleation constant, f is a correction factor and equals to $2T_c/(T_m+T_c)$ and G_0 is a pre-exponential factor.

A major extension of the theory involved the recognition that the deposition of a single critical nucleus may not always occur and that multiple nucleation generate different situation. The situation is handled best in general conceptual terms by considering it to be a competitive situation between the rate at which critical nuclei are deposited on the surface and the rate at which the chains deposit laterally to complete the growth step. This leads to three distinct situations or regimes which is illustrated in Fig. 2.6; regime I the classical situation in which the rate of secondary nucleation is slowest, regime II a situation in which the rates of secondary nucleation and lateral spreading are comparable, and regime III a situation in which the rate of secondary nucleation is the fastest[62, 63].
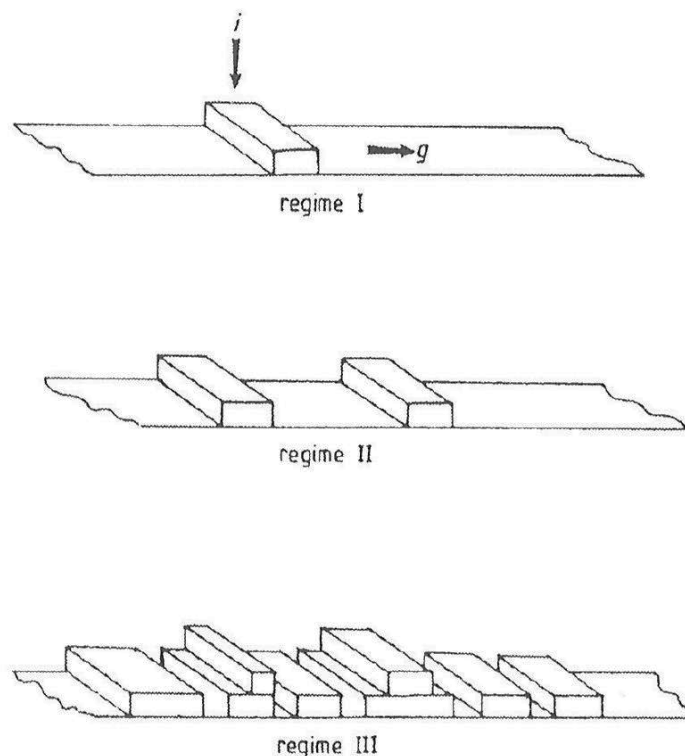

i

g

regime I

regime II

regime III

Figure 2.6 *Schematic representation of growth mechanism of secondary nucleation*

These three situations occur naturally in many polymers as the crystallization temperature is reduced (see Fig. 2.7). The vast majority of polymers studied show

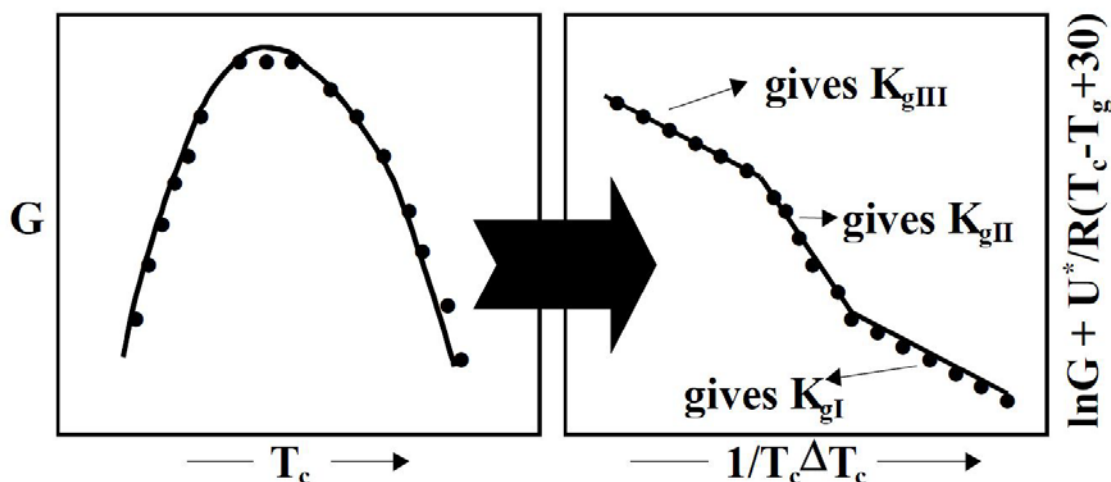regimes II and III, whereas few show regime I which is the classical situation [60, 64].

Figure 2.7 *A schematic illustrating the conversion of growth rate data to a Hoffman-Lauritzen plot showing the three regime transitions*

After detailed discussion about various models which are used, in a following segment, parameter which influences the ability of crystallization is discussed.

2.2 Parameter influences to crystallization

Crystallites in polymers exert a major influence on their bulk properties. Modification of crystallinity can significantly alter mechanical and optical properties. Thus the thermal history of a polymer, in particular between T_g and T_m, greatly influences its end-use value [65]. Understanding the temperature effect, the key parameter influencing industrial crystallization, is essential for rational manufacturing design and operation. Potentially one can exploit the competition between kinetics and thermodynamic driving forces to manipulate the crystallization rate, crystal size, and particle polydispersity. Here the distribution kinetics approach is to represent the dynamics and kinetics of nucleation and growth processes by a cluster size-distribution model. The temperature effect is incorporated into the model by considering the temperature dependence of interfacial energy, equilibrium solubility, and growth rate coefficient. We begin in the next section by reviewing the theory of nucleation, growth, and coarsening for polymer crystallization.

The influences' of blends on their crystallization were discussed here at a length as it was major research area in this doctoral study. A large number of poly-

mer blends contain one or two crystallizable components. The crystallization behavior of a polymer component in a blend is expected to alter by the presence of the second blend component, whether both are completely miscible, partially miscible or totally immiscible. Therefore, a profound scientific understanding of the crystallization behavior and the resulting semicrystalline structure in polymer blends is necessary for effective manipulation and control of their properties. There are a number of important factors governing the change of the crystallization rate and semicrystalline structure of a polymer in blend systems. Those include the degree of miscibility of the constituent polymers, their concentration, their glass-transition and melting temperatures, the phase morphology and the interface structure in the case of immiscible blends, etc. The most intriguing effect in polymer crystallization is the occurrence of chain folding which inevitably leads to the formation of lamellae as the morphological building block of semi-crystalline polymers [47].

An important parameter is the thermal history of the sample. Crystallizable dispersed droplets that were submitted to premelting at higher temperatures for longer time generally display a shift in the heterogeneous nucleation spectrum to greater undercooling. The homogeneous crystallization temperature however is not displaced and thus independent of the thermal history. This may become less evident for blends with unstable phase morphology which occur through rapid phase coarsening upon annealing; long residence times in the melt will cause fine droplets to coarsen. Consequently, the newly formed larger droplets have a higher probability to crystallize close to the bulk crystallization temperature of the homopolymer.

Immiscible polymer blends, where the crystallization takes place within domains of nearly neat component, are largely unaffected by the presence of other polymers. However, while both phases are physically separated, they can exert a deep influence on each other. The presence of the second component can disturb the normal crystallization process, thus influencing crystallization kinetics, spherulite growth rate, semicrystalline morphology, etc.

Important factors which can influence crystallization are:

o Molecular structure and molecular mass of the components,
o Blend composition,
o Type and degree of dispersion of the phases in the melt state,
o Phase interactions *(e.g.,* nature of the interface, migration of nuclei, etc.),
o Melt history,
o Crystallization conditions (for example T_c, cooling rate, etc.),

o Physical crystallization conditions (surrounded by melt or solidified material).

These factors influence the crystalline morphology development, resulting in changes of crystallization parameters such as:

o Nucleation density, *N,*
o Spherulite growth rate, G,
o Overall crystallization rate, *K,*
o Total degree of crystallinity, X_c,
o Semicrystalline morphology, i.e., shape, size and texture of the spherulites, inter spherulitic boundaries, etc.

In a following section, in general terms, purpose of crystallization study are presented and discussed.

2.3   Purpose of crystallization study

Understanding the mechanism of self-assembly during polymer crystallization also has practical importance in industry. Synthetic polymers show unique features in their nucleation and crystallization. Understanding the mechanism of nucleation and crystal growth is critical for manufacturing process and determination of the final product properties, such as crystal size distribution, thermal stability and mechanical properties. The average crystal size can be manipulated by appropriately varying the crystallization temperature. The mechanical properties of polymers can also be manipulated through the extent of crystallization. As the crystallization temperature decreases from the melting temperature, T_m, to the point where the maximum nucleation rate is expected, the extent of crystallization increases, thus the friability of the polymer products increases.

Despite various existing models, the mechanism of polymer crystallization is not settled yet. The key factor that impedes the investigation of crystallization in polymers is the fact that the polymer chains fold back upon themselves during crystallization. One of the difficulties derived from chain folding is that chain–folded crystals are thermodynamically unstable and for that reason they tend to rearrange towards the equilibrium shape. The rapid rearrangement of the crystals together with the slow sample preparation needed.

In the traditionally used experimental techniques observation of the originally grown crystals is difficult. Advances in instrumental development and experimental techniques are correlated with fundamental breakthroughs in the understanding of

polymer crystallization. The established models frequently fail to explain new experimental observations. Real–time microscopy and X–ray diffraction techniques have provided a deeper insight into the molecular organization of polymers during the crystallization process. These findings concern the early stages of crystal growth, the existence of metastable phases, and the evolution of single crystals in time to form superstructures. The observations resulted in the revision of the existing models and the proposal of new concepts of polymer crystallization.

There are some of the problems related to crystallization usually arising in polymer industries:

o Minimization of the time until a certain degree of crystallization is reached
o Optimization of the morphology; in particular the distribution of interfaces between the crystals
o Optimization of crystal size distribution

Due to above mentioned problems, for semi-crystalline polymers, crystal morphology is always a fundamental factor of the later physical properties and the behavior of the final product is strongly influenced by the microstructure of the crystallized material. Concretely, how to choose comparatively easily controllable temperature range to end up with homogenous structure of small spherulites having excellent quality of the polymer product is always a principal concern.

REFERENCES

[1] KELLER, A. A Note on Single Crystals in Polymers: Evidence for a Folded Chain Configuration. *Philos. Mag.* 1957, vol. 2, no. 21, p. 1171-1175.

[2] GHIJSELS, A., GROESBEEK, N., YIP, C.W. Multiple crystallization behaviour of polypropylene/thermoplastic rubber blends and its use in assessing blend morphology. *Polymer* 1982, vol. 23, no. 13, p. 1913-1916.

[3] MARTUSCELLI, E., SILVESTRE, C., ABATE, G. Morphology, crystallization and meltingbehaviour of films of isotacticpolypropyleneblended with ethylene-propylenecopolymers and polyisobutylene. *Polymer* 1982, vol. 23, no. 2, p. 229-237.

[4] MARTUSCELLI, E. Influence of composition, crystallization conditions and melt phase structure on solid morphology, kinetics of crystallization and thermal behavior of binary polymer/polymer blends. *Polym. Eng. Sci.* 1984, vol. 24, no. 8, p. 563-586.

[5] FRENSCH, H., HARNISCHFEGER, P., JUNGNICKEL, B.J. Fractionated Crystallization in Incompatible Polymer Blends. *Acs Symposium Series* 1989, vol. 395, no., p. 101-125.

[6] LI, Y., JUNGNICKEL, B.J. The competition between crystallization and phase-seperation in polymer blends. 2. Small-angle X-ray scattering studies on the crystalline morphology of poly(epsilon-caprolactone) in its blends with polystyrene. *Polymer* 1993, vol. 34, no. 1, p. 9-15.

[7] PENNING, J.P., MANLEY, R.S.J. Miscible blends of two crystalline polymers .2. Crystallization kinetics and morphology in blends of poly(vinylidene fluoride) and poly(1,4-butylene adipate). *Macromolecules* 1996, vol. 29, no. 1, p. 84-90.

[8] SUN, D.H., ZHANG, R., LIU, Z.M., HUANG, Y., WANG, Y., HE, J., HAN, B.X., YANG, G.Y. Polypropylene/silica nanocomposites prepared by in-situ sol-gel reaction with the aid of CO_2. *Macromolecules* 2005, vol. 38, no. 13, p. 5617-5624.

[9] MA, J., BILOTTI, E., PEIJS, T., DARR, J.A. Preparation of polypropylene/sepiolite nanocomposites using supercritical CO_2 assisted mixing. *Eur. Polym. J.* 2007, vol. 43, no. 12, p. 4931-4939.

[10] ZHAI, W.T., KUBOKI, T., WANG, L.L., PARK, C.B., LEE, E.K., NAGUIB, H.E. Cell Structure Evolution and the Crystallization Behavior of Polypropylene/Clay Nanocomposites Foams Blown in Continuous Extrusion. *Ind. Eng. Chem. Res.* 2010, vol. 49, no. 20, p. 9834-9845.

[11] HAMBIR, S., BULAKH, N., JOG, J.P. Polypropylene/clay nanocomposites: Effect of compatibilizer on the thermal, crystallization and dynamic mechanical behavior. *Polym. Eng. Sci.* 2002, vol. 42, no. 9, p. 1800-1807.

[12] MAITI, P., NAM, P.H., OKAMOTO, M., HASEGAWA, N., USUKI, A. Influence of crystallization on intercalation, morphology, and mechanical properties of polypropylene/clay nanocomposites. *Macromolecules* 2002, vol. 35, no. 6, p. 2042-2049.

[13] HE, J.D., CHEUNG, M.K., YANG, M.S., QI, Z.N. Thermal stability and crystallization kinetics of isotactic polypropylene/organomontmorillonite nanocomposites. *J. Appl. Polym. Sci.* 2003, vol. 89, no. 12, p. 3404-3415.

[14] AVELLA, M., COSCO, S., VOLPE, G.D., ERRICO, M.E. Crystallization behavior and properties of exfoliated isotactic polypropylene/organoclay nanocomposites. *Adv. Polym. Technol.* 2005, vol. 24, no. 2, p. 132-144.

[15] SEN, K., KUMAR, P. Influence of gamma-irradiation on structural and mechanical properties of polypropylene yarn. *J. Appl. Polym. Sci.* 1995, vol. 55, no. 6, p. 857-863.

[16] LUGAO, A.B., HUTZLER, B., OJEDA, T., TOKUMOTO, S., SIEMENS, R., MAKUUCHI, K., VILLAVICENCIO, A. Reaction mechanism and rheological properties of polypropylene irradiated under various atmospheres. *Radiat. Phys. Chem.* 2000, vol. 57, no. 3-6, p. 389-392.

[17] KRUPA, I., LUYT, A.S. Thermal properties of isotactic polypropylene degraded with gamma irradiation. *Polym. Degrad. Stabil.* 2001, vol. 72, no. 3, p. 505-508.

[18] KRAUSE, B., VOIGT, D., HAUSSLER, L., AUHL, D., MUNSTEDT, H. Characterization of electron beam irradiated polypropylene: Influence of irradiation temperature on molecular and rheological properties. *J. Appl. Polym. Sci.* 2006, vol. 100, no. 4, p. 2770-2780.

[19] MORANCHO, J.M., RAMIS, X., FERNANDEZ, X., CADENATO, A., SALLA, J.M., VALLES, A., CONTAT, L., RIBES, A. Calorimetric and thermogravimetric studies of UV-irradiated polypropylene/starch-based materials aged in soil. *Polym. Degrad. Stabil.* 2006, vol. 91, no. 1, p. 44-51.

[20] ZHAO, Y., LUO, Y.X., JIANG, B.Z. Effect of irradiation on crystallinity and mechanical properties of ultrahigh molecular weight polyethylene. *J. Appl. Polym. Sci.* 1993, vol. 50, no. 10, p. 1797-1801.

[21] SHEN, F.W., MCKELLOP, H.A., SALOVEY, R. Irradiation of chemically crosslinked ultrahigh molecular weight polyethylene. *J. Polym. Sci. Pt. B-Polym. Phys.* 1996, vol. 34, no. 6, p. 1063-1077.

[22] ANDJELIC, S., RICHARD, R.E. Crystallization behavior of ultrahigh molecular weight polyethylene as a function of in vacuo gamma-irradiation. *Macromolecules* 2001, vol. 34, no. 4, p. 896-906.

[23] GHEYSARI, D., BEHJAT, A., HAJI-SAEID, M. The effect of high-energy electron beam on mechanical and thermal properties of LDPE and HDPE. *Eur. Polym. J.* 2001, vol. 37, no. 2, p. 295-302.

[24] KHONAKDAR, H.A., JAFARI, S.H., WAGENKNECHT, U., JEHNICHEN, D. Effect of electron-irradiation on cross-link density and crystalline structure of low- and high-density polyethylene. *Radiat. Phys. Chem.* 2006, vol. 75, no. 1, p. 78-86.

[25] KOJIMA, Y., USUKI, A., KAWASUMI, M., OKADA, A., FUKUSHIMA, Y., KURAUCHI, T., KAMIGAITO, O. Mechanical properties of nylon 6-clay hybrid. *J. Mater. Res.* 1993, vol. 8, no. 5, p. 1185-1189.

[26] USUKI, A., KAWASUMI, M., KOJIMA, Y., OKADA, A., KURAUCHI, T., KAMIGAITO, O. Swelling behaviour of montmorillonite cation exchanged for omega-amino acids by epsilon-caprolactam. *J. Mater. Res.* 1993, vol. 8, no. 5, p. 1174-1178.

[27] USUKI, A., KOJIMA, Y., KAWASUMI, M., OKADA, A., FUKUSHIMA, Y., KURAUCHI, T., KAMIGAITO, O. Synthesis of nylon 6-clay hybrid. *J. Mater. Res.* 1993, vol. 8, no. 5, p. 1179-1184.

[28] UTRACKI, L.A., Polymer Blends Handbook, Volumes 1-2, Springer - Verlag, 2002 ISBN 978-1-4020-1114-6.

[29] BRANDRUP, J., IMMERGUT, E.H., GRULKE, E.A., ABE, A., BLOCH, D.R., Polymer Handbook (4th Edition), John Wiley & Sons, p. 280-391, ISBN 978-0-471-16628-3.

[30] KULSHRESHTHA, A.K., VASILE, C., Handbook of Polymer Blends and Composites, Volumes 1-4, Smithers Rapra Technology, 2002 ISBN 978-1-85957-309-6.

[31] BALAZS, A.C., EMRICK, T., RUSSELL, T.P. Nanoparticle polymer composites: Where two small worlds meet. *Science* 2006, vol. 314, no. 5802, p. 1107-1110.

[32] PAUL, D.R., ROBESON, L.M. Polymer nanotechnology: Nanocomposites. *Polymer* 2008, vol. 49, no. 15, p. 3187-3204.

[33] PAUL, D.R., BARLOW, J.W. Polymer blends (or alloys). *J. Macromol. Sci.-Rev. Macromol. Chem. Phys.* 1980, vol. C18, no. 1, p. 109-168.

[34] SCHMIDT, D., SHAH, D., GIANNELIS, E.P. New advances in polymer/layered silicate nanocomposites. *Curr. Opin. Solid State Mat. Sci.* 2002, vol. 6, no. 3, p. 205-212.

[35] RICHARDSON, M.J., FLORY, P.J., JACKSON, J.B. Crystallization and melting of copolymers of polymethylene. *Polymer* 1963, vol. 4, no. 2, p. 221-236.

[36] KEITH, H.D., PADDEN, F.J. Spherulitic Crystallization from the Melt. I. Fractionation and Impurity Segregation and Their Influence on Crystalline Morphology. *J. Appl. Phys.* 1964, vol. 35, no. 4, p. 1270.

[37] CHATTERJEE, A.M., PRICE, F.P., NEWMAN, S. Heterogeneous nucleation of crystallization of high polymers from melt. 1. Substrate-induced morphologies. *J. Polym. Sci. Pt. B-Polym. Phys.* 1975, vol. 13, no. 12, p. 2369-2383.

[38] CHATTERJEE, A.M., PRICE, F.P., NEWMAN, S. Heterogeneous nucleation of crystallization of high polymers from melt. 3. Nucleation kinetics and interfacial energies. *J. Polym. Sci. Pt. B-Polym. Phys.* 1975, vol. 13, no. 12, p. 2391-2400.

[39] LEGRAS, R., MERCIER, J.P., NIELD, E. Polymer crystallization by chemical nucleation. *Nature* 1983, vol. 304, no. 5925, p. 432-434.

[40] MERCIER, J.P. Nucleation in polymer crystallization: A physical or a chemical mechanism. *Polym. Eng. Sci.* 1990, vol. 30, no. 5, p. 270-278.

[41] HIKOSAKA, M., AMANO, K., RASTOGI, S., KELLER, A. Lamellar thickening growth of an extended chain single crystal of polyethylene .1. Pointers to a new crystallization mechanism of polymers. *Macromolecules* 1997, vol. 30, no. 7, p. 2067-2074.

[42] SADLER, D.M. Roughness of growth faces of polymer crystals: Evidence from morphology and implications for growth mechanisms and types of folding. *Polymer* 1983, vol. 24, no. 11, p. 1401-1409.

[43] BURGER, M., Crystal growth and impingement in polymer melts, Birkhauser Verlag Ag, Basel, 2004 3-7643-2193-8.

[44] MANDELKERN, L., QUINN, F.A., FLORY, P.J. Crystallization kinetics in high polymers. 1. Bulk polymers. *J. Appl. Phys.* 1954, vol. 25, no. 7, p. 830-839.

[45] MANDELKERN, L. The crystallization of flexible polymer molecules. *Chem. Rev.* 1956, vol. 56, no. 5, p. 903-958.

[46] DI LORENZO, M.L. Spherulite growth rates in binary polymer blends. *Prog. Polym. Sci.* 2003, vol. 28, no. 4, p. 663-689.

[47] LIU, J.P., JUNGNICKEL, B.J. Crystallization kinetical and morphological peculiarities in binary crystalline/crystalline polymer blends. *J. Polym. Sci. Pt. B-Polym. Phys.* 2007, vol. 45, no. 15, p. 1917-1931.

[48] LONG, Y., SHANKS, R.A., STACHURSKI, Z.H. Kinetics of poymer crystallization *Prog. Polym. Sci.* 1995, vol. 20, no. 4, p. 651-701.

[49] AVRAMI, M. Kinetics of phase change I - General theory. *J. Chem. Phys.* 1939, vol. 7, no. 12, p. 1103-1112.

[50] AVRAMI, M. Granulation, Phase Change, and Microstructure - Kinetics of Phase Change. III. *J. Chem. Phys.* 1941, vol. 9, no. 2, p. 177-184.

[51] DEBRUIJN, T.J.W., DEJONG, W.A., VANDENBERG, P.J. Kinetic-parameters in avrami-erofeev type reactions from isothermal and non-isothermal experiments *Thermochim. Acta* 1981, vol. 45, no. 3, p. 315-325.

[52] HARNISCH, K., MUSCHIK, H. Determination of the Avrami exponent of partially crystallized polymers by DSC- (DTA-) analyses. *Colloid Polym. Sci.* 1983, vol. 261, no. 11, p. 908-913.

[53] CAZE, C., DEVAUX, E., CRESPY, A., CAVROT, J.P. A new method to determine the Avrami exponent by dsc studies of non-isothermal crystallization from the molten state. *Polymer* 1997, vol. 38, no. 3, p. 497-502.

[54] PRADELL, T., CRESPO, D., CLAVAGUERA, N., CLAVAGUERA-MORA, M.T. Diffusion controlled grain growth in primary crystallization: Avrami exponents revisited. *J. Phys.-Condes. Matter* 1998, vol. 10, no. 17, p. 3833-3844.

[55] HOFFMAN, J.D., WEEKS, J.J. Melting Process and the Equilibrium Melting Temperature of Polychlorotrifluoroethylene. *J. res. Nat. Bur. Stand. Sect. A. Phys. chem.* 1962, vol. 66, no. JAN-F, p. 13.

[56] HOFFMAN, J.D., LAURITZEN, J.I. Crystallization of bulk polymers with chain folding: theory of growth of lamellar spherulites. *J. Res. Natl. Bur. Stand.* 1961, vol. A 65, no. 4, p. 297.

[57] HOFFMAN, J.D. Theoretical aspects of polymer crystallization with chain folds: Bulk polymers. *Spe Transactions* 1964, vol. 4, no. 4, p. 315-362.

[58] HOFFMAN, J.D., LAURITZE.J.I, PASSAGLI, E., ROSS, G.S., FROLEN, L.J., WEEKS, J.J. Kinetics of polymer crystallization from solution and the melt. *Colloid Polym. Sci.* 1969, vol. 231, no. 1-2, p. 564-592.

[59] LAURITZEN, J.I., HOFFMAN, J.D. Extension of theory of growth of chain-folded polymer crystals to large undercoolings. *J. Appl. Phys.* 1973, vol. 44, no. 10, p. 4340-4352.

[60] HOFFMAN, J.D., FROLEN, L.J., ROSS, G.S., LAURITZEN, J.I. On the growth rate of spherulites and axialites from the melt in polyethylene fractions: Regime I and regime II crystallization. *J. res. Nat. Bur. Stand. Sect. A. Phys. chem.* 1975, vol. 79, no. 6, p. 671-699.

[61] MARAND, H., XU, J.N., SRINIVAS, S. Determination of the equilibrium melting temperature of polymer crystals: Linear and nonlinear Hoffman-Weeks extrapolations. *Macromolecules* 1998, vol. 31, no. 23, p. 8219-8229.

[62] HOFFMAN, J.D. Regime III crystallization in melt-crystallized polymers: The variable cluster model of chain folding. *Polymer* 1983, vol. 24, no. 1, p. 3-26.

[63] CLARK, E.J., HOFFMAN, J.D. Regime-III crystallization in polypropylene. *Macromolecules* 1984, vol. 17, no. 4, p. 878-885.

[64] HOFFMAN, J.D., MILLER, R.L. Kinetics of crystallization from the melt and chain folding in polyethylene fractions revisited: Theory and experiment. *Polymer* 1997, vol. 38, no. 13, p. 3151-3212.

[65] LEISEN, J., BECKHAM, H.W., SHARAF, M.A. Evolution of crystallinity, chain mobility, and crystallite size during polymer crystallization. *Macromolecules* 2004, vol. 37, no. 21, p. 8028-8034.

AIM OF THE DOCTORAL STUDY

There is a need to understand crystallization behavior in course to apply this knowledge at industrial level. Therefore, the main objective of the study was to determine crystallization behavior for polyolefins, its blends and nanocomposites at various conditions by various analytical methods and existing models.

Accordingly the main consideration within this work is particularly divided to following topics:

✓   The effect of various polypropylene/ethylene-octene copolymer blends on its crystallization ability.

✓   The effect of initial melting temperature on the crystallization ability of various polypropylene/organoclay nanocomposites.

✓   A study of crystallization behavior for the polypropylene based nanocomposite under the influence of supercritical CO_2 and initial melting temperature.

✓   The influence of electron beam irradiation on polypropylene and high-density polyethylene.

LIST OF PAPERS

I.   Isothermal crystallization in polypropylene/ethylene–octene copolymer blends
Petr Svoboda, Krunal Trivedi, Dagmar Svobodova, Pavel Mokrejs, Vladimir Vasek, Keisuke Mori, Toshiaki Ougizawa, Takashi Inoue
Materials Chemistry and Physics
Volume 131, Issues 1–2, 15 December 2011, Pages 84–93

II.   Effect of Initial Melting Temperature on Crystallization of Polypropylene/Organoclay Nanocomposites
Petr Svoboda, Krunal Trivedi, Dagmar Svobodova, Pavel Mokrejs, and Karel Kolomaznik
Macromolecular Research
Accepted (2011)

III.   Influence of supercritical CO_2 and initial melting temperature on crystallization of polypropylene/organoclay nanocomposite
Petr Svoboda, Krunal Trivedi, Dagmar Svobodova, Karel Kolomaznik, Takashi Inoue
Polymer Testing
Volume 31, Issues 3, May 2012, Pages 444-454

IV.   A study on the crystallization behavior of electron beam irradiated polypropylene and high-density polyethylene
Krunal Trivedi, Petr Svoboda, Dagmar Svobodova, Zdenek Holik, Michal Danek, Kittisak Jantanasakulwong, Toshiaki Ougizawa
Submitted for publication

SUMMARIES OF PAPERS

Short summaries and the major results of Papers I-IV are presented below:

Paper I focuses on the effect of blends composition on crystallization ability of polypropylene/ethylene-octene copolymer blends. Crystallization kinetics of polypropylene (PP)/ethylene-octene copolymer (EOC) blends was measured by differential scanning calorimetry (DSC) and by optical microscopy at various temperatures (123-140°C). The crystallization kinetics is greatly affected by the blend composition. As it was found by DSC, small amounts of EOC (10-30%) increased the bulk crystallization kinetics. On the other hand, larger amounts of EOC (50-80%) caused the decrease in kinetics. Optical microscopy revealed a decrease in a single spherulite growth rate caused by EOC obstacles, and at the same time larger number of spherulites. EOC acts as a nucleation agent increasing the bulk crystallization rate and at the same time it acts as an obstacle to the growing front of a spherulite when the PP lamellae have to go around the EOC obstacle. This was confirmed by detailed analyses according to Avrami and Hoffmann-Lauritzen. TEM also revealed presence of PP lamellae in EOC regions that together with T_g shift of PP and also EOC suggested partial miscibility. While at low temperatures the crystallization is very fast, at higher temperatures there is a competition of phase separation and crystallization.

The effect of initial melting temperature on crystallization behavior of polypropylene/organoclay nanocomposites was discussed in **paper II**. Polypropylene (PP) nanocomposites were prepared by melt intercalation in an intermeshing co-rotating twin-screw extruder. The influence of organoclay (Cloisite 20A) and maleic anhydride modified polypropylene (PPMA) on various properties was explored. The effect of the initial melting temperature on crystallization kinetics was investigated by differential scanning calorimetry (DSC) and optical microscopy. DSC has revealed a gradual decrease in crystallization kinetics with an increase in initial melting temperature for two-component systems (PP/PP-MA and PP/20A). However, in the case of a three-component system (PP/PP-MA/20A), the decrease of crystallization kinetics in the range of initial melting temperature being 200-240°C was followed by an increase in the temperature range 240-260°C. After initial melting at 250°C, many spherulites were discovered in the three-component system. This unusual crystallization behavior was explained with the help of Fourier transform infrared spectroscopy (FTIR), where an increase in the Si-O peak with the increasing initial melting temperature was detected, which indicates the presence of large surface of clay layers. The X-ray diffraction (XRD) analysis has revealed a decrease in the

peak intensity with an increase in initial melting temperature, which suggests exfoliation caused by fast diffusion at high temperatures.

The influence of supercritical CO_2 and initial melting temperature on crystallization kinetics of polypropylene/organoclay nanocomposite was investigated in **paper III**. Polypropylene/clay nanocomposite with maleic anhydride modified polypropylene (PP-MA) was prepared using a twin-screw extruder. The effect of supercritical carbon dioxide ($scCO_2$) on mixing was investigated. Isothermal crystallization of the nanocomposites was investigated by differential scanning calorimetry (DSC) and also by optical microscopy as a function of initial melting temperature. Increasing initial melting temperature causes a gradual decrease in bulk crystallization kinetics, with the exception of the 240–260°C temperature range for the system without CO_2. Optical microscopy revealed a large number of small spherulites for the system without CO2 after initial melting at 250°C. After 28 min initial induction period of crystallization many small spherulites appeared in the vicinity of large spherulites for the system with CO_2, indicating the beginning of homogenous nucleation. X-ray diffraction (XRD) and direct observation of the samples after tensile testing revealed better dispersion of nanoclay for the system without CO_2.

Paper IV deals with effect of electron beam irradiation on crystallization behavior of polypropylene and high-density polyethylene. Polypropylene copolymer and high-density polyethylene sheets were prepared by compression molding. Sheet was irradiated by electron beam at the room temperature in normal atmosphere. High temperature (200°C) creep test has revealed that HDPE gradually more and more crosslinks in the range 30-120 kGy while PP does not crosslink at all. Mechanical properties were measured in range -150 to 200°C by dynamical mechanical analysis (DMA). Small presence of C=C and C=O bonds was found in irradiated PP by Fourier transform infrared spectroscopy (FTIR). Crystallization kinetics study revealed tremendous decrease in crosslinked HDPE and rather moderate decrease in case of PP. Also while crystallinity was unchanged for PP, HDPE was decreased by irradiation significantly (from 60 to 47%). Optical microscopy clearly illustrated smaller number of nucleation centers after irradiation and also decreased rate of crystallization of individual spherulites. XRD analysis exposed lower crystallinity for HDPE and very interesting increase of β-phase in case of PP with maximum being at 60kGy.

CONTRIBUTIONS TO THE SCIENCE AND PRACTICE

The presented doctoral thesis deals with the crystallization study of polyolefins, its blends and nanocomposites with various techniques and existing scientific theories. The contributions of the current study to the level of scientific knowledge are as follows:

- o To investigate the effect of polypropylene/ethylene-octene copolymer blends on crystallization activities at wide range of isothermal crystallization temperature. This also provides a better understanding on morphological aspects of blends. It could be helpful to produce better industrial products at certain blend ratio and at precious crystallization temperatures.

- o The study of crucial initial melting temperature effects on the crystallization kinetics of the polypropylene based nanocomposites gives a better understanding on how crystallization affects nanocomposites mechanical properties.

- o The study of processing of polypropylene based nanocomposite with the help of supercritical CO_2 followed by study of crystallization behaviour after initial melting temperature results could be significant for industrial application.

- o The study of crystallization behavior of electron beam irradiated polypropylene and high-density polyethylene holds a practical standpoint.

Obtained results have already been published or been submitted to publication. This study provides a better understanding on crystallization behaviour under different circumstances. This could be of practical importance to the related industries facing the problems with crystallization behaviour.

CURRICULUM VITAE

Name: Krunal

Surname: Trivedi

Nationality: Indian

Date of Birth: 26th October 1983

Permanent Address: 145, Saurabh Society,
GIDC Residential Area,
Opp. Rofel MBA college,
Vapi (GIDC) - 396195,
Gujarat
INDIA

Email: trivedikrunalr@gmail.com

EDUCATION AND ACADEMIC ACTIVITIES

11/2008 – Till date: Tomas Bata University in Zlin – Doctoral student in Faculty of Technology

2004 – 2006: Sardar Patel University - M.Sc. in Plastics Technology

2001 – 2004: Sardar Patel University - B.Sc. in Industrial Polymer Chemistry

INDUSTRIAL TRAINING

- In 2003, six weeks training in *Mayura Industries*, Nani Daman, India.
- In 2005, six weeks training in *Solvay Advance Polymers*, Panoli, India.

HONORS

- Awarded Gold Medal in graduation for securing 1st in the University.
- Securing overall Highest marks in M.Sc.

WORK EXPERIENCE

- 11/2007 – 10/2008: R.R.PACKAGING, Vapi, India.

  Worked as a 'Process Engineer'

  Product: Manufacturing Plastics' printed and non-printed bags and rolls.

- 09/2006 – 11/2007: PI POLYMER (now known as *Rhodia Polymers & Specialties India Private Ltd*), Ankleshwar, India.

Worked as a 'Laboratory Chemist (R&D and QC)'

Product: Engineering Thermoplastics like PC, PPE, PBT, PP, Nylon, ABS and SAN. Handle large range of fillers like Talc, Calcite, Mica, Glass Fiber, Glass Beads and Wollastonite.

- 05/2006 – 09/2006: POLYSIL PIPES, Silavassa, India.

Worked as a 'QC-Officer'

Product: Pipe Tubes & Fittings (PVC).

RESEARCH EXPERIENCE AND PUBLICATIONS

PROJECT: As Master student,

- Morphological and mechanical study of biodegradable LDPE/modified starch blends.

Conference presentation/Publication

✓ Trivedi K., John N. *Processability, morphological study and mechanical properties of biodegradable LDPE/modified starch blends* Conference proceeding, GSC, 2006.

✓ Trivedi K., John N. *Morphological study and mechanical properties of biodegradable LDPE/modified starch blends*", Conference proceeding, Asia Rubtech '06 2006.

MANUSCRIPTS ACCEPTED/SUBMITTED:

✓ Svoboda P., Trivedi K. et al. *Isothermal crystallization in polypropylene/ethylene-octene copolymer blends* Materials Chemistry and Physics Volume 131, Issues 1–2, 15 December 2011, Pages 84–93 (2011)

✓ Svoboda P., Trivedi K. et al. *Effect of Initial Melting Temperature on Crystallization of Polypropylene/Organoclay Nanocomposites* Macromolecular Research Accepted (2011)

✓ Svoboda P., Trivedi K. et al. *Influence of supercritical CO_2 and initial melting temperature on crystallization of polypropylene/organoclay nanocomposite* Polymer Testing Volume 31, Issues 3, May 2012, Pages 444-454 (2012)

✓ Trivedi K, Svoboda P., et al. *A study on the crystallization behavior of electron beam irradiated polypropylene and high-density polyethylene* Submitted

PAPER I
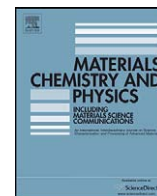
Isothermal crystallization in polypropylene/ethylene–octene copolymer blends

Petr Svoboda [a,*], Krunal Trivedi [a], Dagmar Svobodova [a], Pavel Mokrejs [a], Vladimir Vasek [b], Keisuke Mori [c], Toshiaki Ougizawa [c], Takashi Inoue [d]

[a] Centre of Polymer Systems, Faculty of Technology, Tomas Bata University in Zlin, Nam.T.G.Masaryka 5555, 760 01 Zlin, Czech Republic
[b] Faculty of Applied Informatics, Tomas Bata University in Zlin, Nad Stranemi 4511, 760 05 Zlin, Czech Republic
[c] Department of Organic and Polymeric Materials, Tokyo Institute of Technology, 2-12-1-S8-33, Ookayama, Meguro-ku, Tokyo 152-8552, Japan
[d] Dept. of Polymer Sci. & Eng., Yamagata University, Yonezawa 992-8510, Japan

ARTICLE INFO

ABSTRACT

Crystallization kinetics of polypropylene (PP)/ethylene–octene copolymer (EOC) blends was measured by differential scanning calorimetry (DSC) and by optical microscopy at various temperatures (123–140 °C). By DSC it was found that small amounts of EOC (10–30%) increase the bulk crystallization kinetics; in some cases even 80% increase was observed. Larger amounts of EOC (50–80%) have caused a decrease in crystallization kinetics. Optical microscopy has revealed that crystallization kinetics of a single spherulite is decreased by the presence of EOC, and at the same time there are more spherulites in the blend. EOC acts as a nucleation agent increasing the bulk crystallization rate and at the same time it acts as an obstacle to the growing front of a spherulite when the PP lamellae have to go around the EOC obstacle. This was confirmed by detailed analyses according to Avrami and Hoffman–Lauritzen. Structure was also observed by transmission electron microscopy (TEM). At low PP content (20%) PP forms very small isolated particles with size smaller than 1 micrometer. At 40% of PP a structure resembling a co-continuous one was found. When the PP is a majority phase (20–40% of EOC) rather large EOC particles were found. TEM also revealed presence of PP lamellae in EOC regions that together with T_g shift of PP and also EOC suggested partial miscibility. While at low temperatures the crystallization is very fast, at higher temperatures there is a competition of phase separation and crystallization.

© 2011 Elsevier B.V. All rights reserved.

1. Introduction

The structure of the semi-crystalline polymer is controlled by the mechanism of crystallization and crystallization kinetics. The nucleation, growth and kinetics of development of these crystalline regions are interesting both for basic and applied research. These characteristics are directly linked to understanding of the morphology of these crystalline regions. Crystallization occurs during the manufacturing of the articles made from polymeric materials; the understanding of its mechanism is necessary for macroscopic structure design and final product properties control. Faster crystallization of blend can cause shorter fabrication time in the injection molding machine, which can also lead to lower finished part cost.

Mechanical properties are closely related to the crystalline structure. For example Xu et al. found out that smaller size of the spherulites (in pure PP) may be responsible for the increase in impact strength [1]. Avella et al. discovered that the connectivity of the spherulitic boundaries is the major factor in controlling the fracture toughness [2]. Zhang et al. found out that decrease in

spherulite size caused by addition of nucleating agent in PP/EOC blends has caused tremendous increase in impact strength and moderate increases in tensile strength and flexural strength [3]. All these examples show the importance of controlling the crystalline morphology in relationship with mechanical properties.

Polypropylene (PP) is one of the most versatile low cost commodity polymers. It has good chemical and moisture resistance, good ductility and stiffness and easy processability. Although PP has seen widespread application, its limited impact strength, especially at lower temperature due to its relatively high T_g is an obstacle to broader utilization as an engineering plastic. The impact properties of PP can be considerably improved by incorporation of a rubbery phase. Accordingly, rubber-toughened PP blends with various impact modifiers have been studied, including ethylene–propylene rubber (EPR), ethylene–propylene–diene rubber (EPDM), and ethylene–propylene–styrene rubber (SEBS). Recently, impact modification of PP, using metallocene-catalyzed ethylene–octene copolymer (EOC) has attracted attention. EOC provides better efficiency of impact modification than EPR, and is more cost effective than EPDM [4].

In 1993, DuPont Dow Elastomers has introduced POEs under the brand name ENGAGE®. They are ethylene–octene copolymers produced via advanced INSITE™ catalyst and process technology

* Corresponding author. Tel.: +420 576 031 335; fax: +420 577 210 172.
E-mail address: svoboda@ft.utb.cz (P. Svoboda).

designed to be processed like thermoplastic but can be also compounded like elastomers. The exceptional performance of ENGAGE® is attributed to extraordinary control over polymer structure, molecular weight distribution, uniform comonomer composition and rheology. They are being considered for use in diverse applications such as cushioning agents, gaskets, and particularly good alternative for sealing application due to their structural regularity and non-toxic composition.

The PP/EOC blend has been investigated from different aspects such as crystallization and melting behavior [5], mechanical properties [6,7], morphology and rheology [8,9]. Moreover, there have been studies on thermal expansion [10], adhesion [11,12], and non-isothermal crystallization [13–17]. However, no comprehensive study has been done on the isothermal crystallization behavior of PP/EOC blends with high EOC content and in wide-range of crystallization temperatures and blend compositions.

The main objective of this research was to analyze quantitatively the influence of blend composition on isothermal crystallization kinetics of PP/EOC blends. The morphology of the blends was observed by transmission electron microscopy (TEM). The crystallization behavior of PP in the blends was investigated by differential scanning calorimetry (DSC). The crystallization kinetics was also measured by optical microscopy. Crystallization kinetics parameters based on the isothermal crystallization were analyzed according to by the Avrami's equation [18,19] and by Hoffman–Lauritzen equation [20,21].

2. Experimental

The isotactic polypropylene (PP) was a commercial polymer supplied by Mitsui Chemicals Inc. (J3HG, $M_w = 3.5 \times 10^5$ g mol^{-1} and $M_n = 5 \times 10^4$ g mol^{-1}).

Ethylene–octene copolymer was a special sample prepared by Dow Chemicals. The octene content is 40 wt% (or 14.29 mol%) which means that there are about 6 ethylene units per 1 octene unit. Molecular weight M_n was 2.28×10^5 g mol^{-1}.

The PP and EOC were melt-mixed (charge 5 g) at 200 °C for 5 min at 50 rpm in a miniature HAAKE MiniLabmixer, two screws being in counter-rotating mode. Blend ratio was gradually varied across the whole blend composition. The melt-mixed blend was extruded and quenched.

The isothermal crystallization of the PP/EOC samples was analyzed by a Perkin-Elmer DSC-1. Temperature calibration was performed using indium standard. Nitrogen atmosphere was employed during the experiment at heat flow rate being 20 mL min^{-1}. For the isothermal crystallization of the PP/EOC samples, the samples were heated up to 200 °C (at 100 °C min^{-1} of heating rate) and then cooled (at 50 °C min^{-1}) to the isothermal crystallization temperatures (124, 126, 128, 130, 132, 134, and 136 °C). In all cases, sample was held at 200 °C for 1 min to eliminate previous thermal history.

For the transmission electron microscopy (TEM) analysis, the specimens were stained with RuO$_4$ vapor at room temperature for 4 h and then microtomed to an ultrathin section of about 70 nm thick using a Reichert-Jung ultracryomicrotome with a diamond knife at room temperature. The structure was observed by an electron microscope, HITACHI H-7650 (accelerating voltage 100 kV).

For the optical microscopy observations, the specimen was melt-pressed for 1 min between two cover glasses on a hot stage at 200 °C. The melted specimen was then placed onto a LINKAM hot stage of the microscope set to temperatures in range 130–140 °C. Structural development during the isothermal annealing was observed under the optical microscope (LMU 406 SP) equipped with a video recording system.

3. Theoretical background

Whenever a polymer crystallizes, the extent of the phase transformation depends upon the crystallizing species and the experimental conditions. High molecular weight polymers do not crystallize completely because of topological constraints that lower crystallinity considerably. The classical isothermal transformation kinetics, initially formulated by Kolmogorov and Goler et al. were extended later by the Avrami theory that was initially formulated for metals and later modified, for example, by Evans and others, for polymers [22].

The fraction X_t is obtained from the area of the exothermic peak in DSC isothermal crystallization analysis at a crystallization time t divided by the total area under the exothermic peak [23]:

$$X_t = \frac{\int_0^t (dH/dt)dt}{\int_0^\infty (dH/dt)dt} \tag{1}$$

where the numerator is the heat generated at time t and the denominator is the total heat generated up to the complete crystallization.

The crystallization kinetics of polymers is analyzed using a classical Avrami equation as given in Eq. (2):

$$1 - X_t = \exp(-kt^n) \tag{2}$$

where the k value is the Avrami rate constant and the n value is the Avrami exponent. Both k and n depend on the nucleation and growth mechanisms of spherulites. In order to deal conveniently with the operation, Eq. (2) is usually rewritten as the double logarithmic form as follows:

$$\ln[-\ln(1 - X_t)] = \ln k + n \ln t \tag{3}$$

The k and n values could be directly obtained using Eq. (3) from the slope and intercept of the best-fit line.

The crystallization behavior of the polymers was also studied according to the relationship between chain folded crystal growth rates and undercooling proposed by Hoffman and Lauritzen [20,21]:

$$G = G_0 \ \exp\left[\frac{-U^*}{R(T_c - T_\infty)} - \frac{K_g}{T_c(\Delta T)f}\right] \tag{4}$$

where G is the crystal growth rate, U^* is a constant characteristic of the activation energy for repetitive chain motion and is equal to 1500 cal mol^{-1} [24,25], R is the gas constant, T_c is the crystallization temperature (K), $T_\infty = T_g - 30$ K and (for PP the glass transition temperature $T_g = 270$ K [26]), $\Delta T = T_m^0 - T_c$, T_m^0 is the equilibrium melting temperature of an infinitely thick crystal, K_g is the nucleation constant, f is a correction factor and equals to $2T_c/(T_m^0 + T_c)$ and G_0 is a pre-exponential factor. In order to perform nonlinear regression by software Mathematica 8 it was necessary to rewrite the equation form into a computer language. The sequence of simplification is shown by Eqs. (5)–(7) and example of equation for pure PP where $T_\infty = 233$ K and $T_m^0 = 459$ K is given by Eq. (8).

$$G = G_0 \exp\left[\frac{-U^*}{R(T_c - T_\infty)} - \frac{K_g}{T_c(T_m^0 - T_c)(2T_c/(T_m^0 + T_c))}\right] \tag{5}$$

$$G = G_0 \exp\left[\frac{-U^*}{R(T_c - T_\infty)} - \frac{K_g(T_m^0 + T_c)}{2T_c^2(T_m^0 - T_c)}\right] \tag{6}$$

$$y = a \exp\left[\frac{-b}{8.314(x - T_\infty)} - \frac{c(T_m^0 + x)}{2x^2(T_m^0 - x)}\right] \tag{7}$$

$$y = a \exp\left[\frac{-b}{8.314(x - 233)} - \frac{c(459 + x)}{2x^2(459 - x)}\right] \tag{8}$$

For linear data analysis and estimation of initial parameters a, b and c for nonlinear regression, it is convenient to use a logarithmic version of Eq. (4) shown by Eq. (9). This equation was used for optical microscopy evaluation.

$$\ln(G) + \frac{U^*}{R(T_c - T_\infty)} = \ln G_0 - \frac{K_g}{T_c \Delta T f} \tag{9}$$

For the evaluation of DSC results we have replaced G by $1/\tau_{1/2}$.

$$\ln\left(\frac{1}{\tau_{1/2}}\right) + \frac{U^*}{R(T_c - T_\infty)} = \ln G_0 - \frac{K_g}{T_c \Delta T f} \tag{10}$$

A major extension of the theory involved the recognition that the deposition of a single critical nucleus may not always occur and that multiple nucleation generate different situation. The situation is handled best in general conceptual terms by considering it to be a competitive situation between the rate at which critical nuclei are deposited on the surface and the rate at which the chains deposit laterally to complete the growth step. This leads to three distinct situations or regimes; regime I the classical situation in which the rate of secondary nucleation is slowest, regime II a situation in which the rates of secondary nucleation and lateral spreading are comparable, and regime III a situation in which the rate of secondary nucleation is the fastest. These three situations occur naturally in many polymers as the crystallization temperature is reduced. The vast majority of polymers studied show regimes II and III, whereas few show regime I which is the classical situation [27].

Basically, the diffusion process has been described as consisting of two elementary processes: the deposition of the first stem on the growth front (secondary nucleation process) and the attachment of following stems in the chain on the crystal surface (surface spreading process). According to the Hoffman–Lauritzen theory, G is mostly governed by the rate of secondary nucleation, i, in regimes I and III, while it is governed by both i and the rate of surface spreading, g, in regime II:

$$G \propto i \quad \text{for } \frac{i}{g} \ll 1 \text{ (regime I)} \tag{11}$$

$$G \propto (ig)^{1/2} \quad \text{for } \frac{i}{g} \sim 1 \text{ (regime II)} \tag{12}$$

$$G \propto i \quad \text{for } \frac{i}{g} \gg 1 \text{ (regime III)} \tag{13}$$

where i consists of both β_g and $\exp[-K_g/T_c(\Delta T)f]$ and g consists of only β_g. The diffusion coefficients in the surface nucleation process and the substrate completion process are defined as D_M and D_S, respectively. Assuming that β_g is proportional to the diffusion coefficient, i and g may be given by:

$$i \propto D_M \ \exp\left[-\frac{K_g}{T_c \Delta T f}\right] \tag{14}$$

$$g \propto D_s \tag{15}$$

From Eqs. (11)–(15) one can obtain:

$$\beta_g \propto \phi_1 D_M \quad \text{(regime I and III)} \tag{16}$$

$$\beta_g \propto \phi_1^{1/2}(D_M D_s)^{1/2} \quad \text{(regime II)} \tag{17}$$

where a prefactor ϕ_1 is introduced, since i is proportional to the number of crystallizable molecules at the crystal surface, which is proportional to the volume fraction of crystalline polymer ϕ_1 [28].

4. Results and discussion

After 5 min in Haake mixer the blends were extruded to air and pressed between two cold metal plates. Fig. 1 shows the TEM micrographs (at 1000× magnification) of blends with increasing EOC content. For 30 and 40% of EOC the matrix is composed of PP and the dispersed phase is EOC. There seems to be an increase in EOC particle size from about 2 μm to 5 μm when the blend composition is changed from 30 to 40% of EOC. At 60% of EOC the structure resembles a co-continuous one. At 80% of EOC the situation is reversed: EOC became a matrix and PP forms very small droplets with the size smaller than 1 μm. One could expect that the crystallization will be affected quite significantly for these very different morphologies.

While the observation of morphology at 1000× magnification is important for seeing which polymer forms the matrix and which one is the dispersed phase, TEM enables us also to look much deeper
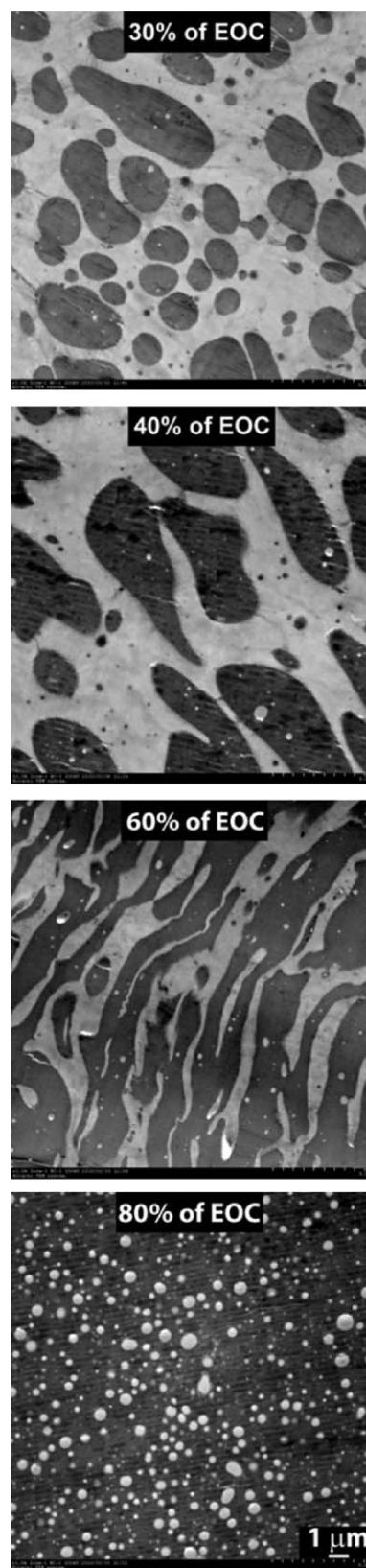

Fig. 1. TEM micrograph of PP/EOC blends after mixing at 50 rpm for 5 min at 200 °C.

at magnification e.g. 30,000× when one can see the lamellar structure.

These structures at much higher magnification are shown in Fig. 2. RuO₄ stains preferably EOC, so the bright phase is PP. In our previous study [29] we have shown the existence of partial
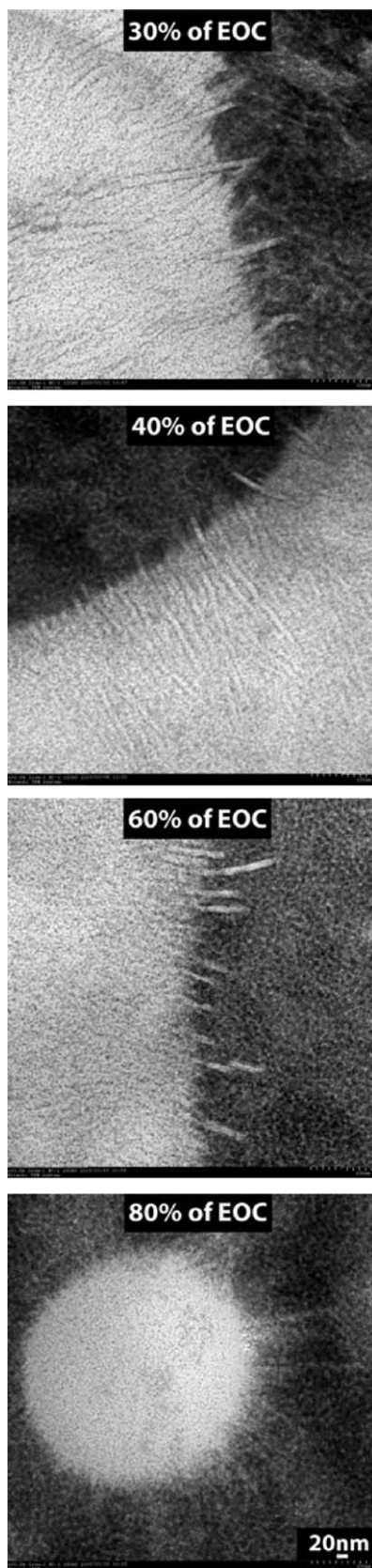
Fig. 2. TEM micrograph of PP/EOC blends after mixing at 50 rpm for 5 min at 200 °C.
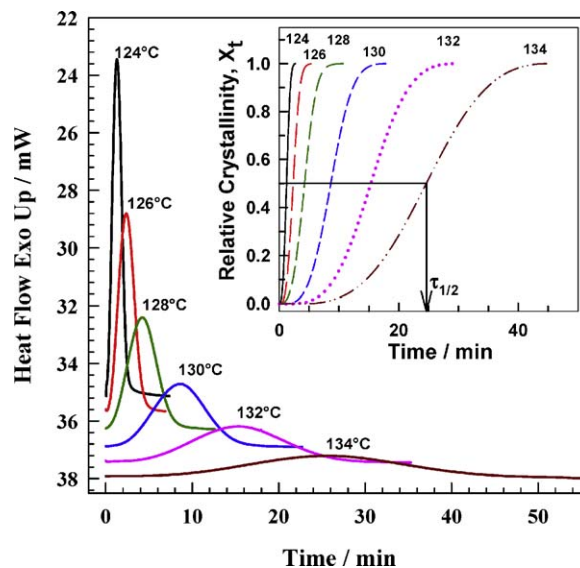

Fig. 3. Isothermal crystallization peaks of PP/EOC (70/30) blend by DSC at various crystallization temperatures.

miscibility between PP and EOC based on the T_g shift for EOC being 3.5 °C and for PP 2.3 °C. The crystallization of PP is most likely affected by the presence of small amount of EOC in PP-rich phase.

In addition to that there are PP lamellae present also in EOC-rich phase. Crystallization of these lamellae could have quite different kinetics compared to lamellae in PP-rich phase. As one can observe the situation is quite complex and we will try to understand it and explain it in following section.

The crystallization was studied at first by DSC and then also by optical microscopy. Fig. 3 illustrates the results from DSC experiments. Initially the samples with weight about 10–15 mg were heated from room temperature to 200 °C at rate 100 °C min^{-1}, then the temperature was kept at 200 °C for 1 min to fully melt the PP crystals (T_m of PP is about 165 °C) and the EOC crystals as well (T_m of EOC is about 48 °C). The next step was fast cooling to desired isothermal crystallization temperature. This cooling at rate 50 °C min^{-1} was attained by a cooling unit capable of cooling to −30 °C. The last step was isothermal crystallization at desired temperature.

When the heat flow curve reaches minimum value and starts to grow to form an exothermal peak we have assigned this time to be 0. By the integration of heat flow curve one can get a relative crystallinity curve shown on the inserted picture of Fig. 3. When the crystallinity reaches 0.5 (or 50%) one gets $\tau_{1/2}$.

Temperature affects the crystallization heat flow curves in a way shown in Fig. 3. While at 124 °C crystallization takes few minutes, at 134 °C crystallization takes almost an hour. One cannot go beyond the 123–136 °C temperature range with DSC experiment very far. When we set the crystallization temperature lower than 123 °C, crystallization starts already during cooling to desired temperature. On the other hand if we choose temperature higher than 136 °C, the heat flow curves have large fluctuations and noises and the $\tau_{1/2}$ evaluation becomes less accurate. For very slowly crystallizing blends this experimental window was limited only to 123–130 °C.

This is shown on the small inserted picture of Fig. 4 for example for PP/EOC (20/80) blend when we had to stop experiments at about 129 °C since the crystallization was extremely slow ($\tau_{1/2}$ being more than 3000 s). It is interesting that pure PP's curve lays somewhere in the middle. As we have mentioned there are blends much slower than pure PP, such as above mentioned PP/EOC (20/80) blend, but there are also blends faster than pure PP, such
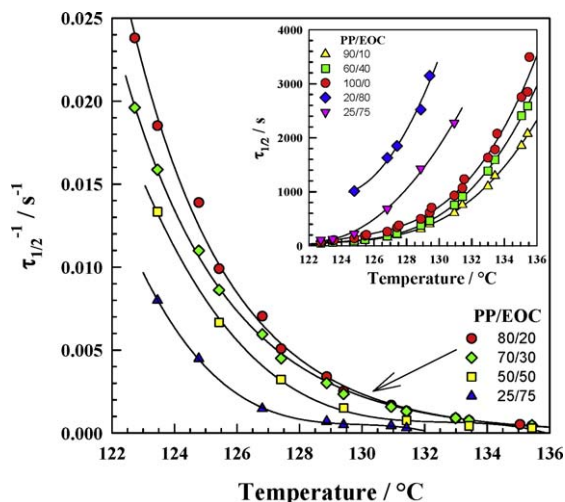
Fig. 4. Crystallization kinetic ($\tau_{1/2}^{-1}$) and half time ($\tau_{1/2}$) from DSC as a function of temperature for PP/EOC blends.

as PP/EOC (90/10 and 60/40), as shown in the small inserted picture of Fig. 4. There is a non-linear increase in $\tau_{1/2}$ as a function of temperature.

More direct way to see the crystallization kinetics is plotting of $\tau_{1/2}^{-1}$ as a function of temperature as shown in main Fig. 4. While there is only a moderate increase in kinetics with decreasing temperature in temperature range $135 \rightarrow 129\,°C$, this increase is much more pronounced in temperature range $129 \rightarrow 123\,°C$. From the composition point of view the kinetics decreases with increasing EOC content 20, 30, 50 and 75%.

To see the effect of EOC content and the morphology on the crystallization kinetics represented by $\tau_{1/2}^{-1}$ we have focused on lower temperatures (124–128 °C) in Fig. 5. For example there is about 80% increase in crystallization kinetics from pure PP to 20% of EOC, then the kinetics decreases with increasing EOC content. How the morphology affects the kinetics it is possible to see in the inserted TEM pictures. Absolutely slowest crystallization was found for 80% of EOC when PP exists in very small droplets (smaller than 1 µm). For 90% of EOC we were not able to detect PP crystallization by this isothermal DSC method. Muller et al. [30] presented similar shape curves for blends of copolymers of ethylene/butene and ethylene/hexene initially heated above UCST curve (upper critical solution temperature) and then crystallized below UCST where in 0–15 and 85–100% partial miscibility still existed. This could be similar to our case.

To analyze the crystallization behavior further we have carried out an Avrami and Hoffman–Lauritzen analyses as follows.

Avrami equation is describing relative crystallinity as a function of time (see Eq. (2)). One has to do the integration step (shown in Fig. 3) to get the relative crystallinity curve. Convenient way to evaluate the constants from Avrami equation is using the double logarithmic form of this equation (see Eq. (3)). The comparison of the pure PP and PP/EOC 70/30 blend at 132 °C is shown in Fig. 6. When we plotted the data from the whole experiments we got a curve rather than a single straight line. It is possible to divide the curve into two straight regions. To understand the problem deeper we have connected the Avrami curve with the original heat flow curve as shown on the inserted picture in Fig. 6. The Avrami curve's straight regions can be limited by points shown as AB and BD. At the heat flow curve also the maximum is an interesting point (called C in Fig. 6). The conclusion of this analysis is this. The majority of the crystallization process happened between points B and D while only very early stage of crystallization happened between points A and B. This is not obvious when one looks only at Avrami
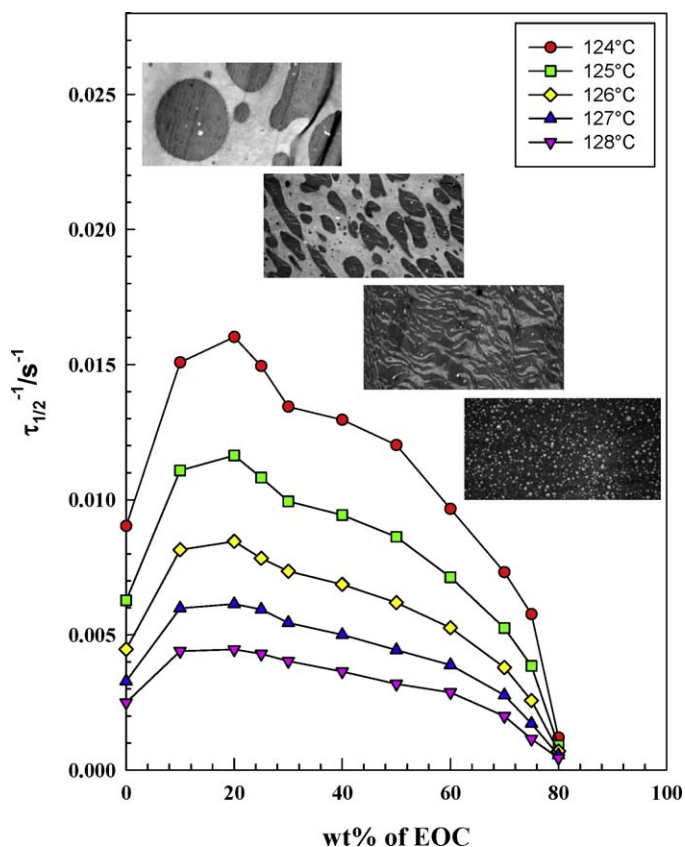
Fig. 5. Crystallization kinetics ($\tau_{1/2}^{-1}$) from DSC as a function of EOC content in PP/EOC blends. The structure of the four corresponding blends (20, 40, 60, and 80% of EOC) is shown by 4 inserted TEM pictures.

curve when the AB section seems to have the same length like BD section. It is clear that the Avrami curves for pure PP and PP/EOC 70/30 are different. Table 1 summarizes the Avrami exponents n and rate constants k for selected blend compositions and crystallization temperatures. At 124 °C the exponent n for pure PP was found to be 2.12 which is close to value 1.97 mentioned by Huang [25] and corresponds to two-dimensional spherulite growth. In
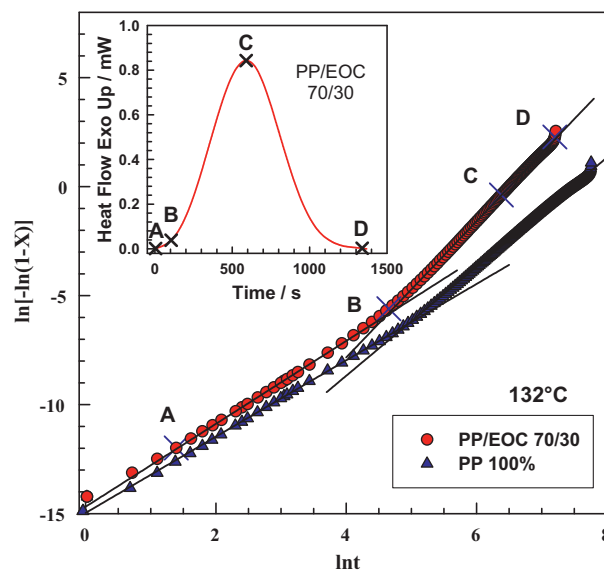

Fig. 6. Avrami plots for pure PP and PP/EOC (70/30) blend isothermally crystallized at 132 °C.

Table 1
Avrami parameters from linear regression.

Wt.% of EOC	124 °C		126 °C		128 °C		130 °C		132 °C		134 °C	
	n	k (min⁻¹)	n	k (min⁻¹)	n	k (min⁻¹)	n	k (min⁻¹)	n	k (min⁻¹)	n	k (min⁻¹)
0	2.12	0.11798	2.26	0.02842	2.34	0.00756	2.53	0.00113	2.52	0.000316	2.52	0.000094
10	2.98	0.76721	2.80	0.26405	2.77	0.04294	2.83	0.00292	2.76	0.001121	2.64	0.000211
30	2.77	0.66801	2.76	0.16869	2.75	0.02317	3.01	0.00206	2.85	0.000596	3.06	0.000147
40	2.67	0.53584	2.74	0.11433	2.87	0.01416	2.83	0.00194	2.78	0.000336	2.71	0.000117
60	2.70	0.26101	2.75	0.04678	2.69	0.00914	2.50	0.00103	2.43	0.000282	2.31	0.000090
75	2.31	0.02222	2.26	0.00309	2.19	0.00082	2.14	0.00047	–	–	–	–
80	2.35	0.00251	2.28	0.00073	2.21	0.00066	2.26	0.00013	–	–	–	–

contrast the blend containing 10% of EOC had the exponent $n = 2.99$ which is very close to 3, and can be attributed to heterogeneous nucleation of a three-dimensional growth in a spherical form. With increasing EOC content this n value gradually decreased up to 2.36 for 80% of EOC. The tendency for changes in n value is due to the transition between heterogeneous and homogeneous nucleation. This tendency was observed for all crystallization temperatures. The n values are not seriously affected by crystallization a temperature which is not a case for rate constant k which is extremely influence by crystallization temperatures. For given crystallization temperatures, the dependence of k on EOC content is very similar to $\tau_{1/2}^{-1}$ dependence shown in Fig. 5 and the dependence of k on crystallization temperature is very similar to the one shown in Fig. 4. In connection with TEM observations the mechanism of crystallization should be very much different for blends with 40% and 80% of EOC. In case of 40% of EOC once nucleus is formed the spherulite can grow through the continuous PP phase. However in case of 80% of EOC nucleus has to be formed in each small PP droplet which influenced not only the kinetics (k) but also the Avrami exponent n.

Next analysis was done according to Hoffman–Lauritzen equation (Eq. (4)). For this treatment we also needed to obtain equilibrium melting points T_m^0 according to Hoffman–Weeks [31] plot. The T_m^0 for pure PP was found to be 183 °C and for the PP/EOC blends in range 177–181 °C. PP/EOC blends have only slightly lower T_m^0 than PP. This observation goes well with Nishi and Wang [32] theory and the fact of only partial miscibility between the two polymers.

According to Eq. (10) the Hoffman–Lauritzen plots are shown in Fig. 7a and b. Some of the blends exhibit two slopes representing regime II and III of crystallization with transition being around 130 °C. Nucleation constant K_g values and pre-exponential factor G_0 values for selected blends are listed in Table 2. Initially the pure PP and PP/EOC (70/30) blend are compared in Fig. 7a. They show similar behavior with a small shift in absolute values affecting the ln G_0 values. These values correspond with different kinetics. The K_g values are very similar. The slope of the line changed quite significantly from about 5.9 to 3.8. In literature it is usually interpreted as different crystallization regime. At the lowest temperature (123–130 °C), so called regime III, there is a multiple nucleation on the surface of lamellae and the crystallization is the fastest. K_g value was found

to be about 5.9×10^5 for pure PP and also for the blend. Then at 130 °C there is transition from regime III to regime II where the rates of secondary nucleation and lateral spreading are comparable. The K_g was found to be about 3.8×10^5 again for pure PP and the blend. In literature we found values K_g 7.76×10^5 for regime III
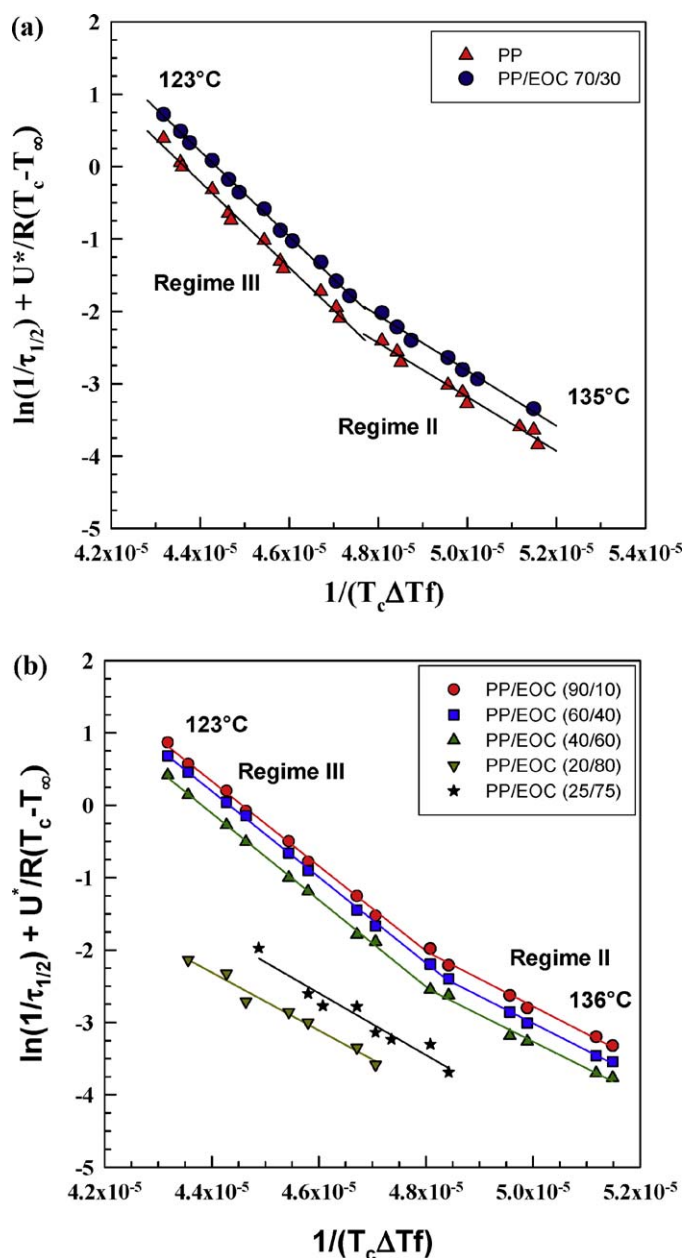

Table 2
Hoffman–Lauritzen parameters from linear regression.

Wt.% of EOC	Regime II		Regime III		Transition (°C)
	$K_g \times 10^{-5}$ (K²)	ln G_0	$K_g \times 10^{-5}$ (K²)	ln G_0	
0	3.731	15.47	5.916	25.82	130.0
10	3.798	16.21	5.863	26.13	130.5
30	3.811	16.24	5.897	26.16	131.0
40	3.747	15.72	5.929	26.28	131.5
60	3.698	15.22	5.988	26.24	132.5
75	–	–	4.275	17.71	–
80	–	–	4.005	15.31	–

Fig. 7. (a) and (b). Hoffman–Lauritzen plots for various PP/EOC blends from DSC.

and 4.46×10^5 for regime II [33], K_g 3.33×10^5 for regime III and 1.68×10^5 for regime II [34], K_g 4.805×10^5 for regime III [35], K_g 5.2×10^5 for regime III [36]. Our values lay in the range reported by other authors for iPP.

How the EOC content influences the Hoffman–Lauritzen plot is shown in Fig. 7b. The curves for 10, 40 and 60 wt.% of EOC show very similar trend and are only little bit shifted to lower values with increasing EOC content. The situation is completely different for 75 and 80% of EOC. Both the K_g and ln G_0 values are much lower (see Table 2). As shown by TEM pictures (Fig. 1) in case of high amount of EOC the PP is located in small islands and therefore the crystallization kinetics is dramatically reduced (which is reflected by pre-exponential factor G_0) and also nucleation parameter K_g is reduced from about 6 to 4×10^{-5} K^2.

In Hoffman–Lauritzen equation some researchers use a constant value for activation energy $U^* = 6300$ J mol^{-1} [34]. This is very convenient in first evaluation (or estimation) of HL parameters K_g and ln G_0 according to logarithmic Hoffman–Lauritzen Eq. (10) which is shown in Fig. 7a and b. Many researchers are calculating the activation energy U^* by nonlinear regression because it is the most important material constant and it is changing with blend/composites composition [37–42]. The nonlinear regression was done by *Mathematica 8* software using Eqs. (7) and (8).

The activation energy U^* calculated in this way is shown by Fig. 8. The activation energy for the blends was found higher than for the pure PP. The meaning of this observation is this. EOC acts as an obstacle (barrier) for crystallization of PP and therefore more
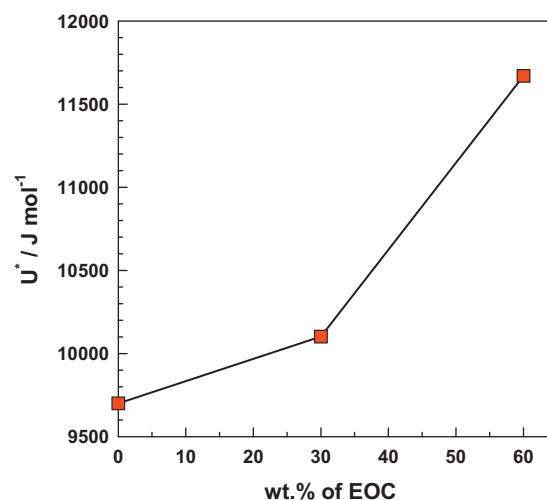
Fig. 8. Activation energy (U^*) as a function of EOC content according to nonlinear regression of Hoffman–Lauritzen equation.

energy is required for crystallization. Similar increase in activation energy was discovered by Huang [25] who has concluded that foreign particles act not only as nucleating agent but also as a hindrance to retard the crystallization.
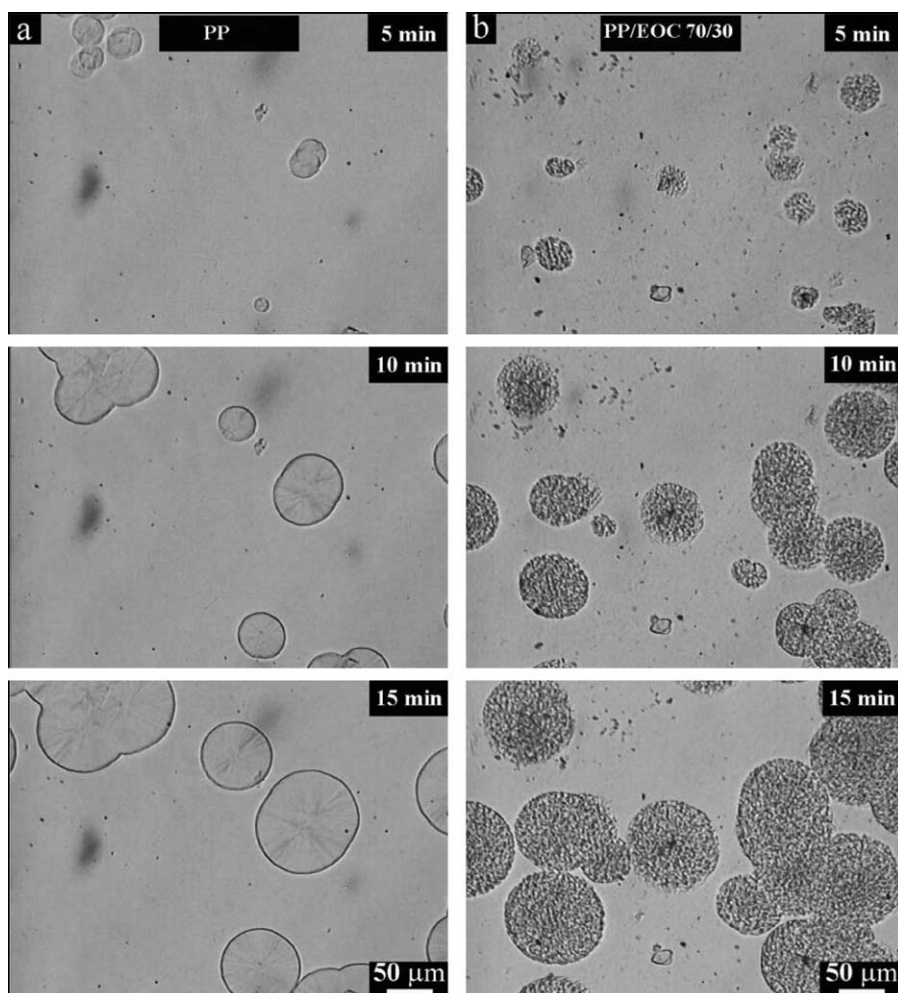
Fig. 9. Growth of spherulites in time at $T_c = 135$ °C in pure PP and PP/EOC (70/30) blend by hot-stage optical microscopy after 1 min pre-heating at 200 °C.
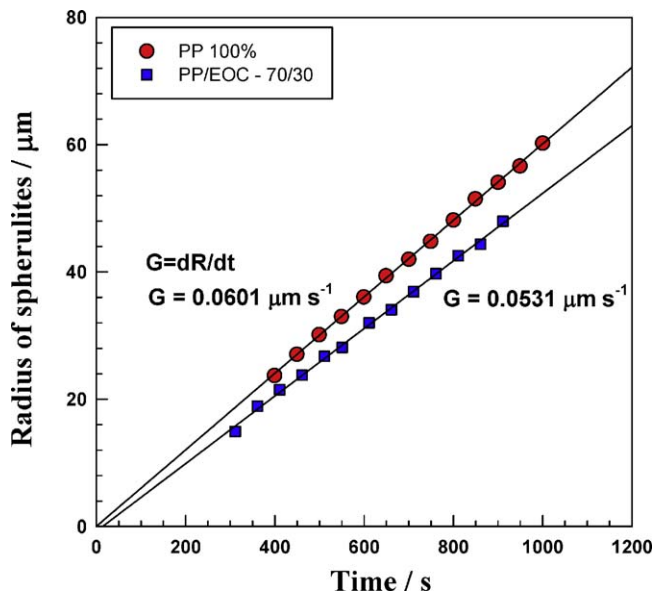
Fig. 10. Two examples of spherulite growth rate evaluation from the plot of radius of spherulite vs. time for pure PP and PP/EOC 70/30 blend at $T_c = 135\,°C$.

Fig. 11. Spherulite growth rate evaluation for PP/EOC (70/30) blend from optical microscopy.

Both of these models, Avrami and Hoffman–Lauritzen, attempt to describe the crystallization behavior. While Avrami is focused on the time dependence of crystallinity at given temperature, Hoffman–Lauritzen is capturing crystallization rate as a function of temperature. We have observed relation of Avrami exponent n with HL K_g values and also Avrami k rate constant and HL ln G_0 values (decrease in 40–80 wt.% of EOC range).

To understand this phenomenon better we have carried out another independent experiment, optical microscopy. We have recorded the structure development in the computer equipped with a TV video card for later precise analysis.

Examples of pictures taken from the video at certain time intervals are shown in Fig. 9. The spherulites are growing in time in both cases, in pure PP and in PP/EOC (70/30) blend. While the PP spherulites are clear, the spherulites growing in blend are quite coarse. The EOC does not prevent spherulite growth at this concentration. There are more spherulites in case of the blend. And the volume fills with them faster in case of the blend. Most likely EOC acts as nucleating agent for PP. This is quite surprising fact bearing in mind that at the measurement temperature (135 °C) the EOC is a liquid (T_m of EOC is 48 °C). Nevertheless it is a foreign subject in PP and causes faster bulk crystallization.

We have also analyzed the growth rate of individual spherulites to see if EOC affects the crystallization kinetics of individual spherulite (see Fig. 10). In contrast with DSC observations we have found the crystallization kinetics of the blend to be slower than that of pure PP. This behavior is quite understandable. Growing PP lamella hits an obstacle in the form of EOC and has to go around this obstacle. Then the overall growth rate of spherulite is slower.

In conclusion the EOC is slowing down the growth of individual spherulites but also acts as nucleation agent causing faster bulk crystallization. This result is in good agreement with above mentioned increase in activation energy.

The PP/EOC 70/30 blend was investigated in the temperature range 130–140 °C by optical microscopy. Fig. 11 shows that the growth was linear for all temperatures. Again we have used the Hoffman–Lauritzen theory to plot the data according to Eq. (5) as shown in Fig. 12. The K_g value in the temperature range 130–136 °C is very similar to that one received by DSC (3.7×10^5) and corresponds to regime II crystallization. Then at the highest temperatures (136–140 °C) the crystallization is very slow, the K_g
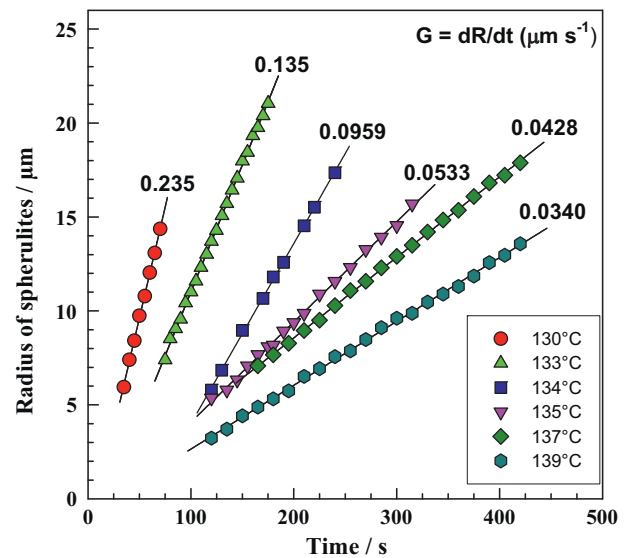
value is 1.7×10^5 and the crystallization proceeds in regime I when the secondary nucleation is the slowest.

As mentioned earlier partial miscibility between PP and EOC does exist. During mixing at high shear PP gets into EOC regions and EOC penetrates into PP. Thus we have to use "PP-rich" and "EOC-rich" terms. When mixing stops and blend is quickly quenched the structure with fine morphology and partial miscibility is preserved. However when the sample is heated again for the crystallization experiment, this time there is no shear, the blend is in quiescent state. The blend is thermodynamically unstable and the polymers tend to phase separate. The example of such phase separation at 200 °C is shown in Fig. 13 [29]. Clearly a phase coarsening is happening at 200 °C. Because of the shift in thermodynamics conditions (high shear → zero shear), also the miscibility is probably affected. This has been shown in past by shifting of LCST (UCST) due to the presence of high shear. The term "flow-induced mixing and demixing" was established [43]. On this basis we can assume that in quiescent state at high temperature where both PP and EOC are
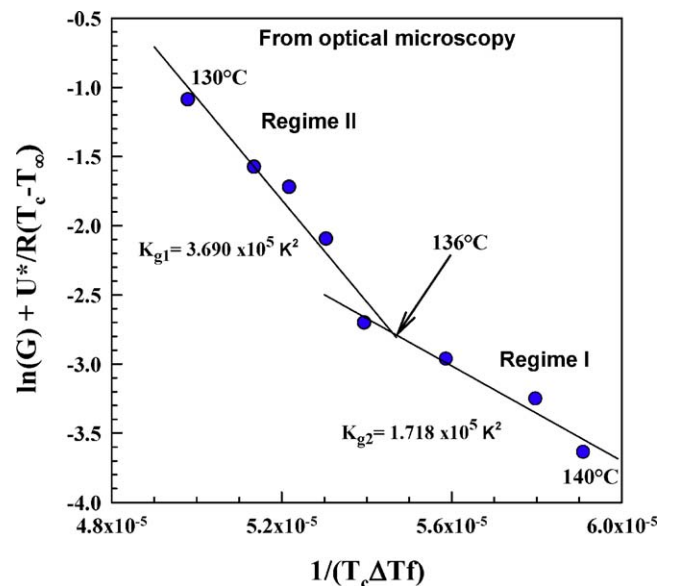

Fig. 12. Hoffman–Lauritzen plots for PP/EOC (70/30) blend from optical microscopy.
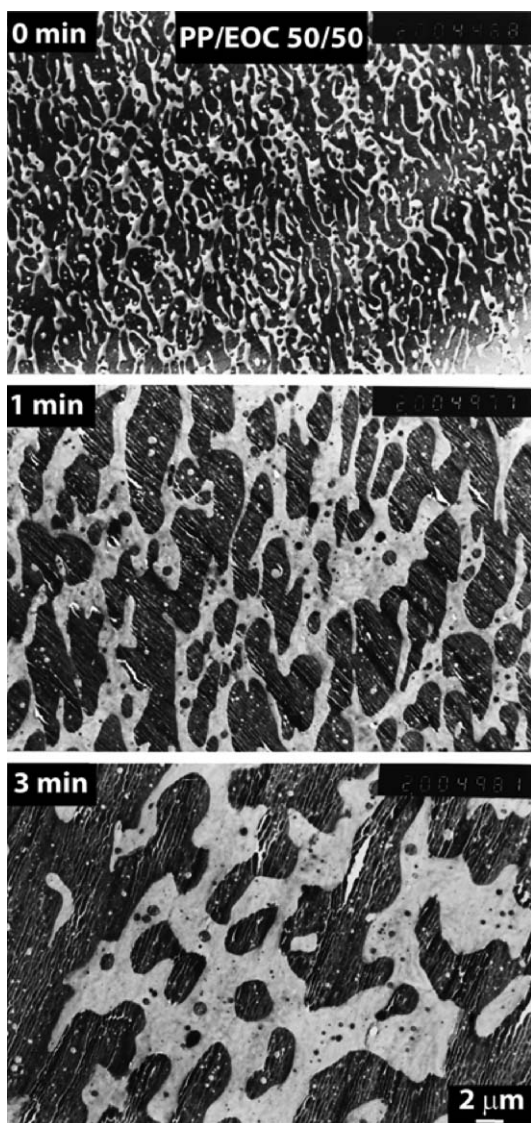
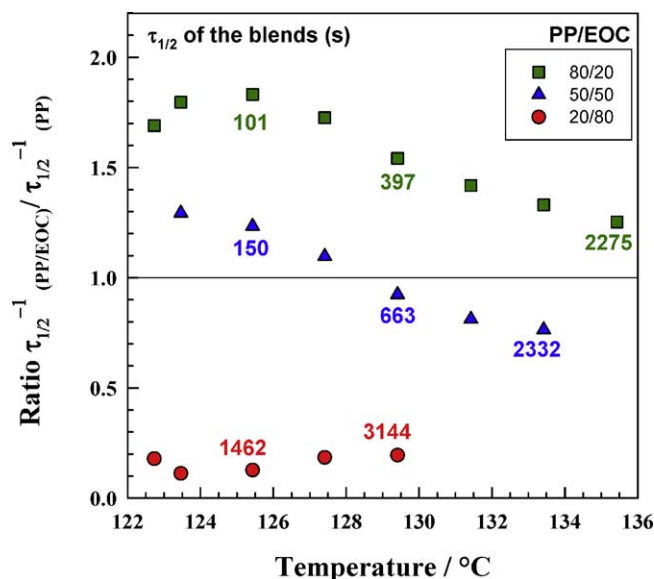**Fig. 13.** Coarsening of PP/EOC (50/50) blend at 200 °C by TEM.

Fig. 14. Ratio of crystallization kinetics ($\tau_{1/2}^{-1}$) of PP/EOC blends over neat PP for various temperatures.

liquids, there is a strong thermodynamic driving force that causes movement of EOC molecules out of PP-rich phase and PP molecules out of EOC-rich phase.

Formally we have mentioned that EOC most likely acts in PP as nucleating agent causing faster bulk crystallization. This was observed in highest extent (e.g. for PP/EOC 80/20 blend) at low crystallization temperatures (122–126 °C) when the crystallization takes just few minutes. It is clearly visible in Fig. 14 where we compare the kinetics of a blend to that of pure PP. The ratio for PP/EOC 80/20 blend at 126 °C has 1.8 value, meaning 80% increases in crystallization kinetics. However at high crystallization temperatures (132–136 °C) when the crystallization takes more than 1 h the ratio has decreased to about 1.2. The difference between the blend and pure PP is not that high. Most likely the EOC had enough time to move from PP-rich phase back to EOC-rich phase causing decreased number of nucleation centres in PP-rich phase. Then the bulk crystallization kinetics of the blend is just slightly higher (20%) than that of pure PP. The 50/50 blend has very interesting behavior. In 124–128 °C temperature range the crystallization of the blend is faster than that of pure PP. Then in the temperature range 128–134 °C the crystallization of pure PP is faster than that of the 50/50 blend. Finally for PP/EOC (20/80) blend the

crystallization kinetics is always much slower than that of pure PP (the ratio is about 0.19).

5. Conclusions

The crystallization kinetics is greatly affected by the blend composition. As it was found by DSC, small amounts of EOC (10–30%) increased the bulk crystallization kinetics. On the other hand, larger amounts of EOC (50–80%) caused the decrease in kinetics. Optical microscopy revealed a decrease in a single spherulite growth rate caused by EOC obstacles, and at the same time larger number of spherulites. EOC in small amount acts as a nucleation agent for PP and increases the bulk crystallization rate.

Crystallization kinetics was tremendously decreased when the EOC content was very high (such as 70–80%). As it was shown by TEM, in this case PP formed small islands in EOC matrix and crystallization in these isolated domains had to wait till nucleation happened in each of them. This is very slow process. We were not able to measure the isothermal kinetics for blends with only 10% of PP.

The analysis according to Avrami's equation revealed that rate constant k and also the Avrami exponent n follow the same trend like $\tau_{1/2}^{-1}$, initially increase and then decrease with increasing EOC content. The Hoffman–Lauritzen equation was at first analyzed in linear form which produced parameters K_g and $\ln G_0$ that decreased significantly when the EOC content was 75–80%. Initial parameters K_g and $\ln G_0$ were then used in nonlinear regression that revealed increase in activation energy U^* caused by addition of EOC into PP. EOC acts as nucleating agent which increases the bulk crystallization rate, but also acts as hindrance to crystallization which decreases the growth rate of individual PP spherulite. This conclusion was confirmed by direct observation of spherulites growth on the hot stage in the polarized optical microscope. The analysis according to Hoffman–Lauritzen theory revealed also interesting transitions in crystallization regimes at 130 and 136 °C.

Comparison of crystallization of the blend to pure PP revealed an existence of competition of crystallization with phase separation. At lower temperatures the crystallization proceeds fast and is not affected by phase separation that much. At high temperatures when the crystallization kinetics is very slow the phase separation

has enough time to proceed before crystallization which results in crystallization kinetics of the blend being close to that one of pure PP (for PP/EOC 80/20).

Acknowledgements

References

[1] T. Xu, J. Yu, Z. Jin, Effects of crystalline morphology on the impact behavior of polypropylene, Mater. Des. 22 (2001) 27.

[2] M. Avella, R. Dellerba, E. Martuscelli, G. Ragosta, Influence of molecular mass, thermal treatment and nucleating agent on structure and fracture toughness of isotactic polypropylene, Polymer 34 (1993) 2951.

[3] X. Zhang, F. Xie, Z. Pen, Y. Zhang, Y. Zhang, W. Zhou, Effect of nucleating agent on the structure and properties of polypropylene/poly(ethylene–octene) blends, Eur. Polym. J. 38 (2002) 1.

[4] S. Hom, A.R. Bhattacharyya, R.A. Khare, A.R. Kulkarni, M. Saroop, A. Biswas, Blends of polypropylene and ethylene octene comonomer with conducting fillers: influence of state of dispersion of conducting fillers on electrical conductivity, Polym. Eng. Sci. 49 (2009) 1502.

[5] R. Adhikari, R. Godehardt, W. Lebek, G.H. Michler, Blends of high density polyethylene and ethylene/1-octene copolymers: structure and properties, J. Appl. Polym. Sci. 103 (2007) 1887.

[6] R.R. Babu, N.K. Singha, K. Naskar, Dynamically vulcanized blends of polypropylene and ethylene–octene copolymer: comparison of different peroxides on mechanical, thermal, and morphological characteristics, J. Appl. Polym. Sci. 113 (2009) 1836.

[7] S. Mohanty, S.K. Nayak, Dynamic-mechanical and thermal characterization of polypropylene/ethylene–octene copolymer blend, J. Appl. Polym. Sci. 104 (2007) 3137.

[8] J.W. Lim, A. Hassan, A.R. Rahmat, M.U. Wahit, Morphology, thermal and mechanical behavior of polypropylene nanocomposites toughened with poly(ethylene-co-octene), Polym. Int. 55 (2006) 204.

[9] A.L.N.D. Silva, M.C.G. Rocha, F.M.B. Coutinhoa, R. Bretas, C. Scuracchiod, Rheological and morphological properties of blends based on ethylene–octene copolymer and polypropylene, Polym. Test. 19 (2000) 363.

[10] M. Onoa, J. Washiyamaa, K. Nakajimab, T. Nishi, Anisotropic thermal expansion in polypropylene/poly(ethylene-co-octene) binary blends: influence of arrays of elastomer domains, Polymer 46 (2005) 4899.

[11] L. Godail, D.E. Packham, Adhesion of ethylene–octene copolymers to polypropylene: interfacial structure and mechanical properties, J. Adhes. Sci. Technol. 15 (2001) 1285.

[12] P. Dias, Y.J. Lin, B. Poon, H.Y. Chen, A. Hiltner, E. Baer, Adhesion of statistical and blocky ethylene–octene copolymers to polypropylene, Polymer 49 (2008) 2937.

[13] J.-R. Ying, S.-P. Liu, F. Guo, X.-P. Zhou, X.-L. Xie, Non-isothermal crystallization and crystalline structure of PP/POE blends, J. Therm. Anal. Calorim. 91 (2008) 723.

[14] G. Bogoeva-Gaceva, A. Janevski, A. Grozdanov, Crystallization and melting behavior of iPP studied by DSC, J. Appl. Polym. Sci. 67 (1998) 395.

[15] D. Rana, K. Cho, T. Woo, B.H. Lee, S. Choe, Blends of ethylene 1-octene copolymer synthesized by ziegler–natta and metallocene catalysts. I. Thermal and mechanical properties, J. Appl. Polym. Sci. 74 (1999) 1169.

[16] J.-W. Huang, Y.-L. Wen, C.-C. Kang, M.-Y. Yeh, S.-B. Wen, Crystallization of poly(butylene terephthalate)/poly(ethylene octene) blends: isothermal crystallization, J. Appl. Polym. Sci. 109 (2008) 3070.

[17] H. Lu, Y. Hu, M. Li, L. Song, Clay intercalation and influence on flammability and crystallization behaviors of POE-based nanocomposites, Polym. Compos. 29 (2008) 1358.

[18] M. Avrami, J.B. Little, Diffusion of heat through a rectangular bar and the cooling and insulating effect of fins. I. The steady state, J. Appl. Phys. 13 (1942) 255.

[19] M. Avrami, Kinetics of phase change. I. General theory, J. Chem. Phys. 7 (1939) 1103.

[20] J.I.J. Lauritzen, J.D. Hoffman, Extension of theory of growth of chain-folded polymer crystals to large undercoolings, J. Appl. Phys. 44 (1973) 4340.

[21] J.D. Hoffman, L.J. Frolen, G.S. Ross, J.I.J. Lauritzen, On the growth rate of spherulites and axialites from the melt in polyethylene fractions: regime I and regime II crystallization, J. Res. Natl. Bur. Stand. Sect. A: Phys. Chem. 79 A (1975) 671.

[22] J. Brandrup, E.H. Immergut, E.A. Grulke, A. Abe, D.R. Bloch, Polymer Handbook, 4th ed., John Wiley & Sons, 2005.

[23] P.D. Hong, W.T. Chung, C.F. Hsu, Crystallization kinetics and morphology of poly(trimethylene terephthalate), Polymer 43 (2002) 3335.

[24] J.D. Hoffman, G.T. Davis, J.I.J. Lauritzen, in: N.B. Hannay (Ed.), Treatise on Solid State Chemistry, Plenum press, New York, 1976, p. p497.

[25] J.-W. Huang, Dispersion crystallization kinetics, and parameters of Hoffman–Lauritzen theory of polypropylene and nanoscale calcium carbonate composite, Polym. Eng. Sci. 49 (2009) 1855.

[26] G.Z. Papageorgiou, D.S. Achilias, D.N. Bikiaris, G.P. Karayannidis, Crystallization kinetics and nucleation activity of filler in polypropylene/surface-treated SiO_2 nanocomposites, Thermochim. Acta 427 (2005) 117.

[27] J.D. Hoffman, R.L. Miller, Kinetics of crystallization from the melt and chain folding in polyethylene fractions revisited: theory and experiment, Polymer 38 (1997) 3151.

[28] M. Okamato, T. Inoue, Crystallization kinetics in poly(butylene terephthalate)/copolycarbonate blend, Polymer 36 (1995) 2739.

[29] P. Svoboda, D. Svobodova, P. Slobodian, T. Ougizawa, T. Inoue, Transmission electron microscopy study of phase morphology in polypropylene/ethylene–octene copolymer blends, Eur. Polym. J. 45 (2009) 1485.

[30] A.J. Muller, M.L. Arnal, A.L. Spinelli, E. Canizales, C.C. Puig, H. Wang, Morphology and crystallization kinetics of melt miscible polyolefin blends, Macromol. Chem. Phys. 204 (2003) 1497.

[31] J.D. Hoffman, J.J. Weeks, Rate of spherulitic crystallization with chain folds in polychlorotrifluoroethylene, J. Chem. Phys. 37 (1962) 1723.

[32] T. Nishi, T.T. Wang, Melting point depression and kinetic effects of cooling on crystallization in poly(vinylidene fluoride)-poly(methyl methacrylate) mixtures, Macromolecules 8 (1975) 909.

[33] Q.L. Ni, J.Q. Fan, J.Y. Dong, Crystallization behavior and crystallization kinetic studies of isotactic polypropylene modified by long-chain branching polypropylene, J. Appl. Polym. Sci. 114 (2009) 2180.

[34] Y.G. Shangguan, Y.H. Song, Q. Zheng, Kinetic analysis on spherulite growth rate of polypropylene catalloys, Polymer 48 (2007) 4567.

[35] V. Goodarzi, S.H. Jafari, H.A. Khonakdar, S.A. Monemian, R. Hassler, D. Jehnichen, Nonisothermal crystallization kinetics and determination of surface-folding free energy of PP/EVA/OMMT nanocomposites, J. Polym. Sci. Part B-Polym. Phys. 47 (2009) 674.

[36] Y. Feng, X. Jin, J.N. Hay, Effect of nucleating agent addition on crystallization of isotactic polypropylene, J. Appl. Polym. Sci. 69 (1998) 2089.

[37] S. Nandi, A.K. Ghosh, Crystallization kinetics of impact modified polypropylene, J. Polym. Res. 14 (2007) 387.

[38] W. Leelapornpisit, M.T. Ton-That, F. Perrin-Sarazin, K.C. Cole, J. Denault, B. Simard, Effect of carbon nanotubes on the crystallization and properties of polypropylene, J. Polym. Sci. Part B-Polym. Phys. 43 (2005) 2445.

[39] S. Vyazovkin, N. Sbirrazzuoli, Isoconversional kinetic analysis of thermally stimulated processes in polymers, Macromol. Rapid Commun. 27 (2006) 1515.

[40] S.Y. Liu, Y.N. Yu, Y. Cui, H.F. Zhang, Z.S. Mo, Isothermal and nonisothermal crystallization kinetics of nylon-11, J. Appl. Polym. Sci. 70 (1998) 2371.

[41] F. Marguerat, P.J. Carreau, A. Michel, Morphology and rheological properties of polypropylene/reactive elastomer blends, Polym. Eng. Sci. 42 (2002) 1941.

[42] Y. Seo, J. Kim, K.U. Kim, Y.C. Kim, Study of the crystallization behaviors of polypropylene and maleic anhydride grafted polypropylene, Polymer 41 (2000) 2639.

[43] I.A. Hindawi, J.S. Higgins, R.A. Weiss, Flow-induced mixing and demixing in polymer blends, Polymer 33 (1992) 2522.

PAPER II

Effect of Initial Melting Temperature on Crystallization of Polypropylene/Organoclay Nanocomposites

Petr Svoboda*,[1], Krunal Trivedi[1], Dagmar Svobodova[2], Pavel Mokrejs[1], and Karel Kolomaznik[3]

[1]*Centre of Polymer Systems, Faculty of Technology, Tomas Bata University in Zlin, Nam. T.G. Masaryka 5555, 760 01 Zlin, Czech Republic*
[2]*Faculty of Humanities, Tomas Bata University in Zlin, Mostni 5139, 760 01 Zlin, Czech Republic*
[3]*Faculty of Applied Informatics, Tomas Bata University in Zlin, Nad Stranemi 4511, 760 05 Zlin, Czech Republic*

Abstract: Polypropylene (PP) nanocomposites were prepared by melt intercalation in an intermeshing co-rotating twin-screw extruder. The influence of organoclay (Cloisite 20A) and maleic anhydride modified polypropylene (PP-MA) on various properties was explored. The effect of the initial melting temperature on crystallization kinetics was investigated by differential scanning calorimetry (DSC) and optical microscopy. DSC has revealed a gradual decrease in crystallization kinetics with an increase in initial melting temperature for two-component systems (PP/PP-MA and PP/20A). However, in the case of a three-component system (PP/PP-MA/20A), the decrease of crystallization kinetics in the range of initial melting temperature being 200-240 °C was followed by an increase in the temperature range 240-260 °C. After initial melting at 250 °C, many spherulites were discovered in the three-component system. This unusual crystallization behavior was explained with the help of Fourier transform infrared spectroscopy (FTIR), where an increase in the Si-O peak with the increasing initial melting temperature was detected, which indicates the presence of large surface of clay layers. The morphology of nanocomposites was also investigated by transmission electron microscopy (TEM). The X-ray diffraction (XRD) analysis has revealed a decrease in the peak intensity with an increase in initial melting temperature, which suggests exfoliation caused by fast diffusion at high temperatures.

Keywords: polypropylene, nanocomposite, organoclay, intercalation, crystallization kinetics.

Introduction

Since the past decade remarkable attention has been given to polymer/clay nanocomposites. This has been due to their potential to display synergistically enhanced properties.[1-5] There is an enormous interest amongst researchers to develop high-performance nanocomposites with low-cost inorganic fillers. Inorganic particle-filled nanocomposites of semi-crystalline polymers have been used extensively to improve mechanical properties, notably modulus and tensile strength. The essential properties of semi-crystalline polymers strongly depend on their crystalline morphology. The difficulty in understanding the deformation behavior of semi-crystalline polymers arises from their two-phase structure, i.e. crystalline and amorphous phase.[6-9]

As polypropylene (PP) is a semi-crystalline polymer, it is important to study the crystallization behavior of its nanoclay composites. It is well known that the mechanical properties of PP depend significantly on its crystalline morphology. Therefore, the properties of the PP/clay nanocomposite will

similarly be dependent on the crystalline morphology.[10-12] PP does not include any polar group in its backbone, and silicate layers even modified by non-polar alkyl groups are incompatible with PP. Thus compatibilizer, maleic anhydride modified PP (PP-MA), is often added to facilitate intercalation/exfoliation of the organoclay and maximize its interfacial contact with the polymer matrix.[13] There has been major interest to study thoroughly the crystallization behavior of PP based nanocomposites filled with various fillers and minerals. Understanding of this behavior can lead to shorter production cycle time and also the spherulite size, which directly influences mechanical properties, can be controlled. For example, Xu *et al*. showed for pure PP that smaller size of the spherulites may be responsible for the increase in impact strength.[14] Also, in connection with crystallization, several researchers attempted to enhance the tensile and impact properties of composites.[15-19]

Wang *et al*. discovered that PP-MA of low molecular weight and high MA content led to better interaction with the clay. However, the addition of lower molecular weight PP-MA or high loading of PP-MA had a negative effect on mechanical and thermal properties of the PP/PP-MA/clay

---

*Corresponding Author. E-mail: svoboda@ft.utb.cz

P. Svoboda *et al.*

composites. Therefore, we have focused only on PP-MA with high molecular weight (330000 gmol⁻¹) and low MA content (0.5%).[20]

We found no report of a study on the influence of the initial melting temperature on crystallization behavior of PP nanocomposites. In our present study, crystallization was initially investigated by differential scanning calorimetry (DSC), and then also by optical microscopy. An unusual crystallization behavior (after melting to 240-260 ºC) was then further explored by Fourier transform infrared spectroscopy (FTIR) and by X-ray diffraction (XRD). The dispersion of nano-layers was observed by transmission electron microscopy (TEM). Finally, the influence of the clay on tensile properties and impact strength was evaluated.

Experimental

The PP with trade name P4G4Z-011 (melt flow index 12 g/10 min, ASTM D1238) was obtained from Huntsman. The maleic anhydride modified polypropylene (PP-MA) was obtained from Uniroyal Chemical. Its trade name was PB3150, molecular weight was 330000 g mol⁻¹ and the MA content was 0.5 wt.%.

The nanoclay, Cloisite® 20A (Southern Clay), is a natural montmorillonite modified with a quaternary ammonium salt.

$$CH_3 - \overset{\overset{\displaystyle CH_3}{|}}{\underset{\underset{\displaystyle HT}{|}}{N^+}} - HT$$
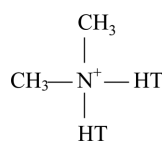
where, HT is a hydrogenated tallow approximately: ~65% -(CH₂)₁₇CH₃; ~30% -(CH₂)₁₅CH₃; ~5% -(CH₂)₁₃CH₃ and the anion is chloride.

Twin screw extruder, Leistritz ZSE 27 with L/D=40 and D=27 mm was used in the co-rotating mode for the melt intercalation of nanocomposites. The barrel temperatures were set at 165-185 ºC and the screw speed was fixed at 300 rpm. In order to achieve desired mixing, the feeding rate was kept low at 2 kg/h.

A Sumitomo 200 ton injection-molding machine was used for the preparation of tensile bars and impact specimens. Mechanical tests were performed according to tensile (ASTM D638) and Izod (ASTM D256) standards, respectively. The tensile properties were measured with the help of Instron tensile tester. There were five experiments used to calculate the average values. For the measurement of notched impact strength, an Izod impact tester from Testing Machines, Inc. was used. Ten experiments were used to obtain average impact strength.

An X-ray diffractometer, X'Pert PRO from PANalytical, was used to analyze the nano-structure of composites with the scanning angle range of 0.5-20º (2θ). Some samples were injection molded and tested at room temperature. Other samples were first melted on Heidolph (MR Hei-End)

hot plate for 1 min at constant temperatures (175, 225, 250 and 275 ºC) and then pressed between two cover glasses for another 1 min. They were then transferred to LINKAM hot stage set to 125 ºC for 2-3 min in order to crystallize always in the same way.

For the TEM analysis, the specimens were microtomed to ultrathin sections with 70 nm thickness using an ultracryomicrotome with a diamond knife. Then the sections were stained with RuO_4. The structure was observed under a transmission electron microscope Phillips CM 12.

Crystallization kinetics of the samples was analyzed by Perkin-Elmer DSC-1. Temperature calibration was performed using the indium standard. Nitrogen atmosphere was employed during the experiment at flow rate 20 mL min⁻¹. For the isothermal crystallization of the samples, the samples were heated up to various initial melting temperatures (at 100 ºC min⁻¹ of heating rate) and then cooled (at 50 ºC min⁻¹) to the isothermal crystallization temperature (130 ºC). In all cases, samples were held at the initial melting temperature for 1 min to eliminate any previous thermal history.

For the observation of growth of the spherulites, an Olympus BH2 polarized optical microscope equipped with a CCD camera connected to a computer and a LINKAM hot stage was used.

For the FTIR study, the Nicolet 320 Avatar FT-IR spectrometer was used in ATR mode.

Results and Discussion

The crystallization was studied at first by DSC and then also by optical microscopy. Initially the samples with weight about 10-15 mg were heated from room temperature to various initial melting temperatures (200-260 ºC) at rate 100 ºC/min, then the temperature was kept constant for 1 min to fully melt the PP crystals (T_m of PP is about 165 ºC). The next step was a fast cooling to the desired isothermal crystallization temperature (130 ºC). This cooling at rate 50 ºC/min was attained by a cooling unit capable of cooling to -30 ºC. The last step was the isothermal crystallization at the desired temperature.

The time when the heat flow curve reaches the minimum value and it starts to grow to form an exothermal peak, was assigned to be 0. By the integration of the heat flow curve one can get a relative crystallinity curve. When the crystallinity reaches 0.5 (or 50%), half time of crystallization $\tau_{1/2}$ is calculated. Then the crystallization kinetics can be expressed as $\tau_{1/2}^{-1}$.

Concerning optical microscopy one can observe several spherulites growing in time at constant crystallization temperature. Crystallization kinetics can be expressed as G=dR/dt, the slope of the line in plot "radius versus time".

Figure 1 shows that for the samples PP/PP-MA (95/5) and PP/20A (95/5) the crystallization kinetics decreases gradually with an increasing initial melting temperature. The rea-

Effect of Initial Melting Temperature on Crystallization of Polypropylene/Organoclay Nanocomposites
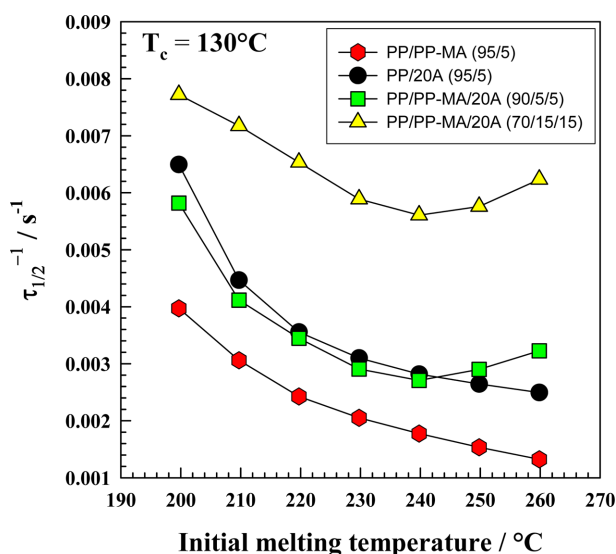

Figure 1. Crystallization kinetic ($\tau_{1/2}^{-1}$) at 130 °C from DSC as a function of initial melting temperature.
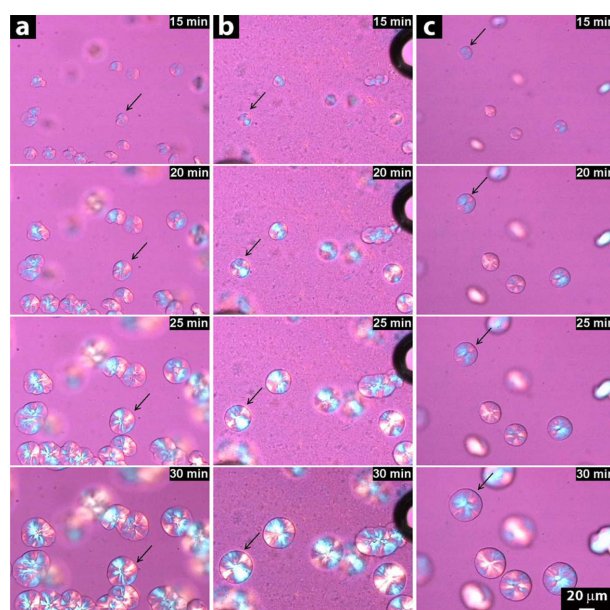

Figure 2. Growth of the spherulites by optical microscopy at 140 °C after initial melting at 225 °C for (a) PP/PP-MA (95/5), (b) PP/20A (95/5) and (c) PP/PP-MA/20A (90/5/5).

son might be in fast diffusion and free movement of molecules at high melting temperatures, i.e. they adopt many different positions compared to their arrangements in the crystal lamella. Consequently, they then require longer time to move back to orderly arrangement in crystal lamella from more disordered state. The three component systems PP/PP-MA/20A (90/5/5) and (70/15/15) exhibited some deviation from the former two-component systems, especially at higher melting temperatures (240-260 °C). Instead of a gradual decrease; there was actually an increase in crystallization kinetics at 250 and 260 °C. This interesting crystallization behavior motivated further optical microscopy observation. The crystallization kinetics was then measured also by optical microscopy, as described in the following section.

From Figure 2 it is clear that the number of spherulites is very similar for all three systems indicating very similar nucleation rate at 225 °C. Also the growth rate of individual spherulites is similar as shown in Figure 4(a). However, the situation is very much different at 250 °C as shown by Figure 3. On the other hand for the two-component systems PP/PP-MA (95/5), and PP/20A (95/5), the number of spherulites and the growth rate are very similar. However, for the three-component system PP/PP-MA-20A (90/5/5) we have discovered a large number of spherulites. The growth rate of individual spherulites is quite similar to the two-component systems as shown also in Figure 4(b). This indicates much higher nucleation rate at 250 °C for the three component system. One possible explanation could be as follows. Initially, the PP-MA was located between the clay layers and also on the surface of the clay layers. However, at high temperature (250 °C) the PP-MA might have segregated into PP-MA micelles, and then the naked clay particles acted as nucleation centers. We had to investigate this hypothesis
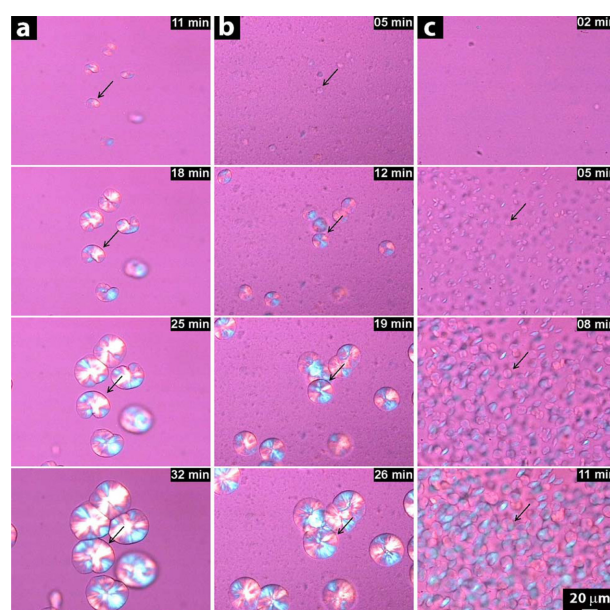
Figure 3. Growth of the spherulites by optical microscopy at 140 °C after initial melting at 250 °C for (a) PP/PP-MA (95/5), (b) PP/20A (95/5) and (c) PP/PP-MA/20A (90/5/5).

also with other methods (FTIR, XRD) and it will be shown in the following sections.

The Figure 5 shows that the spherulite growth rate is gradually decreasing with the crystallization temperature. We have found no significant differences in the crystallization kinetics of individual spherulites for various nanocomposites. We might conclude that is that the differences in the

P. Svoboda *et al.*
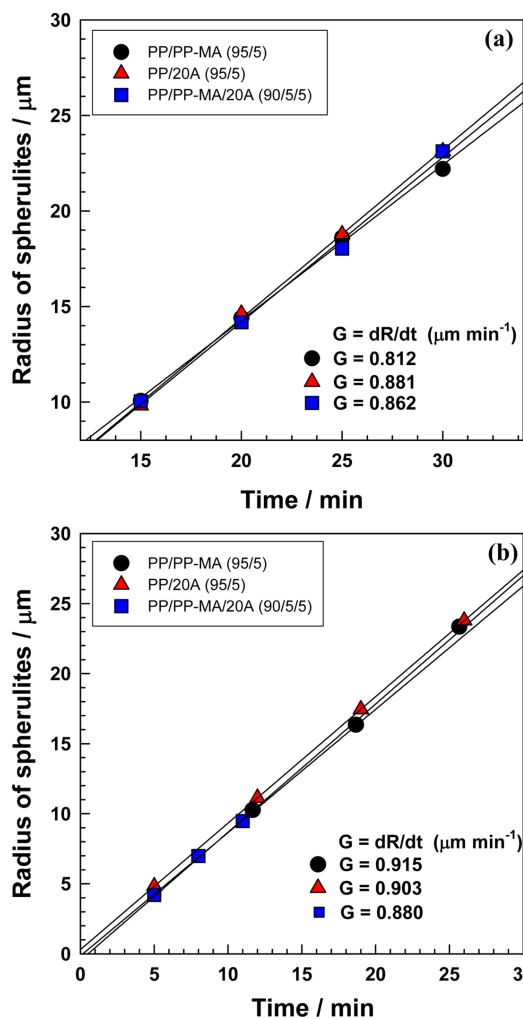
Figure 4. Evaluation of crystallization kinetics at 140 °C based on Figures 2 and 3 after initial melting at (a) 225 °C, (b) 250 °C.
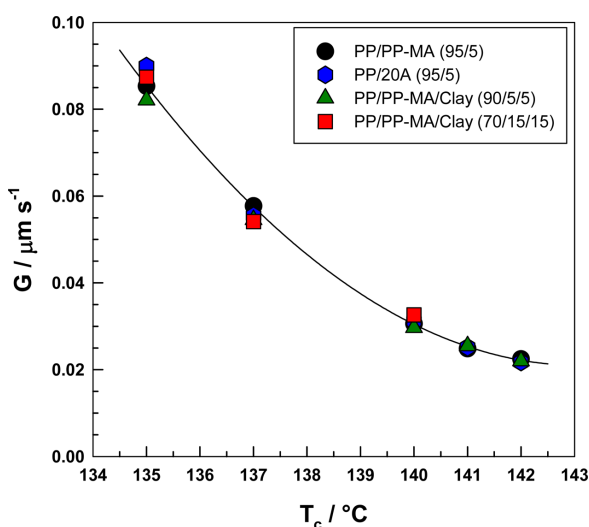

Figure 5. Crystallization kinetics as a function of crystallization temperature (T_c) from optical microscopy after initial melting at 200 °C.
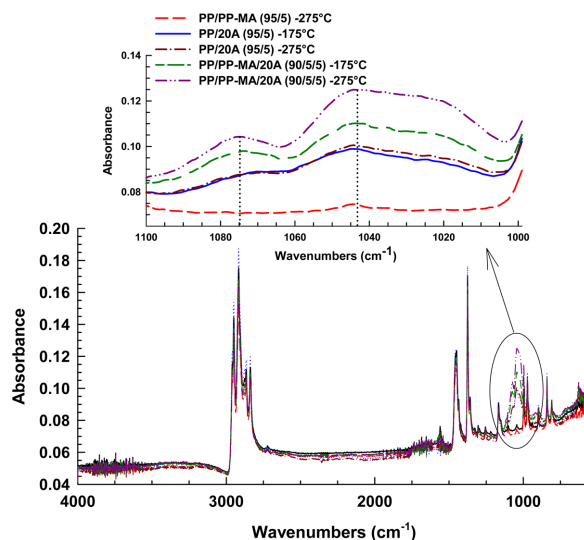

Figure 6. FTIR spectrum of various samples exposed to melting at 175 or 275 °C.

crystallization kinetics observed by DSC are mainly caused by different nucleation rate (see Figure 5).

Figure 6 illustrates the FTIR data of various samples after different thermal history with the focus on 1000-1150 cm^{-1} area where the Si-O peak is located. The baseline sample PP/PP-MA (95/5) without clay shows almost no peak in this area. Then the PP/20A (95/5) sample exhibits a moderate peak which is not influenced by the initial melting temperature. The three-component system PP/PP-MA/20A has the largest Si-O peak, plus there is a noticeable difference between the initial melting temperatures 175 and 275 °C. The PP/PP-MA/20A sample exposed to 275 °C has the largest Si-O
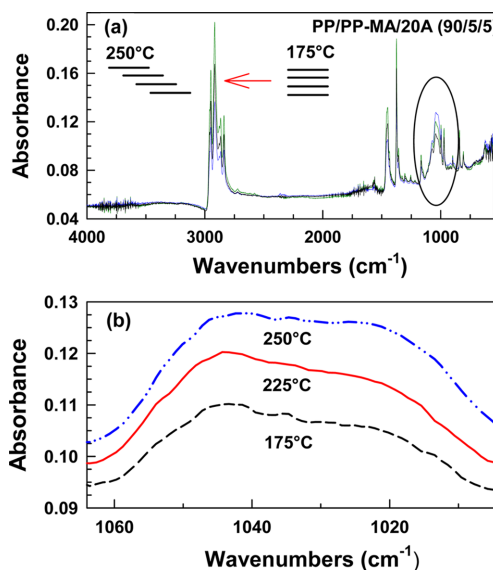
Figure 7. FTIR spectrum of PP/PP-MA/20A (90/5/5) exposed to initial melting at 175, 225 and 250 °C.

Effect of Initial Melting Temperature on Crystallization of Polypropylene/Organoclay Nanocomposites
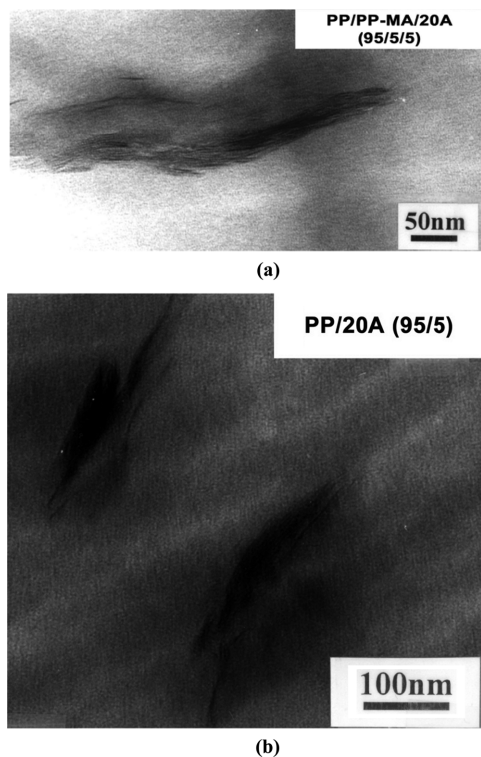
Figure 8. TEM micrographs of the PP nanocomposite: (a) PP/PP-MA/20A (90/5/5) and (b) PP/20A (95/5).
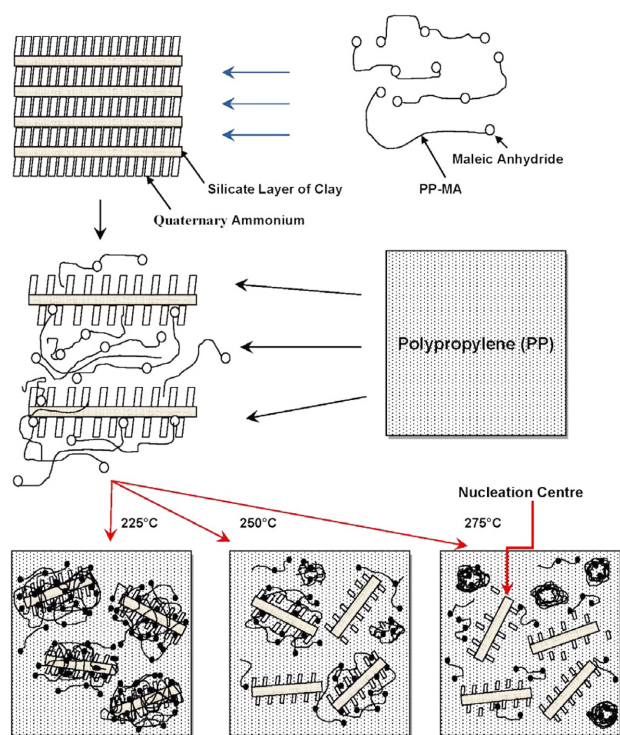

Figure 9. Schematic representation of the dispersion process of PP/PP-MA/20A (90/5/5) at mentioned initial melting temperatures.

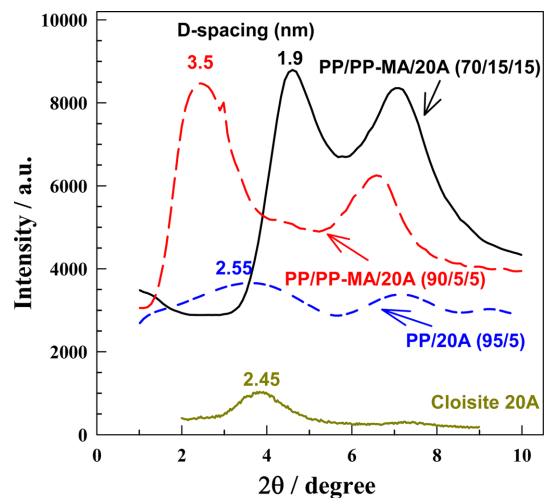**Figure 10.** XRD patterns of the nanocomposites.

peak. Due to the Brownian motion at higher temperatures PP-MA chains move away and the clay surface gets more exposed. This causes an increase in the Si-O peak. Figure 7 illustrates a systematic increase of the Si-O peak with increasing initial melting temperature for the three-component system.

Figure 8 shows the morphology of three-component and two-component nanocomposites. While in two-component system (PP/20A) the clay layers are very close to each other, in case of the three-component system there are signs of intercalation and exfoliation. PP-MA is a very effective compatibilizer between non-polar PP and polar clay because it contains non-polar PP areas and also polar maleic anhydride sites.

Figure 9 schematically illustrates what is most likely happening at different initial melting temperatures. While at 225 °C the clay layers are well covered by PP-MA, at 250 °C there are some layers without PP-MA that can potentially act as new nucleation centers for crystallization, as shown in Figure 3(c) by optical microscopy. Rising the temperature to 275 °C, the process of PP-MA removal from the clay layers continues. Additionally, quaternary ammonium salt starts to degrade and it separates from the clay layers,[21] leaving them uncovered and thus forming new nucleation centers. Due to the polar nature of PP-MA it is probable that it forms micelles in non-polar PP. Most likely PP-MA and PP are immiscible in static conditions.

XRD is a powerful technique for quantitative analysis of

D-spacing in nanocomposites. Figure 10 illustrates XRD results for injection molded nanocomposites in comparison to Cloisite 20A powder. Pure Cloisite 20A has D-spacing about 2.45 nm. Mixing of Cloisite 20A with pure polypropylene by twin screw extruder (high shear rate at 300 rpm) is able to separate the clay layers only up to 2.55 nm. Even higher separation of nanolayers can be achieved by adding PP-MA (D=3.5 nm) for 5% of clay. In case of 15% of clay the average D-spacing is found to be 1.9 nm, it is difficult to disperse well such a large amount of nanoclay. The XRD results shown in
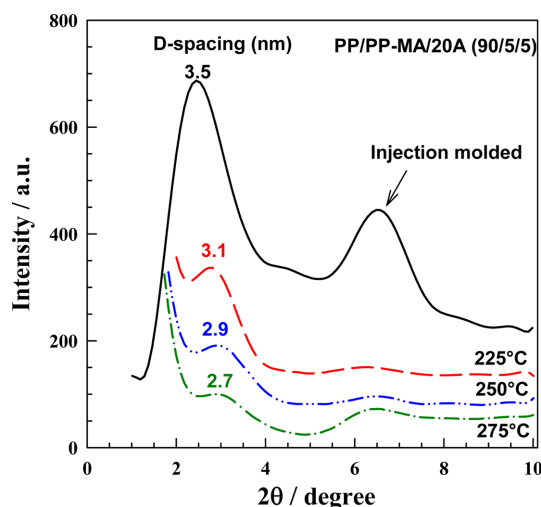
P. Svoboda *et al.*

Figure 11. XRD patterns of PP/PP-MA/20A (90/5/5) measured after exposure to different initial melting temperatures.
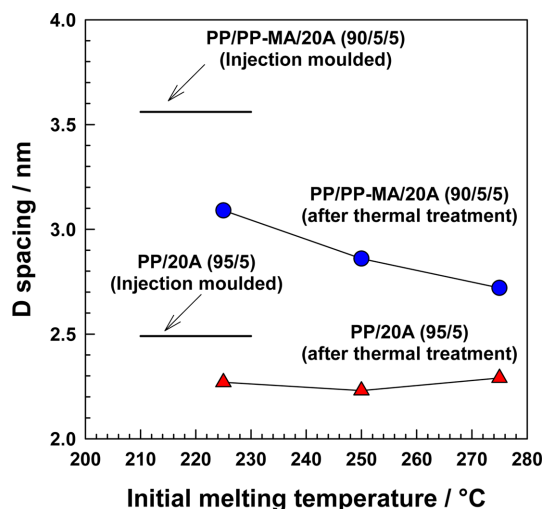

Figure 12. Study of D-spacing after thermal threatment on nanocomposites at different initial melting temperatures.

Figures 11 and 12 can be explained by a schematic representation illustrated in Figure 13. At first, the XRD peak of PP/20A (95/5) sample is not changing its position with the change in initial melting temperatures. The D-spacing remains almost constant (2.23-2.29 nm) in the temperature range 225-275 °C. By incorporating PP-MA, the situation changes dramatically. The D-spacing increases to the range 2.7-3.5 nm which means that PP-MA is present between the silicate layers. The injection molded sample has the highest D-spacing (3.5 nm). Two things are happening when we increase the annealing temperature (in range 225-275 °C). The peak intensity shifts towards a larger angle and the intensity decreases with increasing initial melting temperature (see Figure 11). There are two possible explanations for this behavior. The first possibility involves the PP-MA diffusion out of the interlayer space that causes a decrease in D-spacing with the
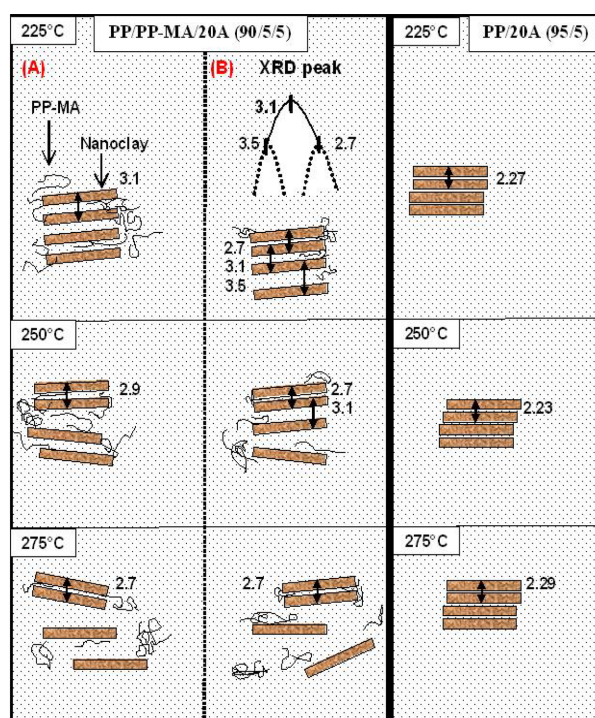
Figure 13. Schematic representation of D-spacing in nanocomposites at different melting temperatures.

increasing annealing temperature. This is shown schematically in Figure 13(A). A second possibility is shown in Figure 13(B). There is distribution in D-spacing (visible also by TEM on Figure 8(a)); schematically we have shown only three distances - 2.7, 3.1 and 3.5 nm. With increasing annealing temperatures, the clay layers separate easily from each other by thermal diffusion when the distance is higher (3.1 or 3.5 nm), but the closest layers (2.7 nm) remain together because the amount of PP-MA between them is lower. The trend in peak intensity in Figure 11 suggests that there is a possibility of a complete disappearance of the peak with further increase in temperature. However, at higher temperatures (more than 300 °C) a serious degradation takes place[21] and such results would have low practical meaning.

In addition to crystallization the kinetics study and morphology analysis, we have performed also mechanical tests. All of the results from the tensile measurements and izod impact strength are summarized in Table I. Figure 14 illustrates original stress-strain curves. Let us first examine the effect of the clay alone (PP/20A vs. PP/PP-MA). Addition of 5% of clay influences yield stress and elongation at MAX only a little, however it decreases the elongation at break significantly. An increase was observed for Young's modulus and for impact strength. Secondly, let us test the effect of the addition of PP-MA (PP/PP-MA/20A vs. PP/20A). PP-MA has caused the increase in yield stress, Young's modulus and impact strength, on the other hand it has led to a decrease in elongation at MAX and elongation at break. Finally, let us

Effect of Initial Melting Temperature on Crystallization of Polypropylene/Organoclay Nanocomposites

Table I. Mechanical Properties

Samples	Ratio	Yield Stress (MPa)	Elongation at MAX (%)	Elongation at Break (%)	Young's Modulus (MPa)	Notched Izod Impact Strength (J/m)
PP/PP-MA	90/5	35.41	8.39	20.16	1670	19.0
PP/20A	95/5	35.85	7.42	14.45	1984	22.8
PP/PP-MA/20A	90/5/5	37.70	7.08	12.40	2070	25.8
PP/PP-MA/20A	70/15/15	38.87	4.09	4.14	3486	21.9
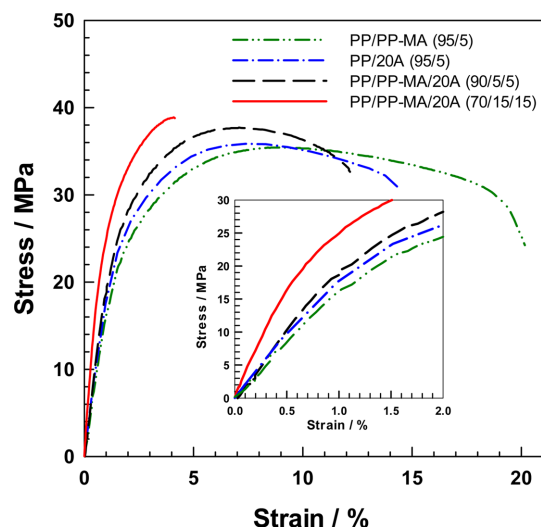
Figure 14. Stress-strain curves for various nanocomposites.

examine the effect of increase in clay concentration in three-component systems (5 vs. 15 wt.% of clay). Although the increased level of clay has caused the increase in yield stress and Young's modulus, it has on the contrary caused a decrease in elongation at MAX, elongation at break and impact strength. It is worth to mention that the increase in Young's modulus was extremely large (3486 vs. 2070 MPa).

Xu *et al*. showed for the pure PP that smaller size of the spherulites may be responsible for the increase in impact strength.[14] Clay particles act as nucleation centers. Increased amount of clay can generate more nucleation centers. When there is large number of nucleation centers, spherulites impinge upon each other and truncate which means that they cannot grow to large size. From this point of view increasing amount of clay can be responsible for the increase in impact strength. From another point of view, while the clay particles are helping extremely with modulus because of high aspect ratio (length to thickness) they act also as stress concentration centers in high speed destruction test such as during the measurement of the impact strength. Then increasing amount of clay increases the number of stress concentration centers which results in decrease in impact strength. Therefore initially we observed increase in impact strength from 19 to 25.8 J/m (for 0 and 5% of clay,

respectively) followed by decrease in impact strength from 25.8 to 21.9 J/m when the amount of clay was increased from 5 to 15 wt.%.

Conclusion

The initial melting temperature greatly influences the crystallization kinetics. For two-component systems, the kinetics decreases gradually with the increasing melting temperature. However, in case of three-component systems (PP/PP-MA/20A), a deviation from this gradual decrease was found. The unusual crystallization behavior of PP/PP-MA/20A three-component systems obtained by DSC analysis was explained with the help of optical microscopy, FTIR and XRD analyses. The optical microscopy revealed an unusually large number of spherulites in case of the three-component system after initial melting at 250 ºC (at 225 ºC, the number of spherulites was comparable to two-component systems). On one hand the crystallization kinetics of a single spherulite was not influenced much by the composition and initial melting temperature; on the other hand it was influenced greatly by the crystallization temperature. FTIR analysis revealed a rise in Si-O peak with increasing melting temperature for a three-component system, while in case of the two-component system, there was almost no change. Apparently, higher melting temperatures caused an increase in surface area of clay layers in the case of the three-component system. XRD analysis revealed a decrease in peak intensity with increasing initial melting temperature, and also a small shift in the peak position in the case of the three-component system. Most likely, the clay layers separate at high temperatures (exfoliation caused by high mobility). Concerning mechanical properties, clay addition increases greatly Young's modulus, but it decreases the elongation significantly too. All investigated nanocomposites had increased impact strength.

P. Svoboda *et al.*

References

(1) Y. W. Chang, J. Y. Shin, and S. H. Ryu, *Polymer International*, **53**, 1047 (2004).

(2) X. B. Hu and A. J. Lesser, *Macromolecular Chemistry and Physics*, **205**, 574 (2004).

(3) Y. Kojima, A. Usuki, M. Kawasumi, A. Okada, T. Kurauchi and O. Kamigaito, *Journal of Polymer Science Part A: Polymer Chemistry*, **31**, 983 (1993).

(4) Y. T. Vu, G. S. Rajan, J. E. Mark, and C. L. Myers, *Polymer International*, **53**, 1071 (2004).

(5) Z. M. Wang, H. Nakajima, E. Manias, and T. C. Chung, *Macromolecules*, **36**, 8919 (2003).

(6) N. Artzi, A. Tzur, M. Narkis, and A. Siegmann, *Polymer Composites*, **26**, 343 (2005).

(7) H. Mirzazadeh and A. A. Katbab, *Polymers for Advanced Technologies*, **17**, 975 (2006).

(8) F. Perrin-Sarazin, M. T. Ton-That, M. N. Bureau, and J. Denault, *Polymer*, **46**, 11624 (2005).

(9) M. T. Ton-That, F. Perrin-Sarazin, K. C. Cole, M. N. Bureau and J. Denault, *Polymer Engineering and Science*, **44**, 1212 (2004).

(10) J. S. Ma, Z. N. Qi, G. Li, and Y. L. Hu, *Acta Polymerica Sinica*, 589 (2001).

(11) A. Pawlak, J. Morawiec, E. Piorkowska, and A. Galeski, in *Interfacial Effects and Novel Properties of Nanomaterials*, W. Lojkowski and J.R. Blizzard, Eds., Trans Tech Publications Ltd, Zurich-Uetikon, 2003, Vol. 94, pp 335.

(12) E. Pavlidou, D. Bikiaris, A. Vassiliou, M. Chiotelli, and G. Karayannidis, in *Second Conference on Microelectronics, Microsystems and Nanotechnology*, A.G. Nassiopoulou, N. Papanikolaou and C. Tsamis, Eds., Iop Publishing Ltd, Bristol, 2005, Vol. 10, pp 190.

(13) M. Kawasumi, N. Hasegawa, M. Kato, A. Usuki, and A. Okada, *Macromolecules*, **30**, 6333 (1997).

(14) T. Xu, J. Yu, and Z. H. Jin, *Mater. Des.*, **22**, 27 (2001).

(15) M. Avella, S. Cosco, M. L. Di Lorenzo, E. D. Pace, M. E. Errico, and G. Gentile, *Macromolecular Symposia*, **234**, 156 (2006).

(16) T. S. Ellis and J. S. D'Angelo, *Journal of Applied Polymer Science*, **90**, 1639 (2003).

(17) G. S. Jang, W. J. Cho, and C. S. Ha, *Journal of Polymer Science Part B-Polymer Physics*, **39**, 1001 (2001).

(18) V. Mittal, *Journal of Applied Polymer Science*, **107**, 1350 (2008).

(19) D. Page and T. G. Gopakumar, *Polymer Journal*, **38**, 920 (2006).

(20) Y. Wang, F. B. Chen, Y. C. Li, and K. C. Wu, *Compos. Pt. B-Eng.*, **35**, 111 (2004).

(21) J. M. Cervantes-Uc, J. V. Cauich-Rodriguez, H. Vazquez-Torres, L. F. Garfias-Mesias, and D. R. Paul, *Thermochimica Acta*, **457**, 92 (2007).
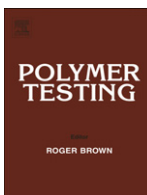
PAPER III

Material behaviour

Influence of supercritical CO_2 and initial melting temperature on crystallization of polypropylene/organoclay nanocomposite

Petr Svoboda [a,*], Krunal Trivedi [a], Dagmar Svobodova [b], Karel Kolomaznik [c], Takashi Inoue [d]

[a] Centre of Polymer Systems, Department of Polymer Engineering, Tomas Bata University in Zlin, Nam. T.G. Masaryka 5555, 760 01 Zlin, Czech Republic
[b] Faculty of Humanities, Tomas Bata University in Zlin, Mostni 5139, 760 01 Zlin, Czech Republic
[c] Faculty of Applied Informatics, Tomas Bata University in Zlin, Nad Stranemi 4511, 760 05 Zlin, Czech Republic
[d] Department of Polymer Science & Engineering, Yamagata University, Yonezawa 992-8510, Japan

ABSTRACT

Polypropylene (PP)/clay nanocomposite with maleic anhydride modified polypropylene (PP-MA) was prepared using a twin-screw extruder. The effect of supercritical carbon dioxide (scCO2) on mixing was investigated. Isothermal crystallization of the nanocomposites was investigated by differential scanning calorimetry (DSC) and also by optical microscopy as a function of initial melting temperature. Increasing initial melting temperature causes a gradual decrease in bulk crystallization kinetics, with the exception of the 240–260 °C temperature range for the system without CO2. Optical microscopy revealed a large number of small spherulites for the system without CO2 after initial melting at 250 °C. After 28 min initial induction period of crystallization many small spherulites appeared in the vicinity of large spherulites for the system with CO2, indicating the beginning of homogenous nucleation. X-ray diffraction (XRD) and direct observation of the samples after tensile testing revealed better dispersion of nanoclay for the system without CO2.

© 2012 Elsevier Ltd. All rights reserved.

1. Introduction

Polymer/clay nanocomposites are a class of hybrid materials composed of organic polymer matrix in which inorganic particles with nanoscale dimensions are embodied. Considerable attention has been given to the preparation of nanocomposites with the aid of supercritical carbon dioxide (scCO2) to expand the clay and cause better polymer intercalation [1,2]. scCO2 is one of the nonflammable, nontoxic and relatively inexpensive solvents which offers many advantages compared with conventional solvents. The presence of dissolved scCO2 in a polymer affects its properties in the molten and solid state. Thus, for example, it reduces the melt viscosity and changes the crystallization rate [3–6]. The scCO2-induced crystallization kinetics has not been studied many times recently.

Polypropylene (PP) is a commodity polymer having various excellent mechanical and chemical properties, many of which depend greatly on its crystallinity and crystalline morphology. A few studies have concluded that incorporation of scCO2 in melt processing may adversely affect polymer/nanoclay mechanical properties and slow down the rate of crystallization [1,6,7], while others utilized scCO2 to enhance gas barrier properties, and also as a foaming agent for PP/nanoclay based composites [8–12].

We found no report of a study on the influence of the initial melting temperature on crystallization kinetics in PP/PP-MA/nanoclay systems. Therefore, we have focused on this topic. Additionally, this paper describes the effect of supercritical CO2 on the crystallization with the help of differential scanning calorimetry (DSC), optical microscopy, Fourier transform infrared spectroscopy (FTIR), and also on dispersion by X-ray diffraction (XRD) and transmission electron microscopy (TEM). Tensile properties were also measured.

---

* Corresponding author. Tel.: +420 576 031 335; fax: +420 577 210 172.
E-mail address: svoboda@ft.utb.cz (P. Svoboda).

2. Experimental

2.1. Materials

The PP with trade name P4G4Z-011 (melt flow index 12 g/10 min, ASTM D1238) was obtained from Huntsman. The maleic anhydride modified polypropylene (PP-MA) was obtained from Uniroyal Chemicals. Its trade name was PB3150, molecular weight was 330,000 g mol^{-1} and the MA content was 0.5 wt.%.

The nano-clay, Cloisite® 20A (Southern Clay), is a natural montmorillonite modified with a quaternary ammonium salt, dimethyl, dihydrogenated tallow, quaternary ammonium chloride.

$$CH_3-N^+-HT$$

(with CH_3 above and HT below)
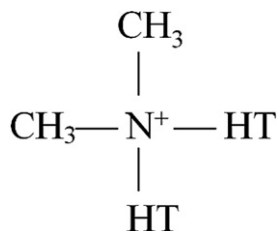
where, HT is a hydrogenated tallow ($\sim$65% C18; $\sim$30% C16; $\sim$5% C14).

2.2. Preparation of PP/PP-MA/20A composites

A twin screw extruder, Leistritz ZSE 27 with L/D = 40 and D = 27 mm was used in the co-rotating mode for the melt intercalation of nanocomposites. The barrel temperatures were set at 165–185 °C and the screw speed was fixed at 300 rpm. In order to achieve desired mixing, the feed rate was kept low at 2 kg/h. A capillary die with a 0.5 mm diameter and 10 mm long nozzle was custom-made to generate a high and rapid pressure drop. CO_2 was delivered from a syringe pump (ISCO 260D) with a cooling jacket, as shown in Fig. 1. The CO_2 pressure and volumetric flow rate can be controlled precisely by the pump controller. CO_2 was compressed to the required pressure in the syringe pump at 40 °C, reaching a super-critical state. Then, approximately 4 wt.% of scCO_2 was injected into the extruder barrel with carefully controlled pressure and volumetric flow rate. On injection into the barrel, scCO_2 was mixed with the polypropylene/PP-MA/20A melt by screw rotation. Nucleation occurs in the die because of the quick and large pressure drop produced by the narrow capillary nozzle. The foamed extrudate flows freely out of the nozzle and vitrifies in the ambient air. The strings were pelletized and remixed again in the twin-screw extruder with a vacuum pump to remove the CO_2.

2.3. Preparation of PP/PP-MA/20A samples for tensile properties

A Sumitomo 200 ton injection moulding machine was used for the preparation of tensile bars. Tensile tests were performed in general accordance with ISO 527 using an Instron tensile tester. The results are the average of 5 test pieces.
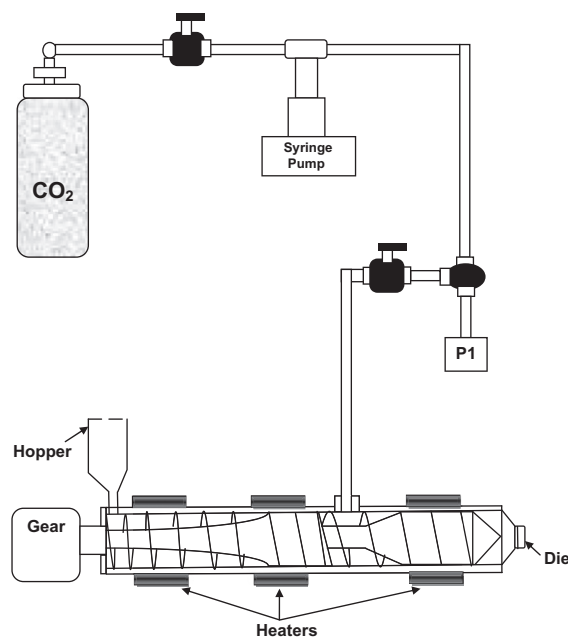

Fig. 1. A schematic of the experimental set-up for the scCO_2-assisted extrusion process.

2.4. Measurements

2.4.1. XRD measurement

An X-ray diffractometer, X'Pert PRO from PANalytical, was used to analyse the nano-structure (D-spacing) of composites with the scanning range of 0.5–20° (2θ). The samples were injection moulded and then tested at room temperature.

2.4.2. Differential scanning calorimetry

The crystallization kinetics of the samples was analysed using a Perkin–Elmer DSC-1. Temperature calibration was performed using the indium standard. A nitrogen atmosphere was employed during the experiment at a flow rate 20 mL min^{-1}. For isothermal crystallization, the samples were heated to various initial melting temperatures (at 100 °C min^{-1} heating rate) and then cooled (at 50 °C min^{-1}) to the isothermal crystallization temperature (127 °C). In all cases, samples were held at the initial melting temperature for 1 min to eliminate any previous thermal history.

2.4.3. Transmission electron microscopy

For the TEM analysis, the specimens were microtomed to ultrathin sections of 70 nm using an ultracryomicrotome with a diamond knife. Then, the sections were stained with RuO$_4$. The structure was observed under a transmission electron microscope Phillips CM 12.

2.4.4. Optical microscopy

For the observation of the growth of the spherulites, an Olympus BH2 polarized optical microscope equipped with

a CCD camera connected to a computer and a LINKAM hot stage were used.

2.4.5. FT-IR measurement

The FTIR study was carried out by the Nicolet 320 Avatar FT-IR spectrometer in ATR mode.

3. Theoretical background

3.1. Avrami analysis

Whenever a polymer crystallizes, the extent of the phase transformation depends on the crystallizing species and the experimental conditions. High molecular weight polymers do not crystallize completely because of topological constraints that lower crystallinity considerably. The classical isothermal transformation kinetics, initially formulated by Kolmogorov and Goler et al. were extended later by the Avrami theory that was initially formulated for metals and later modified.

The crystallization kinetics of polymers can be analysed using a classical Avrami equation as given in Eq. (1) [13]:

$$1 - X_t = \exp(-kt^n) \tag{1}$$

where k is the Avrami rate constant and n is the Avrami exponent. Both k and n depend on the nucleation and growth mechanisms of spherulites.

The fraction X_t is obtained from the area of the exothermic peak in DSC isothermal crystallization analysis at a crystallization time t divided by the total area under the exothermic peak:

$$X_t = \frac{\int_0^t \left(\frac{dH}{dt}\right)dt}{\int_0^\infty \left(\frac{dH}{dt}\right)dt} \tag{2}$$

where the numerator is the heat generated at time t and the denominator is the total heat generated up to complete crystallization.

In order to deal conveniently with the operation, Eq. (1) is usually rewritten as the double logarithmic form as follows:

$$\ln[-\ln(1 - X_t)] = \ln k + n \ln t \tag{3}$$

The k and n values can be directly obtained using Eq. (3) from the slope and intercept of the best-fit line.

3.2. Hoffman–Lauritzen analysis

The crystallization behaviour of the polymers was also studied according to the relationship between chain folded crystal growth rates and undercooling proposed by Hoffman and Lauritzen [14,15]:

$$G = G_0 \exp\left[\frac{-U^*}{R(T_c - T_\infty)} - \frac{K_g}{T_c(\Delta T)f}\right] \tag{4}$$

where G is the crystal growth rate, U^* is a constant characteristic of the activation energy for repetitive chain motion and is equal to 1500 cal mol^{-1}, R is the gas constant, T_c is the crystallization temperature (K), $T_\infty = T_g - 30$ K (for PP the glass transition temperature $T_g = 270$ K), $\Delta T = T_m^0 - T_c$, T_m^0 is the equilibrium melting temperature of an infinitely thick crystal, K_g is the nucleation constant, f is a correction factor and equals to $2T_c/(T_m^0 + T_c)$, and G_0 is a pre-exponential factor. For the evaluation of DSC results, we have replaced G by $1/\tau_{1/2}$.

$$\ln\left(\frac{1}{\tau_{1/2}}\right) + \frac{U^*}{R(T_c - T_\infty)} = \ln G_0 - \frac{K_g}{T_c \Delta T f} \tag{5}$$

A major extension of the theory involved the recognition that the deposition of a single critical nucleus may not always occur and that multiple nucleation generates
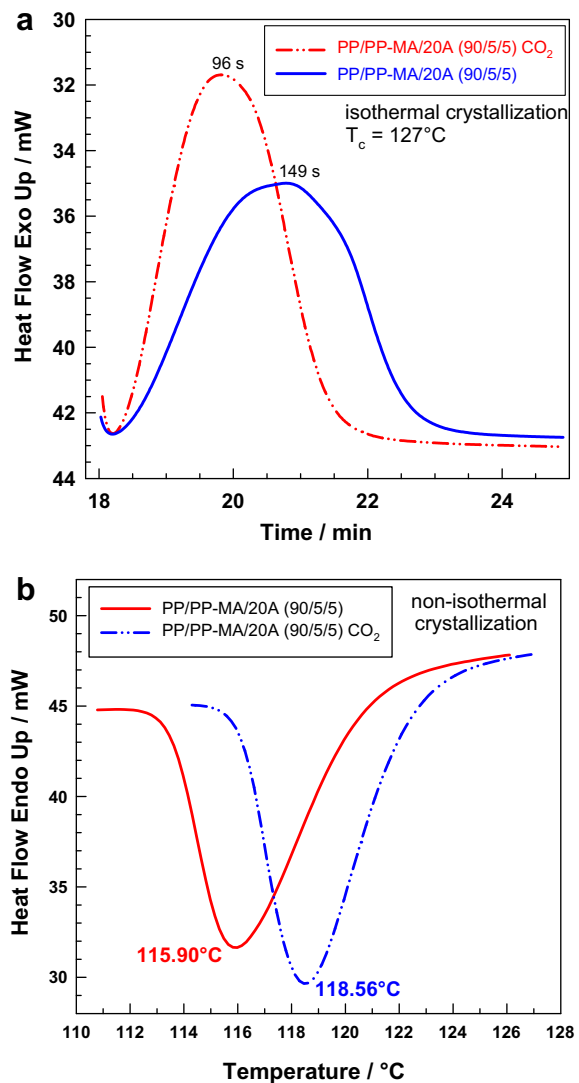
Fig. 2. (a) Isothermal crystallization peak at 127 °C for nanocomposites and (b) crystallization temperature (T_c) for nanocomposites during non-isothermal crystallization after initial melting at 210°C.

a different situation. The situation is handled best in general conceptual terms by considering it to be a competitive situation between the rate at which critical nuclei are deposited on the surface and the rate at which the chains deposit laterally to complete the growth step. This leads to three distinct situations or regimes; regime I the classical situation in which the rate of secondary nucleation is slowest, regime II a situation in which the rates of secondary nucleation and lateral spreading are comparable, and regime III a situation in which the rate of secondary nucleation is the fastest. These three situations occur naturally in many polymers as the crystallization temperature is reduced. The vast majority of polymers studied show regimes II and III, whereas few show regime I which is the classical situation [16].

Basically, the diffusion process has been described as consisting of two elementary processes: the deposition of the first stem on the growth front (secondary nucleation process) and the attachment of following stems in the

Fig. 4. Crystallinity (X_c) of nanocomposites as a function of (a) crystallization temperature and (b) initial melting temperature.

Fig. 3. (a) Crystallization kinetic ($\tau_{1/2}^{-1}$) and (b) half time of crystallization ($\tau_{1/2}$) at 127 °C from DSC as a function of initial melting temperature.
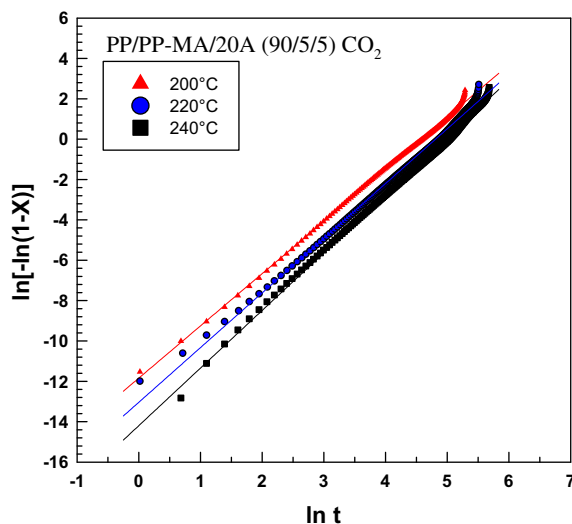
Fig. 5. Avrami plot for PP/PP-MA/20A (90/5/5) CO_2 nanocomposites at 127°C after melting at various initial melting temperatures.
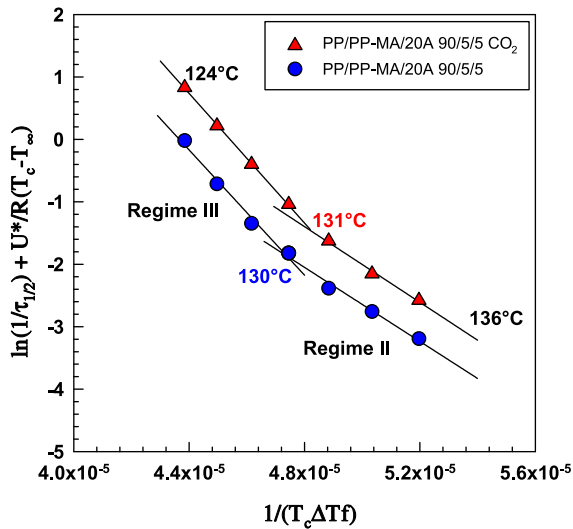
Fig. 6. Hoffman–Lauritzen plots for nanocomposites from DSC.

chain on the crystal surface (surface spreading process). According to the Hoffman–Lauritzen theory, G is mostly governed by the rate of secondary nucleation, i in regimes I and III, while it is governed by both i and the rate of surface spreading, g, in regime II:

$$G \propto i \qquad for \frac{i}{g} \ll 1 (regime\ I) \tag{6}$$

$$G \propto (ig)^{1/2} \qquad for \frac{i}{g} \sim 1 (regime\ II) \tag{7}$$

$$G \propto i \qquad for \frac{i}{g} \gg 1 (regime\ III) \tag{8}$$

where i consists of both β_g and $\exp[-K_g/T_c(\Delta T)f]$ and g consists of only β_g. The diffusion coefficients in the surface nucleation process and the substrate completion process are defined as D_M and D_S, respectively. Assuming that β_g is proportional to the diffusion coefficient, i and g may be given by:

$$i \propto D_M \exp\left[-\frac{K_g}{T_c \Delta Tf}\right] \tag{9}$$

$$g \propto D_S \tag{10}$$

From Eqs. (6)–(10) one can obtain:

$$\beta_g \propto \phi_1 D_M \qquad (regime\ I\ and\ III) \tag{11}$$

$$\beta_g \propto \phi_1^{1/2}\left(D_M D_S\right)^{1/2} \qquad (regime\ II) \tag{12}$$

where a prefactor ϕ_1 is introduced, since i is proportional to the number of crystallizable molecules at the crystal surface, which is proportional to the volume fraction of crystalline polymer ϕ_1 [17].

3.3. XRD study

Nanocomposite formation and the degree of nanoclay dispersion was monitored using a X'Pert PRO wide-angle X-ray diffraction (XRD) system from PANalytical. The d-spacing of clay in nanocomposites was calculated from Bragg's equation using XRD results [18]:

$$d = \frac{n\lambda}{2\sin\theta} \tag{13}$$

where d is the spacing between layers of the clay, λ the wave length of X-ray equal to 0.153 nm, θ the angle at the maximum point of the first peak (lowest θ) in the spectra and n is a whole number, representing the order of diffraction.

4. Results and discussion

Initially, we have investigated the crystallization kinetics by DSC in the isothermal mode (Fig. 2a) and also in a nonisothermal way (Fig. 2b). While the samples PP/PP-MA/20A (95/5/5) crystallize somewhat slowly ($\tau_{1/2} = 149$ s at 127 °C, for nonisothermal $T_c = 115.90$ °C) the crystallization of the sample PP/PP-MA/20A (95/5/5), CO_2 completed much faster ($\tau_{1/2} = 96$ s at 127 °C, $T_c = 118.56$ °C). At this point it is not clear what the true cause of this difference is. It could be different number of nucleation centres or different growth rate of the spherulites. Further investigation by other methods was necessary.

We have investigated also the influence of initial melting temperature (in the range 200–260 °C) on isothermal crystallization kinetics by the DSC method. The sample was always kept 1 min at different melting temperature and then quickly quenched to 127 °C (50 °C/min). For the samples PP/PP-MA/20A (95/5/5) and PP/PP-MA/20A (95/5/5) CO_2, the crystallization kinetics decreases gradually with increasing initial melting temperature in the range 200–240 °C, as shown on Fig. 3a. The reason might be

Table 1
Avrami parameters.

Samples	200 °C		220 °C		240 °C		260 °C	
	n	k (s^{-1})	n	k (s^{-1})	n	k (s^{-1})	n	k (s^{-1})
PP/PP-MA/20A	2.53	3.9×10^{-6}	2.69	8.6×10^{-7}	2.70	6.2×10^{-7}	2.78	4.5×10^{-7}
PP/PP-MA/20A CO_2	2.58	7.2×10^{-6}	2.71	2.1×10^{-6}	2.85	6.8×10^{-7}	2.81	6.8×10^{-7}

Table 2
Hoffman–Lauritzen parameters.

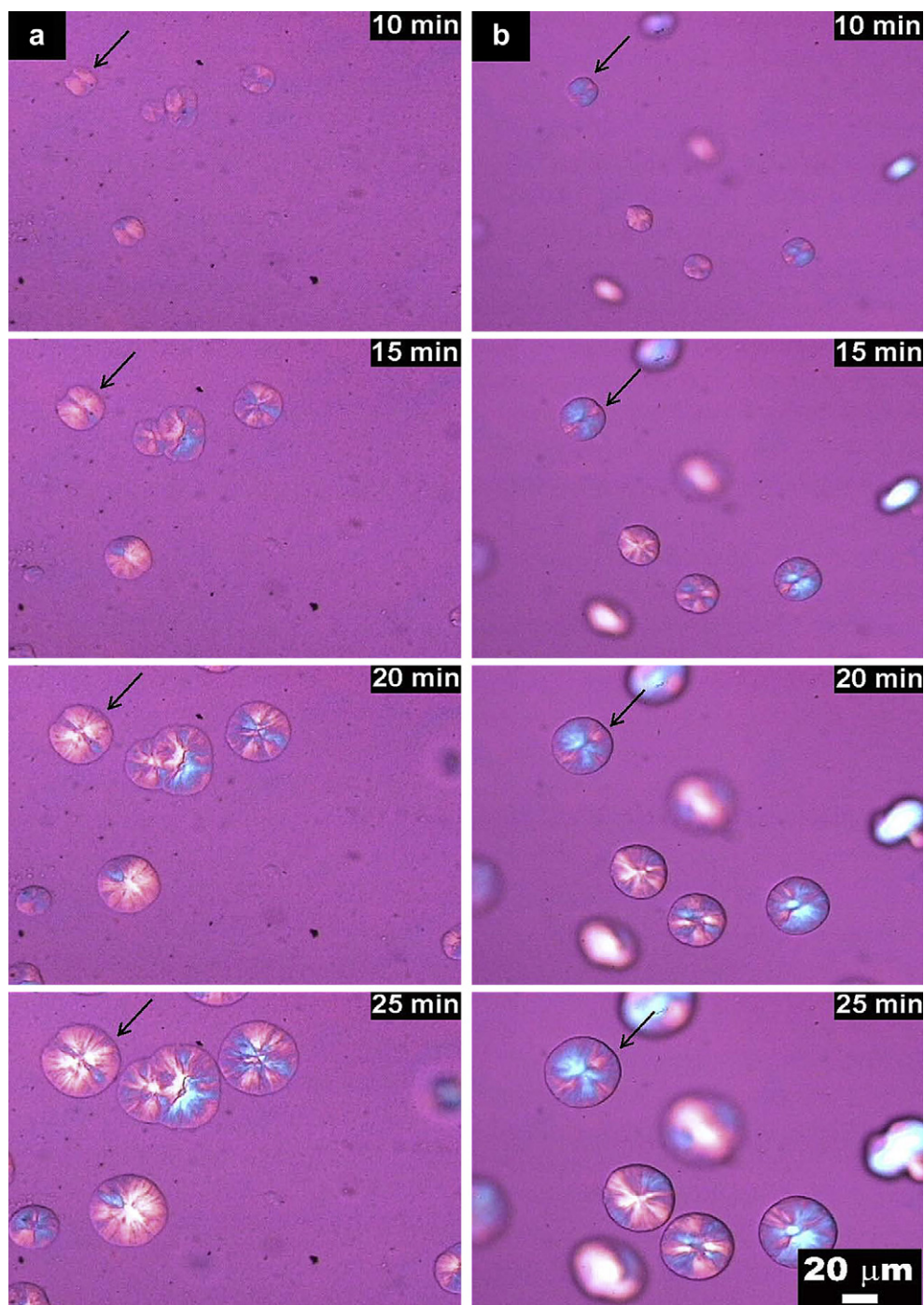| Samples	Regime II		Regime III		Transition (°C)
	$K_g \times 10^{-5}$ (K^2)	$\ln G_0$	$K_g \times 10^{-5}$ (K^2)	$\ln G_0$	
PP/PP-MA/20A	2.96	12.19	5.01	21.90	130.0
PP/PP-MA/20A CO$_2$	3.03	13.15	5.18	23.56	131.0

Fig. 7. Growth of the spherulites by optical microscopy at 140 °C after initial melting at 225 °C for (a) PP/PP-MA/20A (90/5/5) CO$_2$ and (b) PP/PP-MA/20A (95/5/5).

faster diffusion and movement of molecules at higher melting temperatures. The macromolecules arrange to much different positions at higher melting temperature than when they were arranged in crystal lamella. Then, it requires longer time to move back to orderly arrangement

in crystal lamella from the more disordered state. However, at higher melting temperatures (240–260 °C), PP/PP-MA/20A (90/5/5) exhibited some deviation. The deviation is better visible on Fig. 3b for the PP/PP-MA/20A (95/5/5) CO_2 system where $\tau_{1/2}$ increases almost linearly with increasing
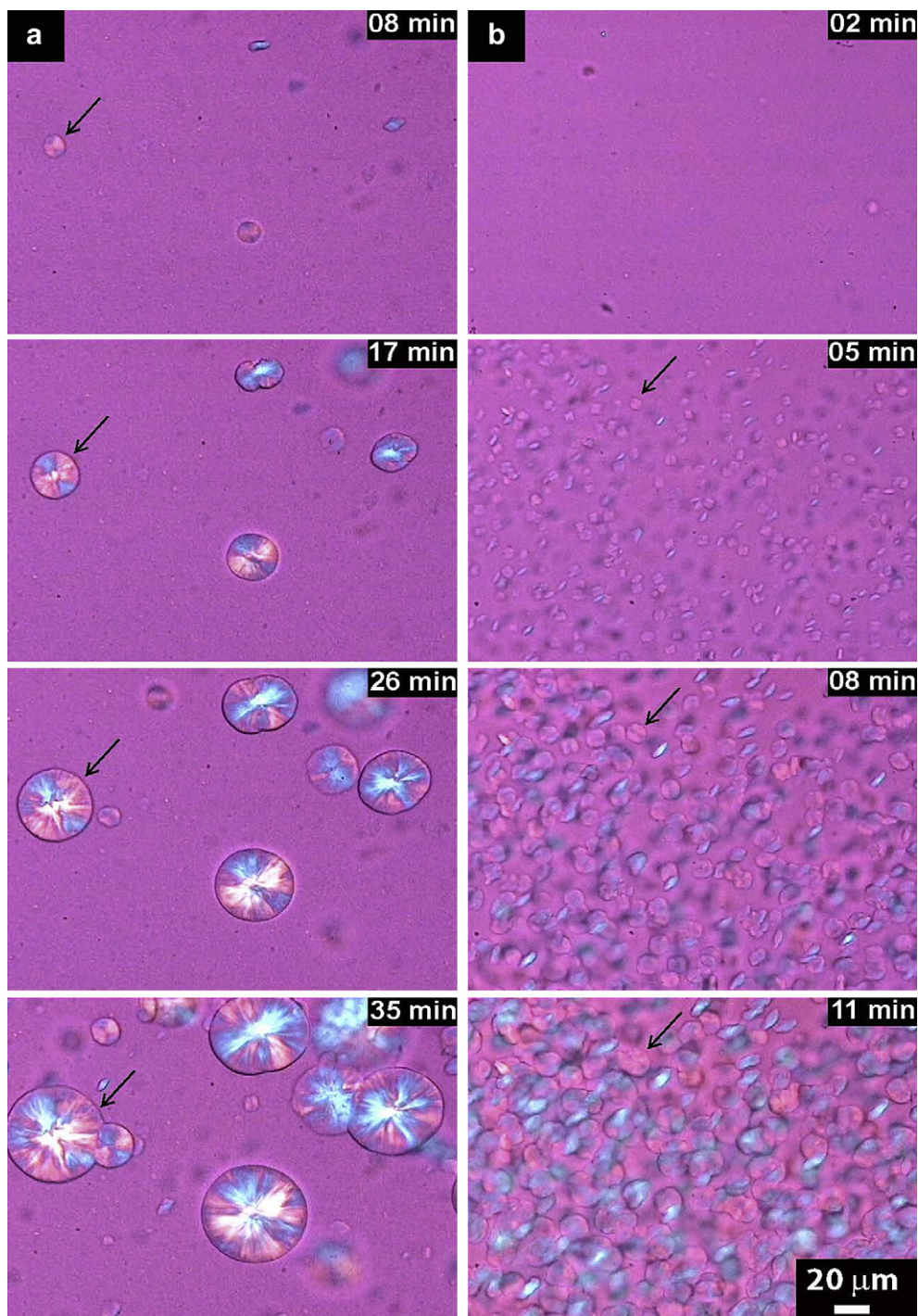
Fig. 8. Growth of the spherulites by optical microscopy at 140 °C after initial melting at 250 °C for (a) PP/PP-MA/20A (90/5/5) CO_2 and (b) PP/PP-MA/20A (95/5/5).

initial melting temperature. However, for the system PP/PP-MA/20A (90/5/5) at 240–260 °C there is a clear deviation from linearity (the curve is bending down). This abnormal behaviour motivated a crystallization kinetics study performed by optical microscopy. Before coming to the optical microscopy results we examine the DSC data in detail.

Fig. 4a illustrates the crystallinity as a function of crystallization temperature. The sample with CO_2 had lower crystallinity at 124–126 °C, but higher in the temperature range 128–132 °C. Li et al. [19] observed increase in crystallinity due to insertion of nucleating agent with the help of the CO_2 (without CO_2 the crystallinity was lower). In our case, we observed the same higher crystallinity for sample with CO_2 in the temperature range 128–132 °C. We also analysed crystallinity as a function of initial melting temperature (Fig. 4b). The lowest crystallinity was found after melting to 200 °C. Then, with increasing initial melting temperature the crystallinity gradually grew to 230 °C and then started to decrease. In the range 200–230 °C, higher temperature helps with faster diffusion of macromolecules
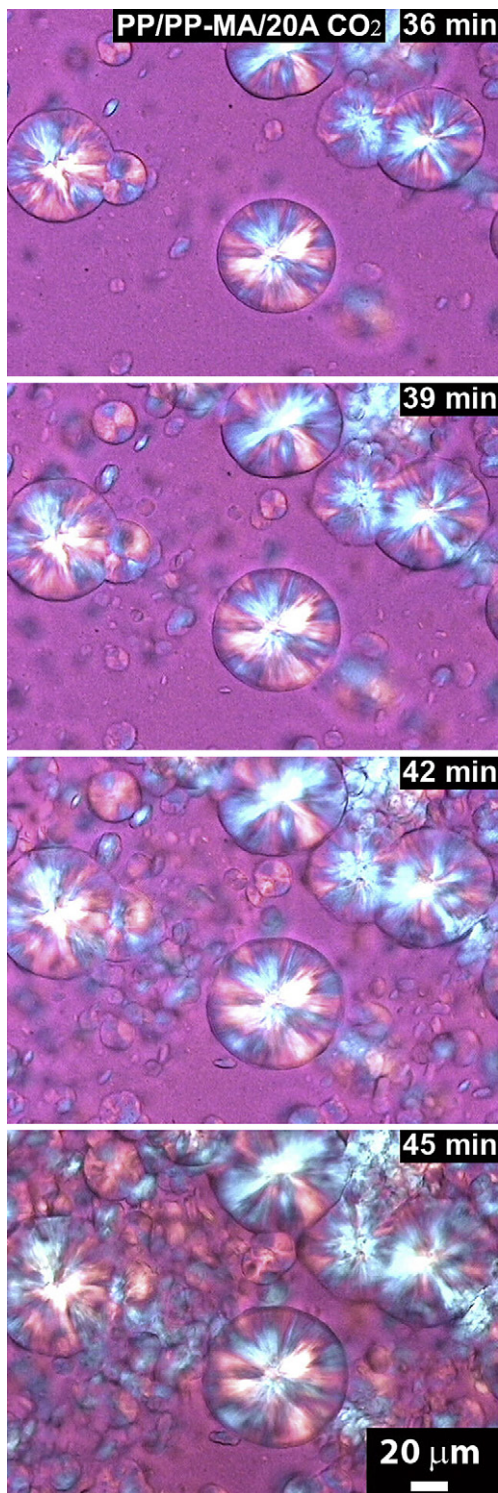
Fig. 9. Continuation of Fig. 8(a) in time.
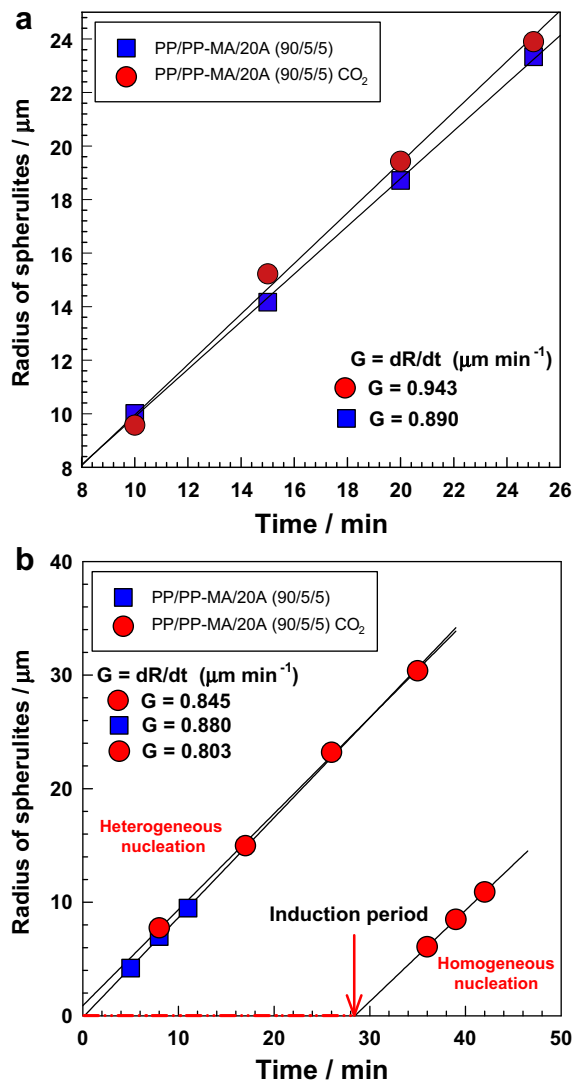
Fig. 10. Evaluation of crystallization kinetics at 140 °C based on Figs. (7) and (8) after initial melting at (a) 225 °C, (b) 250 °C.

in the melt, as then more of them can arrange into lamellae. However, in the temperature range 230–260 °C degradation most likely starts to take place, the macromolecules get shorter which results in lower crystallinity (compare 260 vs. 230 °C). This trend exhibiting maximum at 230 °C was observed for both samples (with or without CO_2). Up to now, we have not come across any other research paper with these data so that comparison was not possible.

We have analysed the DSC data with the help of the Avrami equation and also according to Hoffman–Lauritzen. Results of the two analyses are shown on Figs. 5 and 6 and also in Tables 1 and 2. Sample with CO_2 always crystallizes faster which is represented by k value in Table 1 and also by $\ln G_0$ in Table 2. For both samples, the n exponent increases slightly from about 2.5 to 2.8 and the k value decreases with increasing initial melting temperature. These values are in accordance with literature [3]. We found transition from regime II to regime III around 130 °C and the K_g values, being about 3×10^{-5} and 5×10^{-5} K^2 for regimes II and III, respectively, were not greatly influenced by CO_2.

The DSC results are connected with bulk crystallization, the kinetics can be influenced by the number of nucleating centres or by spherulite growth rate. To understand which of these factors is predominant we have also carried out optical microscopy observations of crystallization at constant elevated temperatures (135–142 °C) on a LINKAM hot stage. From Fig. 7, it is clear that the number of spherulites is very similar for both systems, indicating very similar nucleation rates at 225 °C. Also, the growth rate of individual spherulites is similar, as shown also in Fig. 10a. The situation was very much different after melting to 250 °C, as shown on Fig. 8. While for the PP/PP-MA/20A (95/5/5) CO_2 the number of spherulites and the growth rate are again very similar up to 225 °C (Fig. 7a), for PP/PP-MA/20A (90/5/5) we found a large number of spherulites. This indicates a much higher nucleation rate after melting at 250 °C. PP/PP-MA/20A (90/5/5) had very good dispersion but at high temperature the PP-MA probably segregated
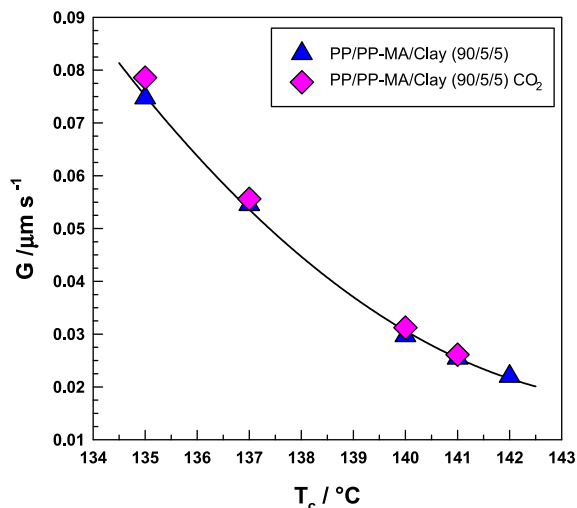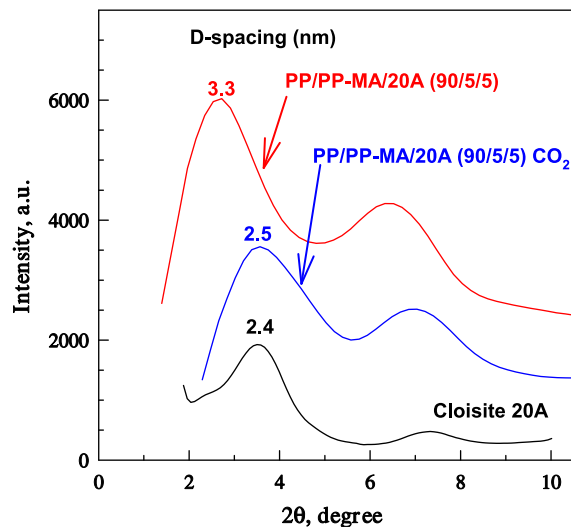

Fig. 12. XRD patterns of the nanocomposites.

into PP-MA micelles, and naked clay particles then acted as nucleation centres. The growth rate of individual spherulites is similar for both systems, as shown also in Fig. 10b. In the case of the system with CO_2, we have discovered interesting crystallization behaviour in the time-frame 35–45 min, which is shown in Fig. 9. In this Figure there are large spherulites and also many new small ones. The explanation of this behaviour could be as follows. Clay particles (foreign substance) act as heterogeneous nucleation centres and the crystallization starts from time zero. After 28 min (induction period of crystallization), homogenous nucleation starts taking place. The growth rate of these small spherulites was not found to be very much different from the growth rate of the large spherulites (see Fig. 10b). The phenomenon of homogenous nucleation could not be observed for the system without CO_2 because the space was already filled with spherulites in about 11 min.

The spherulites growth rate gradually decreased with increasing crystallization temperature, as shown in Fig. 11. We have not found large differences in crystallization kinetics of individual spherulites for both systems. The CO_2 does not influence the crystallization kinetics of individual spherulites.
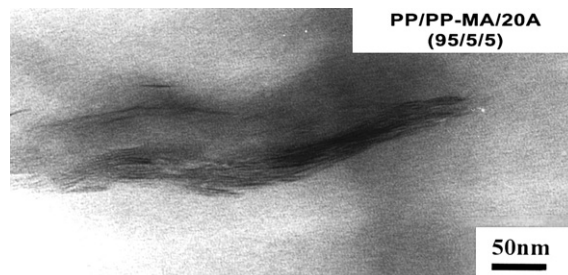

Fig. 11. Crystallization kinetics as a function of crystallization temperature (T_c) from optical microscopy after initial melting at 200 °C.

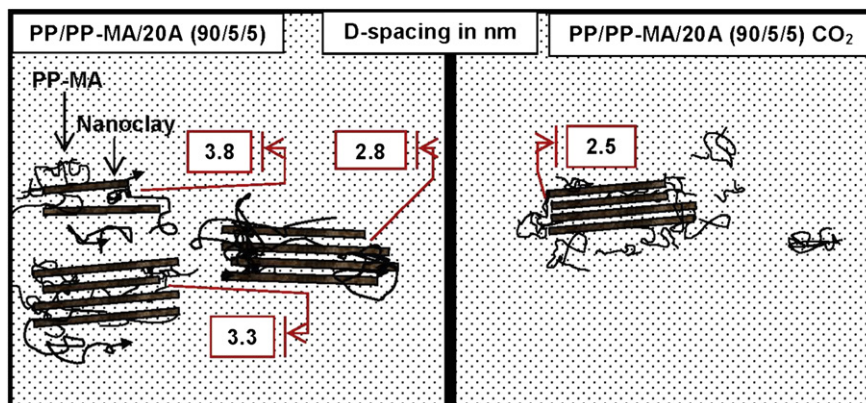**Fig. 13.** TEM micrograph of the PP nanocomposite.

Fig. 14. Schematic representation of clay layers arrangement based on XRD result.
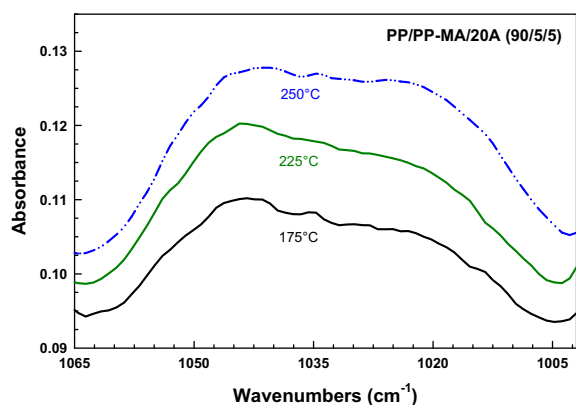

Fig. 15. FT-IR spectrum of PP/PP-MA/20A (90/5/5) exposed to initial melting at 175, 225 and 250 °C.

An XRD result indicates in Fig. 12 that PP/PP-MA/20A (95/5/5) CO_2 has worse dispersion of clay than PP/PP-MA/20A (95/5/5). The system with CO_2 had D-spacing 2.5 nm, while without CO_2 the D-spacing was 3.3 nm. Apparently, CO_2 decreases viscosity during mixing (acts as a plasticizer) which causes smaller shear stress and worse dispersion of nanolayers. From the opposite point of view, higher viscosity (systems without CO_2) is favorable for mixing (higher shear stress) and causes better intercalation of nanolayers.

While XRD results indicate the level of intercalation, we have also made direct observation of the structure by transmission electron microscopy (TEM) for PP/PP-MA/20A (95/5/5), as shown on Fig. 13. Rather broad XRD peak suggests distribution in D-spacing. Some nanolayers are quite close to each other, some are more intercalated and there is a small portion of nanolayers completely exfoliated.

This is schematically illustrated in Fig. 14. The system with CO_2 has nanolayers with shorter D-spacing (2.5 nm) which is very close to the original Cloisite 20A (2.4 nm). The nanolayers stayed together during mixing in a twin-screw extruder and also during processing in the injection moulding machine.

In Figs. 3 and 8b there is rather unusual crystallization behaviour in the temperature range 240–260 °C for the sample without CO_2. This behaviour could be connected with degradation of quaternary ammonium chloride [20] and also with migration of PP-MA out of the surface of the clay into micelles, which in the end could lead to uncovered clay nanolayers. To confirm this hypothesis, we have carried out FTIR measurement of the samples annealed to various temperatures (175–250 °C).

Fig. 15 illustrates the FTIR data of PP/PP-MA/20A (90/5/5) sample after different thermal history with the focus on the 1000–1150 cm^{-1} area where the Si–O peak is located. The PP/PP-MA/20A sample exposed to 250 °C has the largest Si–O peak. Due to the Brownian motion at higher temperatures, the PP-MA moves out and more of the clay surface is exposed. This causes an increase in Si–O peak. There is a systematic increase of Si–O peak with increasing initial melting temperature.

Finally we have measured tensile properties to see if the CO_2 has any effect on the mechanical properties. The results are summarized in Table 3 and illustrated in Fig. 16. All of the mechanical properties were very similar for these two systems except for stress at break which was lower for the system with CO_2. We found differences in appearance of the specimens after tensile tests (see Fig. 17). While the system without CO_2 has very fine particles, in the system with CO_2 there are some larger black particles which act as centres of stress during the mechanical test, finally causing the already mentioned lower stress at break.
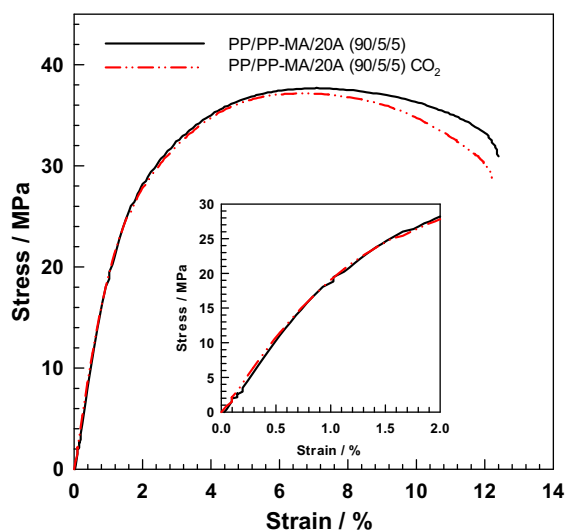
Table 3
Mechanical properties.

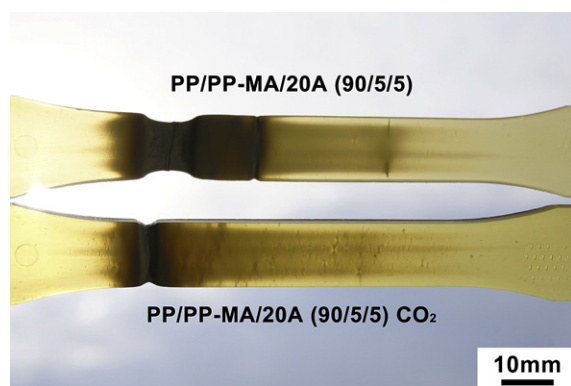| Sample	Ratio	Yield stress (MPa)	Stress at break (MPa)	Elongation at MAX (%)	Elongation at break (%)	Young's modulus (MPa)
PP/PP-MA/20A	90/5/5	37.70	30.85	7.08	12.40	2260
PP/PP-MA/20A CO_2	90/5/5	37.72	28.66	6.69	11.95	2314

Fig. 16. Stress–strain curves.

Fig. 17. Specimens after tensile testing.

5. Conclusions

Increasing initial melting temperature causes decrease in bulk crystallization kinetics observed by DSC. We have found deviation from liner increase in $\tau_{1/2}$ in the temperature range 240–260 °C for the system without CO_2, which motivated optical microscopy observation of the crystallization. While Bin Li et al. [3] observed very fine morphology of PP spherulites for the system with nucleating agent and CO_2; we have not seen such fine morphology with the nanoclay and CO_2 system. In fact, very fine morphology was found for the system without CO_2 after initial melting at 250 °C. At high temperatures (240–260 °C) the PP-MA most likely moved out of the clay surface forming PP-MA micelles, and these naked nanolayers acted as nucleation centres. This behaviour was not found for the system with CO_2, most likely because of the worse dispersion which was found by XRD and by direct observation of the specimens after tensile testing. Most likely, the number of particles is smaller in the case of the system with CO_2. During mixing in a twin-screw extruder the CO_2 most likely acts as plasticizer that causes decrease in viscosity and, finally, the dispersion of clay particles is worse than for the system without CO_2.

References

[1] M. Takada, M. Tanigaki, M. Ohshima, Effects of CO_2 on crystallization kinetics of polypropylene, Polym. Eng. Sci. 41 (11) (2001) 1938–1946.
[2] M. Varma-Nair, P.Y. Handa, A.K. Mehta, P. Agarwal, Effect of compressed CO_2 on crystallization and melting behaviour of isotactic polypropylene, Thermochim. Acta 396 (1–2) (2003) 57–65.
[3] B. Li, G.H. Hu, G.P. Cao, T. Liu, L. Zhao, W.K. Yuan, Effect of super-critical carbon dioxide-assisted nano-scale dispersion of nucleating agents on the crystallization behaviour and properties of polypropylene, J. Supercrit. Fluids 44 (3) (2008) 446–456.
[4] T. Oda, H. Saito, Exclusion effect of carbon dioxide on the crystallization of polypropylene, J. Polym. Sci. Pt. B-Polym. Phys. 42 (9) (2004) 1565–1572.
[5] G. Teramoto, T. Oda, H. Saito, H. Sano, Y. Fujita, Morphology control of polypropylene by crystallization under carbon dioxide, J. Polym. Sci. Pt. B-Polym. Phys. 42 (14) (2004) 2738–2746.
[6] K. Yang, R. Ozisik, Effects of processing parameters on the preparation of nylon 6 nanocomposites, Polymer 47 (8) (2006) 2849–2855.
[7] Z.Y. Zhang, A.V. Nawaby, M. Day, CO_2-delayed crystallization of isotactic polypropylene: a kinetic study, J. Polym. Sci. Pt. B-Polym. Phys. 41 (13) (2003) 1518–1525.
[8] M. Frounchi, S. Dadbin, Z. Salehpour, M. Noferesti, Gas barrier properties of PP/EPDM blend nanocomposites, J. Membr. Sci. 282 (1–2) (2006) 142–148.
[9] X.L. Jiang, J.B. Bao, T. Liu, L. Zhao, Z.M. Xu, W.K. Yuan, Microcellular foaming of polypropylene/clay nanocomposites with supercritical carbon dioxide, J. Cell. Plast. 45 (6) (2009) 515–538.
[10] S.M. Lee, D.C. Shim, J.W. Lee, Rheology of PP/Clay hybrid produced by supercritical CO_2 assisted extrusion, Macromol. Res. 16 (1) (2008) 6–14.
[11] B. Li, G.P. Cao, T. Liu, L. Zhao, W.K. Yuan, Preliminary study on the characteristics of isotactic polypropylene with nucleating agent swollen by supercritical carbon dioxide, Chin. J. Chem. Eng. 13 (5) (2005) 673–677.
[12] H.E. Naguib, C.B. Park, S.W. Song, Effect of supercritical gas on crystallization of linear and branched polypropylene resins with foaming additives, Ind. Eng. Chem. Res. 44 (17) (2005) 6685–6691.
[13] P.D. Hong, W.T. Chung, C.F. Hsu, Crystallization kinetics and morphology of poly(trimethylene terephthalate), Polymer 43 (11) (2002) 3335–3343.
[14] J.D. Hoffman, L.J. Frolen, G.S. Ross, J.I. Lauritzen, Growth-rate of spherulites and axialites from melt in polyethylene fractions – regime-1 and regime-2, J. Res. Natl. Bur. Stand. Sect. a-Physics Chem. 79 (6) (1975) 671–699.
[15] J.I. Lauritze, J.D. Hoffman, Extension of theory of growth of chain-folded polymer crystals to large undercoolings, J. Appl. Phys. 44 (10) (1973) 4340–4352.
[16] J.D. Hoffman, R.L. Miller, Kinetic of crystallization from the melt and chain folding in polyethylene fractions revisited: theory and experiment, Polymer 38 (13) (1997) 3151–3212.
[17] M. Okamoto, T. Inoue, Crystallization kinetics in poly(butylene terephthalate)/copolycarbonate blend, Polymer 36 (14) (1995) 2739–2744.
[18] W. Parrish, B.W. Irwin, Data for X-ray analysis. Volume I. Charts for solution of bragg's equation, J. Franklin Inst. 256 (4) (1953) 391.
[19] B. Li, G.-H. Hu, G.-P. Cao, T. Liu, L. Zhao, W.-K. Yuan, Supercritical carbon dioxide-assisted dispersion of sodium benzoate in polypropylene and crystallization behaviour of the resulting polypropylene, J. Appl. Polym. Sci. 102 (4) (2006) 3212–3220.
[20] J.M. Cervantes-Uc, J.V. Cauich-Rodriguez, H. Vazquez-Torres, L.F. Garfias-Mesias, D.R. Paul, Thermal degradation of commercially available organoclays studied by TGA-FTIR, Thermochim. Acta 457 (1–2) (2007) 92–102.

PAPER IV

A study on the crystallization behavior of electron beam irradiated polypropylene and high-density polyethylene

Krunal Trivedi[a], Petr Svoboda[a,*], Dagmar Svobodova[b], Zdenek Holik[a], Michal Danek[c], Kittisak Jantanasakulwong[d], Toshiaki Ougizawa[d]

[a] Centre of Polymer Systems, Faculty of Technology, Tomas Bata University in Zlin, Nam. T.G. Masaryka 5555, 760 01 Zlin, Czech Republic
[b] Faculty of Humanities, Tomas Bata University in Zlin, Mostni 5139, 760 01 Zlin, Czech Republic
[c] BGS Beta-Gamma-Service GmbH & Co. KG, Fritz-Kotz-Strasse 16, 51674 Wiehl, Germany
[d] Department of Organic and Polymeric Materials, Tokyo Institute of Technology, 2-12-1-S8-33, Ookayama, Meguro-ku, Tokyo 152-8552, Japan

* Corresponding author. Tel. 420–576 031 335, fax. 420–577 210 172.
  E-mail address: svoboda@ft.utb.cz (P. Svoboda)

ABSTRACT:

The influence of e-beam irradiation on polypropylene (PP) and high density polyethylene (HDPE) was investigated with the focus on crystallization. High temperature (200°C) creep test has revealed that HDPE gradually more and more crosslinks in the range 30-120 kGy while PP does not crosslink at all. Mechanical properties were measured in range -150 to 200°C by dynamical mechanical analysis (DMA). Small presence of C=C and C=O bonds was found in irradiated PP by Fourier transform infrared spectroscopy (FTIR). Crystallization kinetics measured by differential scanning calorimetry (DSC) and hot-stage optical microscopy was influenced by irradiation tremendously for HDPE and a little less for PP. Irradiation has caused a decrease in number of nucleation centers and also a decreased growth rate of individual spherulites. Crystallization was analyzed in detail with help of Hoffman-Lauritzen, Avrami and also by Arrhenius equations. Increasing β-crystal formation with increasing irradiation level was discovered for PP by X-ray diffraction (XRD).

Keywords: differential scanning calorimetry (DSC); electron beam irradiation; crystallization; spherulites

INTRODUCTION

The effects of e-beam radiation on polymeric materials can be manifested in one of the three ways. The polymer may undergo one or both of the two possible reactions: those that are molecular weight increasing in nature (crosslinking) or molecular weight reducing in nature (chain scissioning or degradation). During irradiation, chain scissioning occurs simultaneously and competitively with crosslinking, the result being determined by the ratio of the yields of the two reactions. On the other hand, in case of radiation-resistant polymers, no significant change in molecular weight will be observed [1]. In order to predict the behavior of carbon-chain polymers exposed to ionizing radiation, an empirical rule can be used. According to this rule, polymers containing a hydrogen atom at each carbon atom predominantly undergo crosslinking, whereas those polymers containing quaternary carbon atoms and polymers of the $-CH_2-CH_2-$ type, chain scissioning predominates [2]. For some polymers, such as polyvinyl chloride (PVC), polypropylene (PP), and polyethylene terephthalate (PET), both directions of transformation are possible, and certain conditions exist for the predominance of each one.

The crystallization behavior of crystalline polymers is greatly influenced by the molecular structure and crystallization conditions. Subsequently, irradiation treatment of polymer also can change molecular structure and can affect crystallization ability of polymer. Thus, understanding the significance of crystallization behavior of polymers after irradiation treatment is very necessary.

Effect of irradiation on PP has been always an important issue for many years. Commercial linear isotactic polypropylene (iPP) has many desirable and beneficial physical properties such as high stiffness, good resistance to corrosive chemicals and low specific gravity. The molecular structure of linear PP can be significantly modified by electron beam irradiation. The main reactions during the irradiation process are chain scission, chain branching, and crosslinking which can take place simultaneously in the PP. Usually all these reactions coexist. The effect, which predominates, is dependent on several factors, such as chemical structure and morphology of the polymer as well as the irradiation conditions and post treatment. The irradiation of neat PP resin without any additives despite of the formation of few branches predominantly leads to significant decrease in molecular weight due to β-chain scission [3]. In PP, the dominant reactions after formation of free radicals are first β-scission, with molar mass decrease and formation of double bonds. Furthermore, the addition of free radicals to the double bonds takes place with formation of chain branching followed by increase in molar mass. Additionally, a

disproportionation or recombination reaction of two polymer radicals occurs followed by changed molar masses.

The crystallization of irradiated polyethylene has distinctly different co-existing chain configurations because of the polycrystalline and partially crystalline character of the system. Ungar and Keller (1980) [4] has studied the effect of radiation on crystals of PE and paraffins. They reported destruction of crystalline structure of PE above certain dose where the radiation temperature approaches the temperature of orthorhombic-hexagonal transition.

A lot of work has been done on physical and mechanical studies on irradiated PP [5-11] or HDPE [12-14] with or without any filler or blends and with different irradiation sources [15-21]. But, none of them considered working on ability to crystallize with the same irradiation technique for both polymers and their outcomes as ability to crosslink or chain scission.

This research aims to investigate the crystallization behavior of polypropylene (PP) influenced by electron beam irradiation and compare it with electron beam irradiated high-density polyethylene (HDPE).

EXPERIMENTAL

The Polypropylene copolymer with trade name C766-03 was supplied by Dow chemical (Europe) and high-density polyethylene with trade name HTA-002 supplied by ExxonMobil chemical. The main characteristics of both materials as supplied in the manufacturers' data sheets are collected in Table 1.

Polypropylene and high-density polyethylene sheets were prepared by compression molding at 200°C for 6 min and at 150°C for 5 min, respectively. Beta (electron beam) irradiation was performed on PP and HDPE sheets (sample size was 12x6x0.6 mm) in normal air at room temperature, in BGS Beta-Gamma-Service GmbH, Germany. It was made sure that the temperature did not exceed 50°C. Source of radiation was toroid electron accelerator Rhodotron (10 MeV, 200 kW). The irradiation was carried out in a tunnel on a continuously moving conveyer with the irradiation dosage ranging from 30-120 kGy; in steps of 30 kGy per pass.

Tensile samples were cut out of the unirradiated and irradiated sheets and used for the tensile creep experiments according to ISO 899 standard. Creep behavior was studied in Memmert oven with temperature control being +2°C. Creep was recorded by a camera (Sony-SLT-A33 which capable of HD video (1920x1080

pixels) at 25fps) for further analysis. Effect of high temperature (200°C) at stress level 0.1MPa on creep behavior of irradiated and unirradiated polypropylene (PP) and high-density polyethylene (HDPE) were studied.

The crystallization kinetics of the samples was analyzed using a Perkin-Elmer DSC-1. Temperature calibration was performed using the indium standard. A nitrogen atmosphere was employed during the experiment at a flow rate 20 mL min^{-1}. For isothermal crystallization, the samples were heated to 200°C (at 100°C min^{-1} heating rate) and then cooled (at 50°C min^{-1}) to the isothermal crystallization temperature (118-135°C). In all cases, samples were held at the 200°C for 1 min to eliminate any previous thermal history. From DSC, in order to evaluate the relative degree of crystallinity (X) of irradiated and nonirradiated samples, the follow equation was used:

$$X = \frac{\Delta H}{\Delta H_{100}} \times 100$$

where ΔH is the heat of crystallization of the PP or HDPE and ΔH_{100} is the value of heat of crystallization for 100% crystalline PP or HDPE ($\Delta H_{100} = 207$ J g^{-1} for PP and $\Delta H_{100} = 293$ J g^{-1} for HDPE).

Irradiated and pristine polypropylene's spherulites growth was observed by hot-stage optical microscopy. The specimen was melt-pressed for 1-2 min between two cover glasses on a hot stage at 200°C. The melted specimen was then placed onto a LINKAM hot stage of the microscope set to desired temperature in range 130-140°C. Structural development during the isothermal annealing was observed under the optical microscope (LMU-406 SP) equipped with a video recording system.

Dynamic mechanical measurements were carried out on a dynamic mechanical analyzer ITKeisoku-seigyo (DVA-200S). The samples were measured in cyclic tensile strain mode with a frequency of 10 Hz. The heating rate was 5 °C/min in the temperature range -150–200 °C.

The FTIR study was carried out by the Nicolet 320 Avatar FT-IR spectrometer in ATR mode. The sheets were scanned from 4000 to 400 cm^{-1} with scanning number 64.

An X-ray diffractometer, X'Pert PRO from PANalytical, was used to analyze the PP and HDPE sheets with the scanning range of 5–30° (2θ).

THEORETICAL BACKGROUND

Avrami analysis

Whenever a polymer crystallizes, the extent of the phase transformation depends on the crystallizing species and the experimental conditions. High molecular weight polymers do not crystallize completely because of topological constraints that lower crystallinity considerably. The classical isothermal transformation kinetics, initially formulated by Kolmogorov and Goler et al. were extended later by the Avrami theory that was initially formulated for metals and later modified.

The crystallization kinetics of polymers can be analyzed using a classical Avrami equation as given in Eq. (1) [22]:

$$1 - X_t = exp(-kt^n) \qquad (1)$$

where k is the Avrami rate constant and n is the Avrami exponent. Both k and n depend on the nucleation and growth mechanisms of spherulites.

The fraction X_t is obtained from the area of the exothermic peak in DSC isothermal crystallization analysis at a crystallization time t divided by the total area under the exothermic peak:

$$X_t = \frac{\int_0^t \left(\frac{dH}{dt}\right) dt}{\int_0^\infty \left(\frac{dH}{dt}\right) dt} \qquad (2)$$

where the numerator is the heat generated at time t and the denominator is the total heat generated up to complete crystallization.

In order to deal conveniently with the operation, Eq. (1) is usually rewritten as the double logarithmic form as follows:

$$ln[-ln(1 - X_t)] = \ln k + n \ln t \qquad (3)$$

The k and n values can be directly obtained using Eq. (3) from the slope and intercept of the best-fit line.

Hoffman-Lauritzen analysis

The crystallization behavior of the polymers was also studied according to the

relationship between chain folded crystal growth rates and undercooling proposed by Hoffman and Lauritzen [23, 24]:

$$G = G_0 \, exp \left[\frac{-U^*}{R(T_c - T_\infty)} - \frac{K_g}{T_c(\Delta T)f} \right] \qquad (4)$$

where G is the crystal growth rate, U^* is a constant characteristic of the activation energy for repetitive chain motion and is equal to 1500 cal mol^{-1}, R is the gas constant, T_c is the crystallization temperature (K), $T_\infty = T_g-30K$ (for PP the glass transition temperature $T_g=270$ K), $\Delta T = T_m^0-T_c$, T_m^0 is the equilibrium melting temperature of an infinitely thick crystal, K_g is the nucleation constant, f is a correction factor and equals to $2T_c/(T_m^0 + T_c)$ and G_0 is a pre-exponential factor.

$$ln(G) + \frac{U^*}{R(T_c - T_\infty)} = ln \, G_0 - \frac{K_g}{T_c \Delta T f} \qquad (5)$$

Arrhenius Equation

Svante Arrhenius recognized that the typical temperature dependence indicates an exponential increase of the rate, or rate constant, with temperature, which can be conveniently written as,

$$\ln k = Ae^{-\frac{E_a}{RT}} \qquad (6)$$

where A is called the preexponential factor, R is the universal gas constant (8.314 J K^{-1} mol^{-1}), T is absolute temperature in K and E_a is known as the activation energy. With this notation, one writes the logarithmic form of Eq. (6)

$$\ln k = -\frac{E_a}{RT} + \ln A \qquad (7)$$

The empirical constants E_a and A can be deduced from the slope and intercept of a graph of logarithmic k-versus-1/T plot [25]. In our case of crystallization of PP and HDPE in temperature range 120-140°C, we observed exponential decay (as opposed to increase) but the regression according to Arrhenius equation gave us the best result.

RESULTS AND DISCUSSION

Figure 1(a-b) shows high temperature (200°C) creep results for polypropylene copolymer (PP) and high-density polyethylene (HDPE) under a constant stress of

0.1 MPa for various irradiation doses. In Fig. 1(a) it is illustrated that PP samples stretched all the way at 200°C within 55s regardless of irradiation dose (only samples with 0 and 120kGy are shown). Apparently irradiation did not cause crosslinking in case of PP even though it is not pure PP but contains small amount of ethylene copolymer. In contrast with PP, the HDPE (see Fig. 1(b)) exhibits very different high temperature creep results. Even slightly irradiated HDPE (30kGy) demonstrates some resistance to creep. This resistance to creep is gradually improving with increasing radiation level. Apparently irradiation is very effective way to crosslink polyethylene and in observed range of irradiation 30-120kGy the improvement of crosslinking is very systematic. As a result we have two irradiated samples PP and HDPE that could show quite different crystallization behavior. And this detailed crystallization behavior study for two very different materials is the main subject of this paper.

Before coming to the crystallization kinetics study we have investigated mechanical properties in wide temperature range (-150 to 200°C) with the help of dynamical mechanical analysis (DMA). Storage modulus (see Fig. 2) of these two materials is very similar till about 100°C, then HDPE losses its mechanical properties at about 130°C, for PP this transition locates at about 150°C. At the temperatures below melting point there was not a great difference in pure samples versus the irradiated ones. DMA analysis renders also the tanδ curves that are shown on Fig. 3. HDPE has T_g at around -130°C (no effect of irradiation on T_g) and exhibits lower tanδ values for 120kGy sample in temperature range 50-100°C. One can expect better elasticity (lower tanδ) for crosslinked sample. In contrast PP had two tanδ peaks, at about -50 and +10°C. Presence of two T_g is usually interpreted as evidence of immiscibility of two polymers. The detailed composition of the PP is the company's secret and is a part of a knowhow how to improve the toughness of the PP at low temperatures. We can speculate that comonomer ethylene was added to propylene and small amount of ethylene-propylene copolymer was created during polymerization. According to DMA results this ethylene-propylene copolymer is immiscible with PP homopolymer. The irradiation has caused quite significant change in the two tanδ peaks. The one at -50°C increased and the one at +10°C decreased. The interpretation of this behavior could be that some chemical reaction happened at the interface and also inside the phases rendering a little bit different chemical and morphological structure. The increase of tanδ in temperature range 30-120°C is most likely connected with lower elasticity caused by chain scission.

FTIR is quite powerful technique in detection of chemical changes that might be happening with these polymers during irradiation. While we haven't found almost any changes in FTIR spectrum for HDPE (see Fig. 4b) there was a small but detectable change for PP (see Fig. 4a) in 1500-1800 cm^{-1} range. The range 1600-1700cm^{-1} is usually connected with C=C bond and the area 1700-1770cm^{-1} with C=O in aldehydes, ketones or in carboxylic acids. It is perceivable that chain scission leads to a C=C in the end of a chain and that small presence of oxygen could react with macroradical rendering C=O bond. Bearing in mind the results from high temperature creep, DMA and FTIR we will now focus on the crystallization behavior.

The crystallization was studied at first by DSC and then also by optical microscopy. Initially the samples with weight about 10-15 mg were heated from room temperature to 200°C at rate 100 °C/min, then the temperature was kept constant for 1 min to fully melt the PP or HDPE crystals (T$_m$ of PP is about 165 °C and T$_m$ of HDPE is about 134°C). The next step was a fast cooling to the desired isothermal crystallization temperature (in range 118-136°C). This cooling at rate 50 °C/min was attained by a cooling unit capable of cooling to -130 °C. The last step was the isothermal crystallization at the desired temperature. The time when the heat flow curve reaches the minimum value and then starts to grow to form an exothermal peak, was assigned to be 0. By the integration of the heat flow curve one can get a relative crystallinity curve. When the crystallinity reaches 0.5 (or 50%), half time of crystallization $\tau_{1/2}$ is calculated. Then the crystallization kinetics can be expressed as $\tau_{1/2}^{-1}$. Results of this analysis are shown in Fig. 5. Both polymers exhibit decrease in bulk crystallization kinetics with increasing irradiation level. It is clear that HDPE is much more affected than PP; in case of HDPE the $\tau_{1/2}^{-1}$ dropped from about 0.52 to about 0.03 min^{-1} while in case of PP the decrease was much more moderate (from 0.3 to 0.13 min^{-1}), compared were values for 0 and 120kGy. Apparently after the crosslinking the mobility (or diffusion rate) of macromolecules toward the crystallizing front of the lamella is considerably slowed down. Some of the crosslinked molecules could be completely prevented from participation in crystalline phase. This can be deduced form the crystallinity vs. irradiation plot (see Fig. 6). In contrast the crystallinity of PP was not changed by irradiation.

The bulk crystallization measured by DSC was analyzed also by Avrami *Eq. 1*, see Fig. 7 and Table 2. There is a tremendous difference in crystallization kinetics expressed as *k* parameter for HDPE. In case of PP initially there is a notable decrease coming from 0 to 60kGy, then the decrease in kinetics is much smaller;

8

these results correspond well with the ones shown on Fig 5. Additional parameter obtained from Avrami analysis is n. There is quite a difference between HDPE and PP (2.2 vs. 2.7) but not significant difference between pure and irradiated samples. The n parameter is usually being connected with two or three dimensional growth. Apparently irradiation does not influence in how many dimensions crystals grow. In Table 2 PP was crystallized at 127°C. We have done crystallization at other temperatures (121-131°C) and evaluated by Avrami equation. The results are presented in Table 3. The k parameter is always decreasing with increasing crystallization temperature. The n parameters for PP_{0kGy} as value around 2.2 while for PP_{120kGy} the n value slightly higher (range 2.52-2.84).

While Fig. 5 compares the crystallization kinetics at fixed temperature for different irradiation levels Fig. 8 shows the dependence of crystallization kinetics on temperature only for pure PP and PP_{120kGy}. Again the PP_{120kGy} is slower for all evaluated temperatures and the kinetics increases exponentially with decreasing temperature. DSC is very powerful technique for evaluation of bulk crystallization kinetics. However, from the DSC measurement it is not clear if the decrease in crystallization kinetics comes from smaller number of nucleation centers or slowly growing spherulites or perhaps both. Hot stage optical microscopy can clarify these questions.

Figure 9 illustrates growth of spherulites observed by optical microscopy at 140°C. It is clear that pure PP and irradiated to 30kGy have much more spherulites in observed area than samples irradiated to 60, 90 and 120kGy. Increased level of irradiation has caused decrease in number of nucleation centers. This result agrees well with the bulk crystallization kinetics decrease observed by DSC that was shown in Fig. 5. For pure PP and PP irradiated by 30kGy the space is filled very quickly with small spherulites that truncate to each other and then the crystallization stops. Most likely in pure PP the macromolecules do not move very far from the original position during 1 min 200°C melting. The memory of original chain positions remains and makes the nucleation step easier. On the other hand the irradiation 60-120kGy has apparently caused some damage to the supramolecular structure of the macromolecules. The chain scission or branching influenced the ability of chains to fold to a lamellar structure. This is manifested by much smaller number of nucleation centers and also by slower radial growth of individual spherulites. The decrease of growth rate of individual spherulites is quantitatively illustrated in Fig. 11. At all crystallization temperatures the growth rate gradually decreased with increasing radiation level.

The crystallization kinetics of individual spherulites was evaluated in temperature range 130-140°C. An example of this analysis is shown in Fig. 10 for PP irradiated to 90kGy. While at 130°C it took only 7 min to grow about 100μm spherulites, at 140°C the same thing took about an hour. Hence the influence of crystallization temperature is very significant. The strong influence of crystallization temperature is nicely visible in Fig. 12 where the dependence of G on T_c was fitted best by Arrhenius equation (*Eq. 6*).

Initially we have performed the analysis by linear regression of the Arrhenius equation in logarithm form, *Eq. 7* which gave us estimated parameters E_a and A. This linear regression is shown in the insert of Fig. 12. Then these estimated parameters E_a and A were used for much more precise non-linear regression analysis shown in Fig. 12. This non-linear analysis has revealed decrease in activation energy with increasing radiation level (see Table 4) which is mainly caused by a considerable decrease in crystallization kinetics of PP_{60kGy} and PP_{120kGy} samples at lower crystallization temperatures. Again there is a large difference in activation energy between samples PP_{0kGy} and PP_{60kGy} compared to PP_{60kGy} and PP_{120kGy}.

Hoffman-Lauritzen analysis of crystallization was performed for PP samples measured by optical microscopy (see Fig. 13). This analysis revealed two crystallization regimes, II and III with transition being at around 136-138°C. Table 4 summarizes the results of HL analysis. Again the $\ln G_0$ terms (corresponding to kinetics) are decreasing with radiation dosage while the K_g parameters were not influenced much by the irradiation.

In addition to crystallization kinetics analysis performed by DSC and optical microscopy we have analyzed the crystalline structure also by XRD analysis. Fig. 14 shows that irradiation has caused a decrease in intensity of two XRD peaks for HDPE which is in good agreement with lower crystallinity observed by DSC after 2nd melting (see Fig. 6). The peak intensity decreases but also apparently the peaks shift to lower angles. However, this can be explained by the destruction of smaller crystals by radiation (larger crystals remained). Situation was quite different in case of PP (see Fig. 15). The large peaks did not change almost at all which well corresponds with unchanged crystallinity shown on Fig. 6. However we found an interesting increase in peak for β-phase. Apparently irradiation helps with generation of β-phase till about 60kGy, then the intensity at $2\theta=16°$ starts to decrease again (see Fig. 15 b and c).

CONCLUSIONS

We found that e-beam irradiation causes crosslinking in HDPE but does not cause crosslinking in case of PP. This was clearly demonstrated by high temperature (200°C) creep test. DMA's tanδ curves confirmed these results. FTIR has pointed out on presence of C=C and C=O bond in PP after irradiation. Crystallization kinetics study revealed tremendous decrease in crosslinked HDPE and rather moderate decrease in case of PP. Also while crystallinity was unchanged for PP, for HDPE decreased by irradiation significantly (from 60 to 47%). Optical microscopy clearly illustrated smaller number of nucleation centers after irradiation and also decreased rate of crystallization of individual spherulites. XRD analysis exposed lower crystallinity for HDPE and very interesting increase of β-phase in case of PP with maximum being at 60kGy.

ACKNOWLEDGEMENTS

REFERENCES

[1] S. Ajit, *Radiat. Phys. Chem.*, **60**, 453 (2001).

[2] V.S. Ivanov, *Radiation chemistry of polymers*, VSP, (1992).

[3] H. Otaguro, L.F.C.P. de Lima, D.F. Parra, A.B. Lugão, M.A. Chinelatto and S.V. Canevarolo, *Radiat. Phys. Chem.*, **79**, 318 (2010).

[4] A. Keller and G. Ungar, *Radiat. Phys. Chem., (1977)*, **22**, 155 (1983).

[5] B. Krause, D. Voigt, L. Haussler, D. Auhl and H. Munstedt, *J. Appl. Polym. Sci.*, **100**, 2770 (2006).

[6] B. Krause, L. Häußler and D. Voigt, *J. Appl. Polym. Sci.*, **100**, 634 (2006).

[7] S.M. Pawde and S. Parab, *J. Appl. Polym. Sci.*, **119**, 1220 (2011).

[8] A.-H. H.M, *Solid-State Electron.*, **49**, 1163 (2005).

[9] G. Przybytniak, K. Mirkowski, A. Rafalski, A. Nowicki, I. Legocka and Z. Zimek, *Nukleonika*, **50**, 153 (2005).

[10] Z.A. Kadir, F. Yoshii, K. Makuuchi and I. Ishigaki, *Radiat. Phys. Chem.*, **39**, 535 (1992).

[11] M.L. Cerrada, V. Rodríguez-Amor and E. Pérez, *J. Polym. Sci., Part B: Polym. Phys.*, **45**, 1068 (2007).

[12] A. Zaydouri and M. Grivet, *Radiat. Phys. Chem.*, **78**, 770 (2009).

[13] S. Wu, H. Sang, Z. Liu and J. Shen, *J Macromol Sci A*, **41**, 1311 (2004).

[14] H.A. Khonakdar, S.H. Jafari, M. Taheri, U. Wagenknecht, D. Jehnichen and L. Häussler, *J. Appl. Polym. Sci.*, **100**, 3264 (2006).

[15] L.X. Tang, M.G. Yan and B.J. Qu, *J. Appl. Polym. Sci.*, **99**, 2068 (2006).

[16] S. Ahmed and A.A. Basfar, *Nucl. Instrum. Methods Phys. Res. Sect. B-Beam Interact. Mater. Atoms*, **151**, 169 (1999).

[17] P. Castell, F.J. Medel, M.T. Martinez and J.A. Puertolas, *J. Nanosci. Nanotechnol.*, **9**, 6055 (2009).

[18] M.M. Hassan, N.A. El-Kelesh and A.M. Dessouki, *Polym. Compos.*, **29**, 156 (2008).

[19] K. Sen and P. Kumar, *J. Appl. Polym. Sci.*, **55**, 857 (1995).

[20] M. Obadal, R. Cermak, M. Raab, V. Verney, S. Commereuc and F. Fraisse, *Polym. Degrad. Stabil.*, **88**, 532 (2005).

[21] C.H. Jung, J.H. Choi, P.H. Kang and Y.C. Nho, *J. Ind. Eng. Chem.*, **13**, 1131 (2007).

[22] P.D. Hong, W.T. Chung and C.F. Hsu, *Polymer*, **43**, 3335 (2002).

[23] J.D. Hoffman, L.J. Frolen, G.S. Ross and J.I. Lauritzen, *J. res. Nat. Bur. Stand. Sect. A. Phys. chem.*, **79**, 671 (1975).

[24] J.I. Lauritzen and J.D. Hoffman, *J. Appl. Phys.*, **44**, 4340 (1973).

[25] G.M. Barrow, *Physical Chemistry*, McGraw-Hill, Singapore, (1988).

TABLE 1 – Properties of pure materials

	Polypropylene copolymer C766-03	**High-density polyethylene HTA 002**
Melt flow rate	3.5 g/10 min (ISO 1133)	0.15 g/10 min (ASTM D1238)
Flexural modulus	1.156 GPa (ISO 178)	-
Charpy impact strength	10 KJ/m^2 at 23°C (ISO 179)	-
Density	-	0.952 g/cm^3 (ExxonMobil Method)

TABLE 2 – Avrami parameters from DSC

Samples	T_c (°C)	**0kGy**		**60kGy**		**120kGy**	
		n	**k (m^{-1})**	**n**	**k (m^{-1})**	**n**	**k (m^{-1})**
PP	127	2.59	0.0211	2.70	0.0034	2.58	0.0030
HDPE	122	2.07	0.1070	2.20	0.0050	2.24	0.0004

TABLE 3 – Avrami parameters for PP from DSC

Radiation dose (kGy)	Crystallization Temperature (°C)									
	121		123		125		129		131	
	n	k (m^{-1})	n	k (m^{-1})	n	k (m^{-1})	n	k (m^{-1})	n	k (m^{-1})
0	-	-	-	-	2.27	0.1076	2.34	0.0089	2.16	0.0039
120	2.52	0.1065	2.68	0.0217	2.84	0.0053	-	-	-	-

TABLE 4 – Hoffman-Lauritzen parameters and activation energy by Arrhenius plot from optical analysis

Radiation dose (kGy)	Regime III		Regime II		E$_a$ (kJ mol^{-1})
	K$_g$ x10^{-5} (K^2)	lnG$_0$	K$_g$ x10^{-5} (K^2)	lnG$_0$	
0	3.05	13.83	1.60	5.75	303
60	2.73	12.00	1.42	4.55	286
120	2.76	11.87	1.15	2.75	275
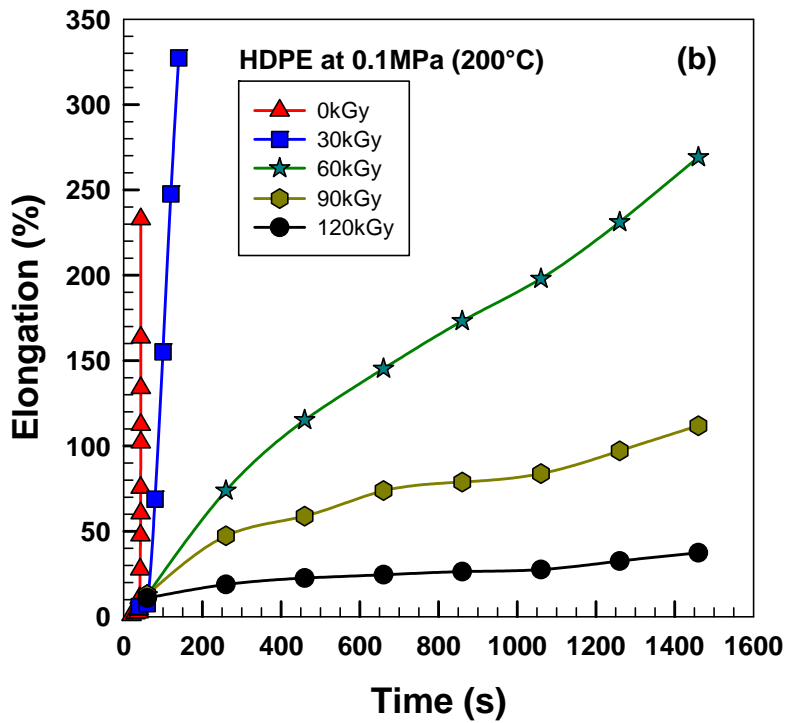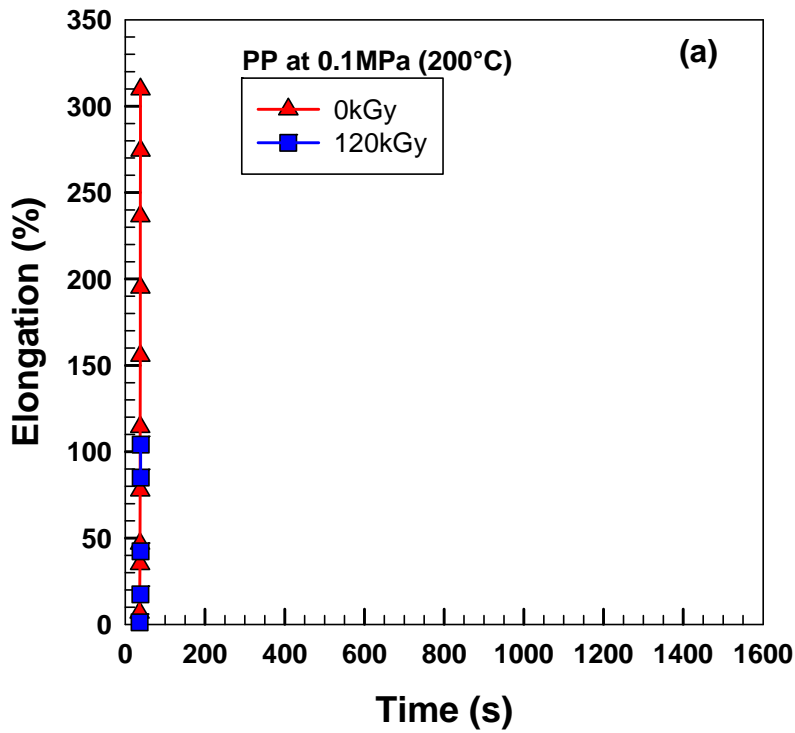
FIG 1. Plot of elongation versus time for (**a**) PP and (**b**) HDPE at 200°C and stress of 0.1MPa for various irradiation doses.
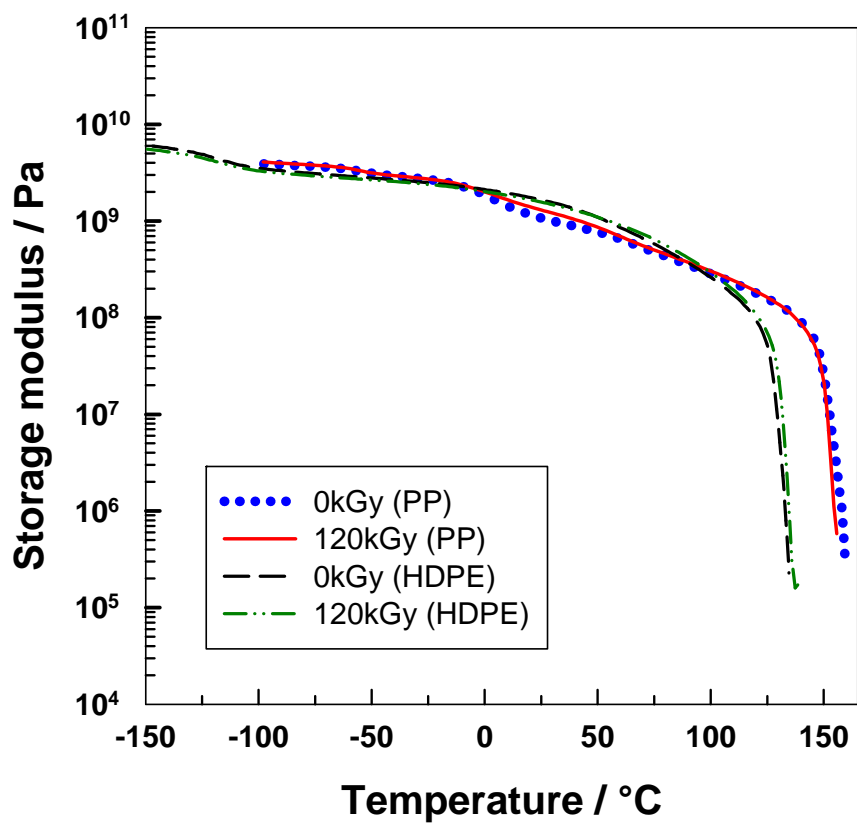
FIG 2. Storage modulus curves as a function of temperature for PP and HDPE.
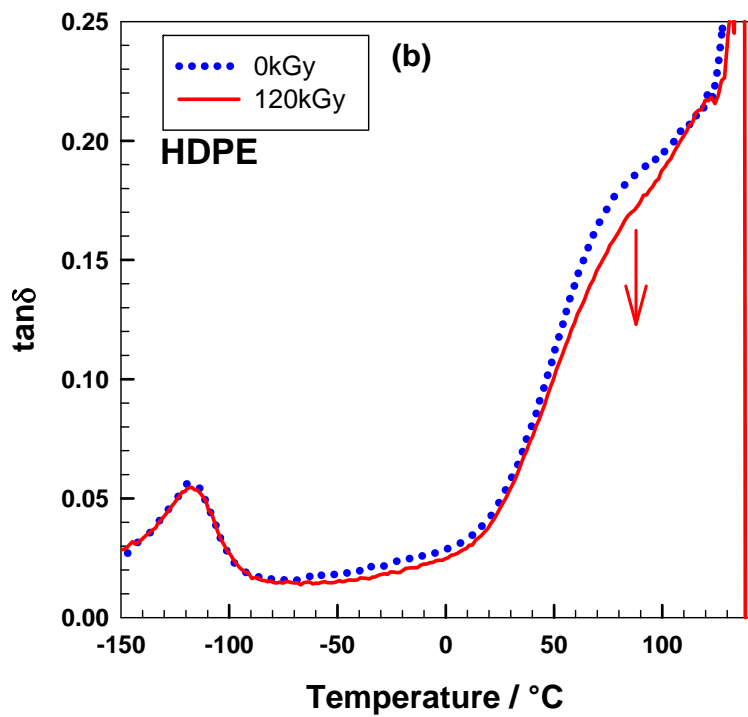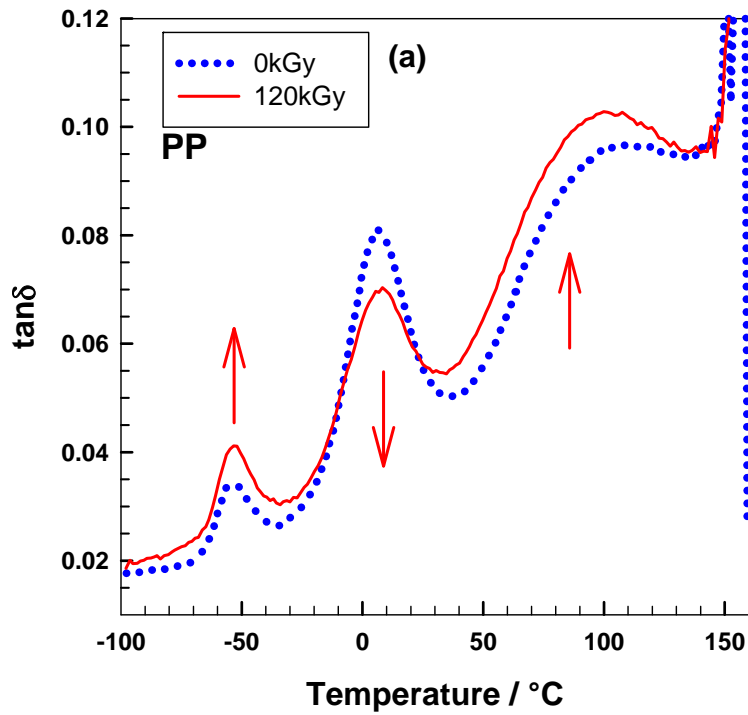
FIG 3. tanδ curves as function of temperature for **(a)** PP and **(b)** HDPE.
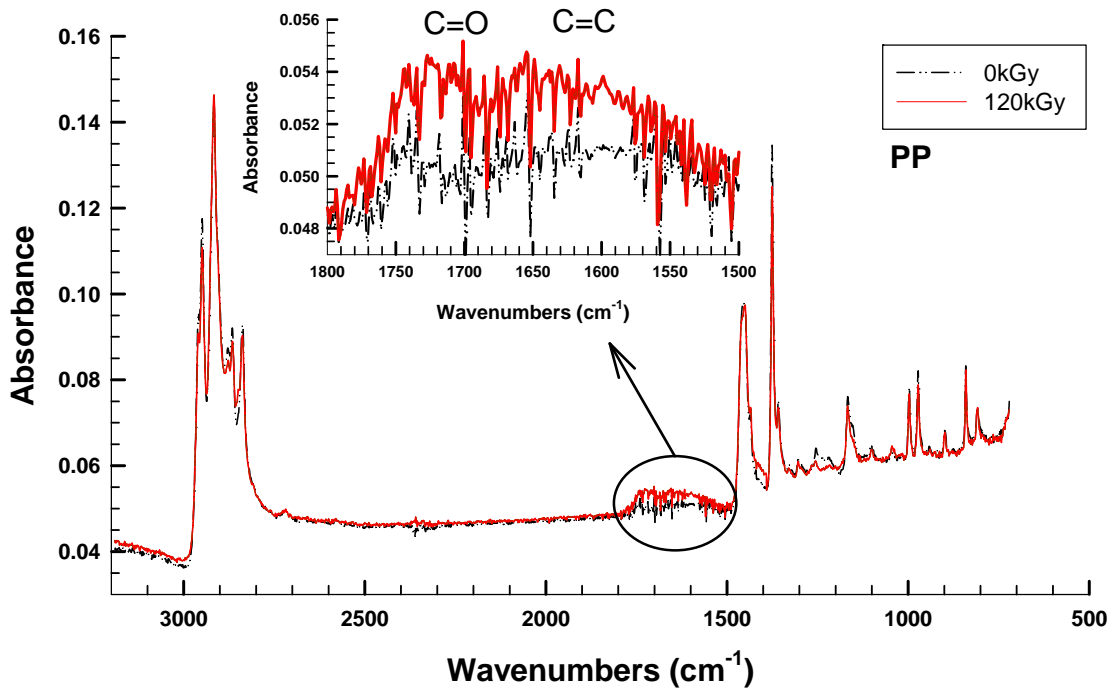
FIG 4a. FTIR spectrum for PP with: 0kGy and 120kGy.
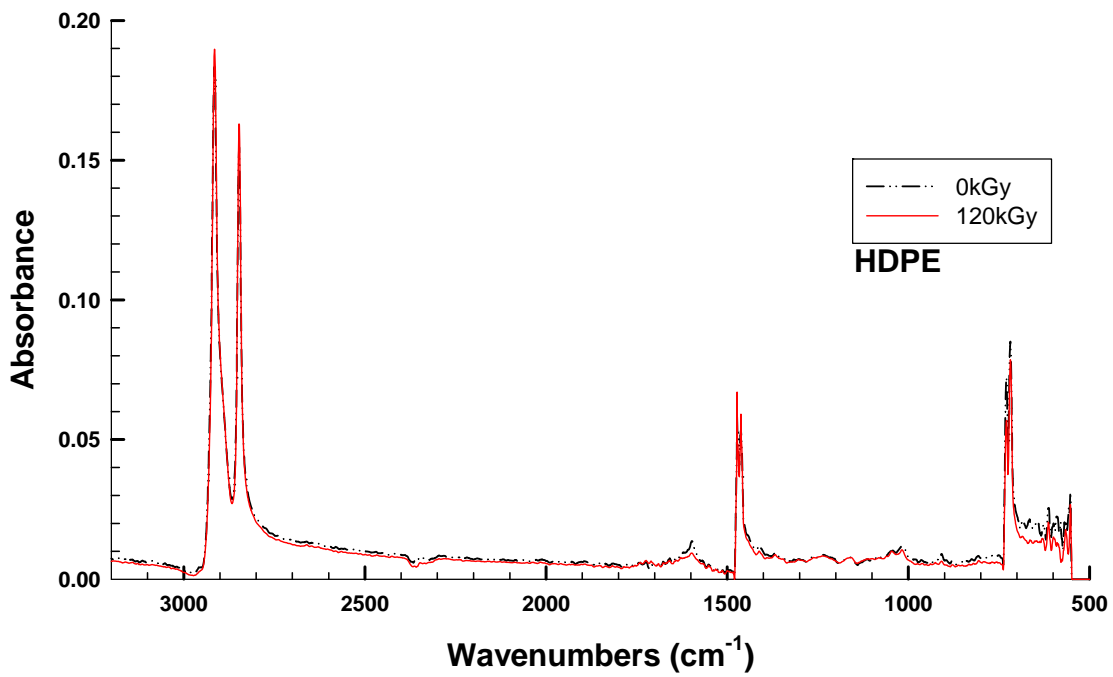
FIG 4b. FTIR spectrum for HDPE with: 0kGy and 120kGy.
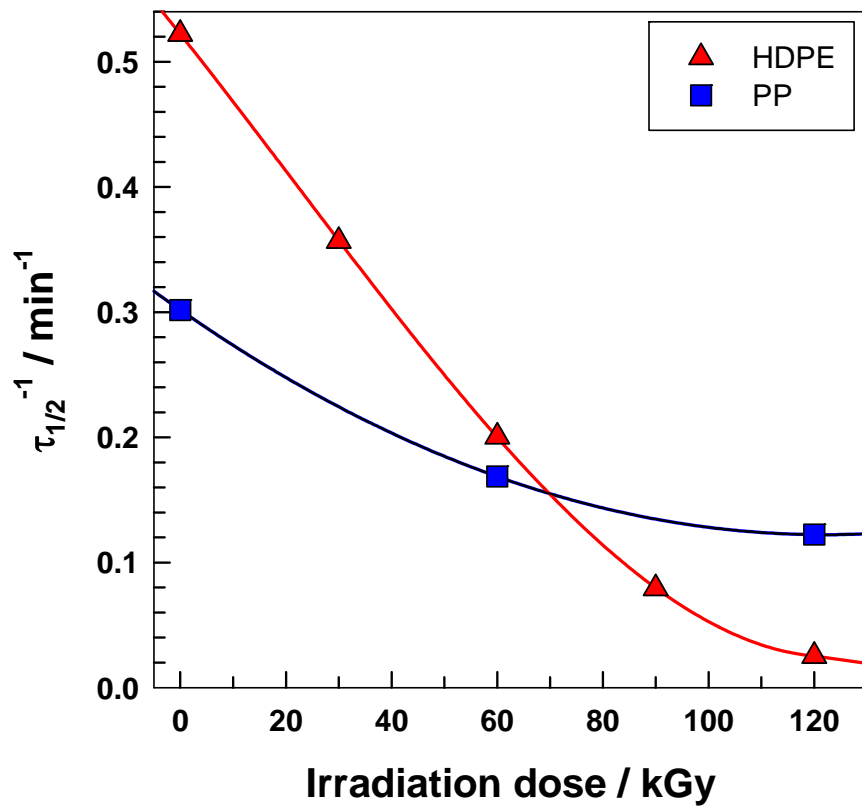
FIG 5. Crystallization kinetics versus irradiation dose (kGy) for PP (T_c = 127°C) and HDPE (T_c = 122°C) from DSC.
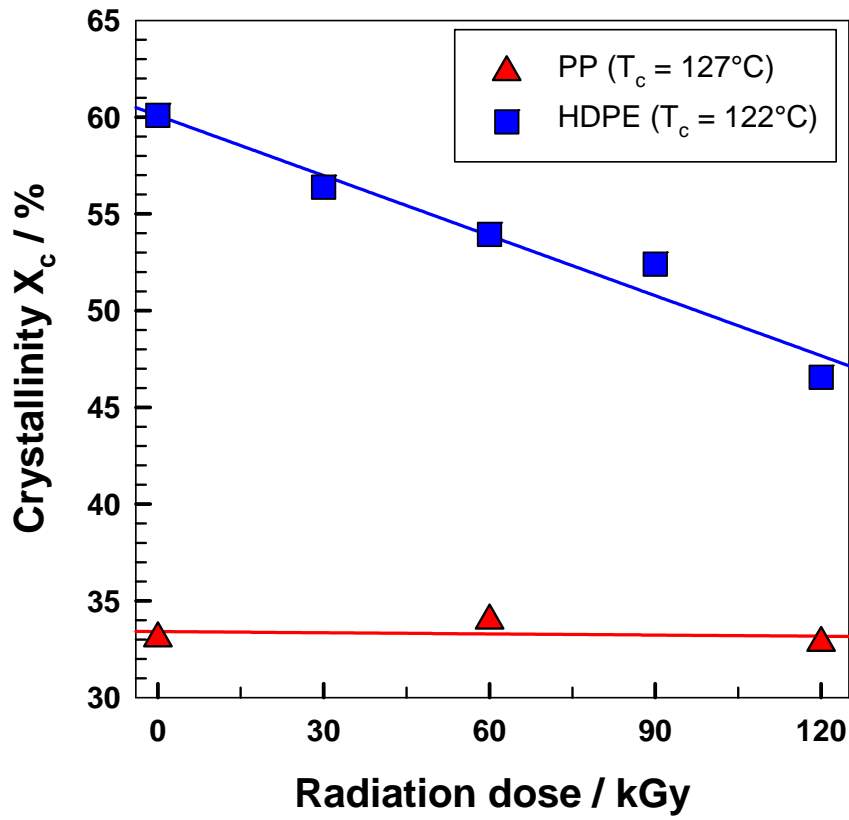
FIG 6. Crystallinity (X_c) (after 2nd heating) versus irradiation dose (kGy) for PP (T_c = 127°C) and HDPE (T_c= 122°C) from DSC.
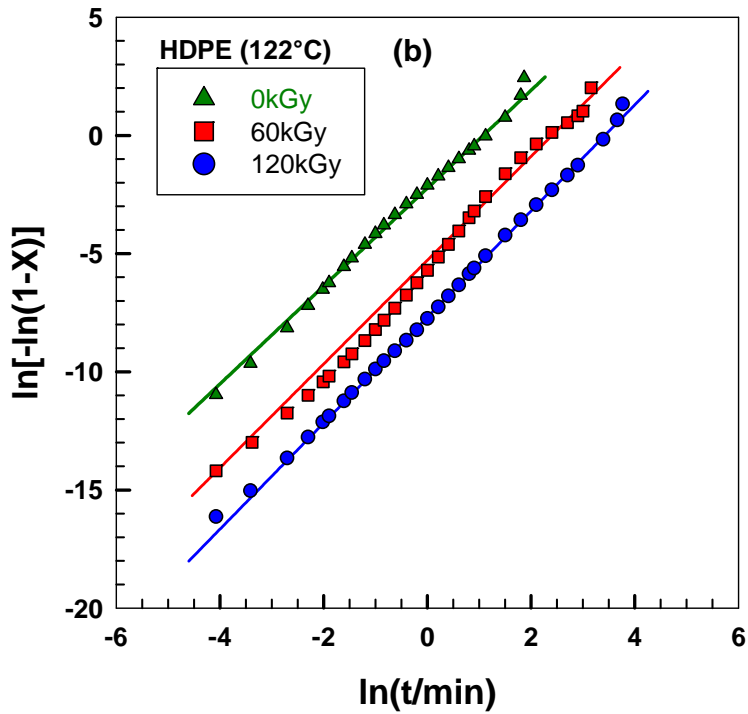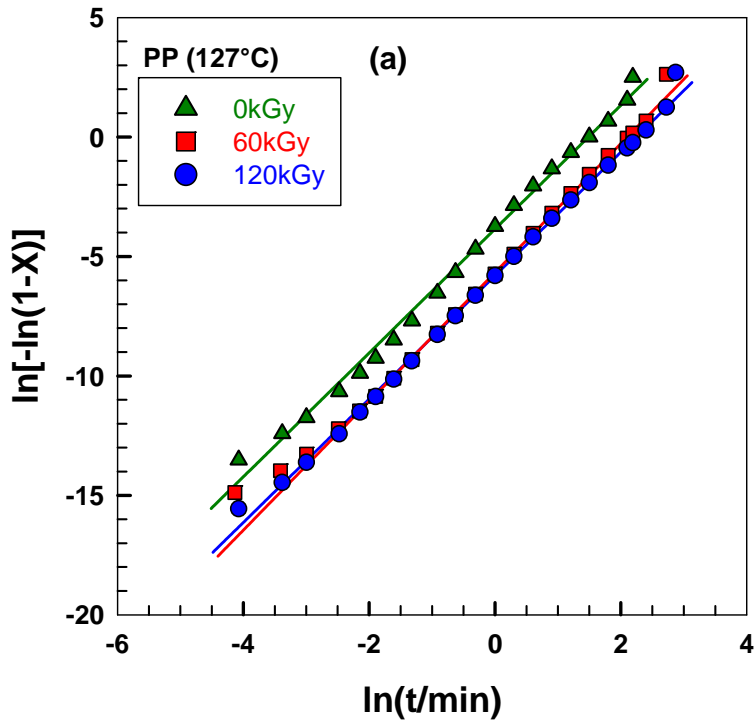
FIG 7. Avrami plots for PP and HDPE at various irradiation doses (kGy) from DSC.
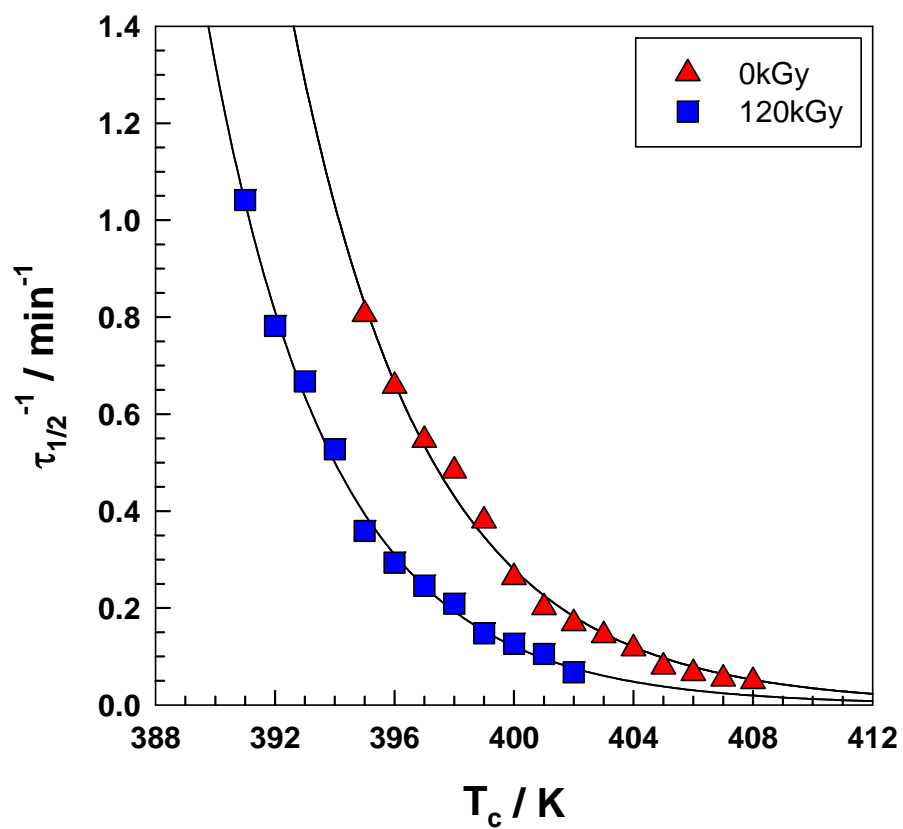
FIG 8. Crystallization temperatures versus crystallization kinetics plot for PP from DSC.
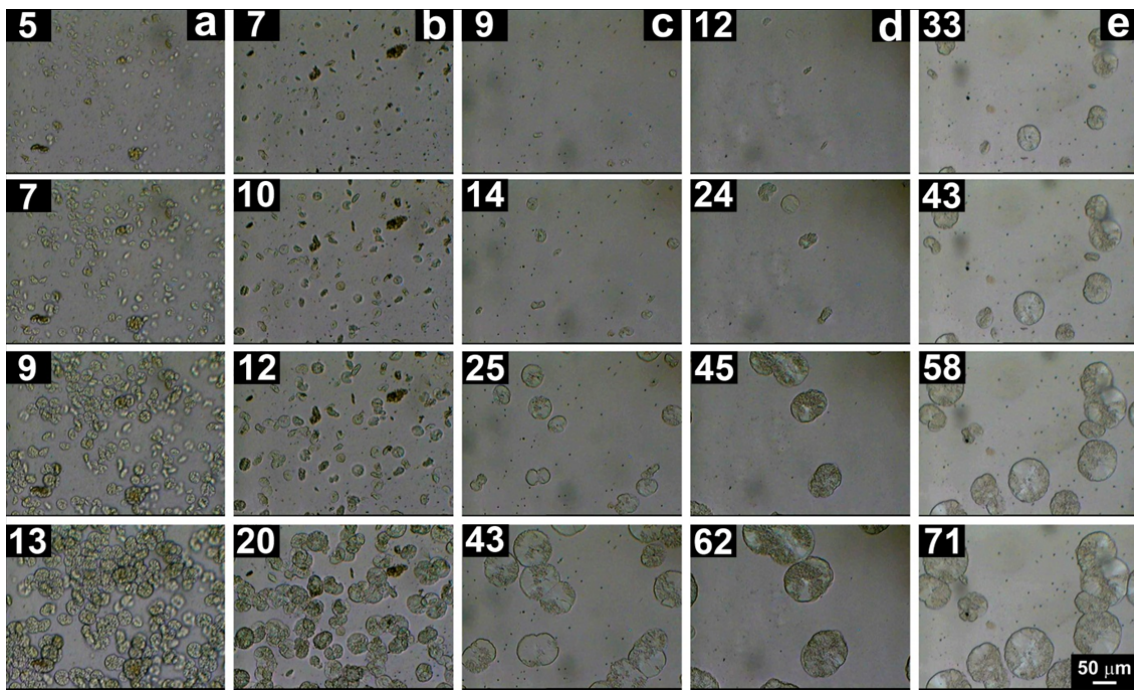
FIG 9. Growth of spherulites in time at $T_c = 140°C$ for various irradiation dose **(a)** 0kGy, **(b)** 30kGy, **(c)** 60kGy, **(d)** 90kGy, and **(e)** 120kGy for PP by hot-stage optical microscopy after 1 min pre-heating at 200°C (Number in upper left corner mean time of crystallization in min).
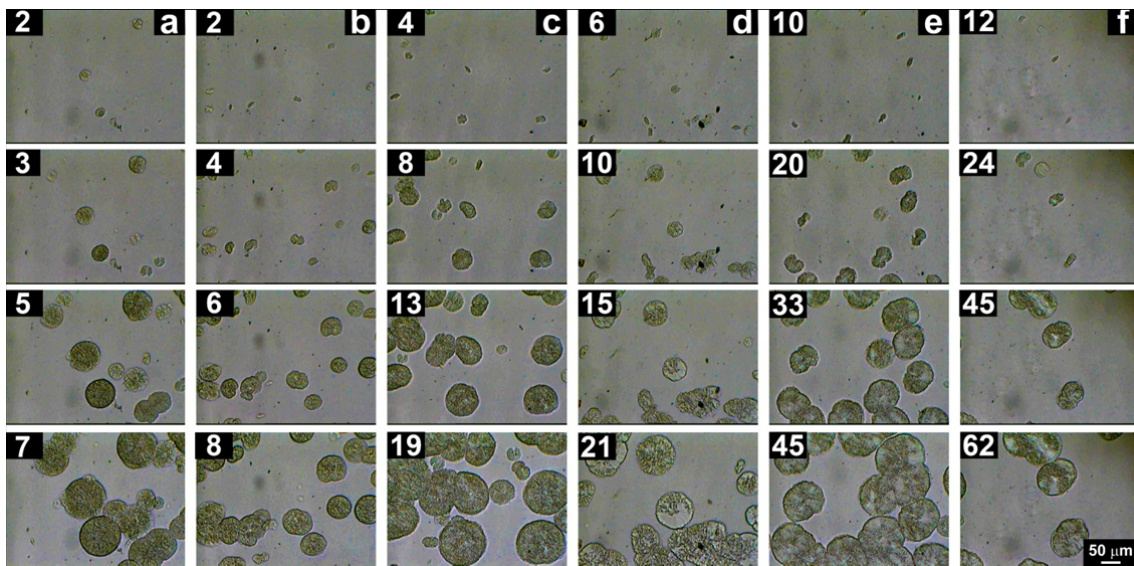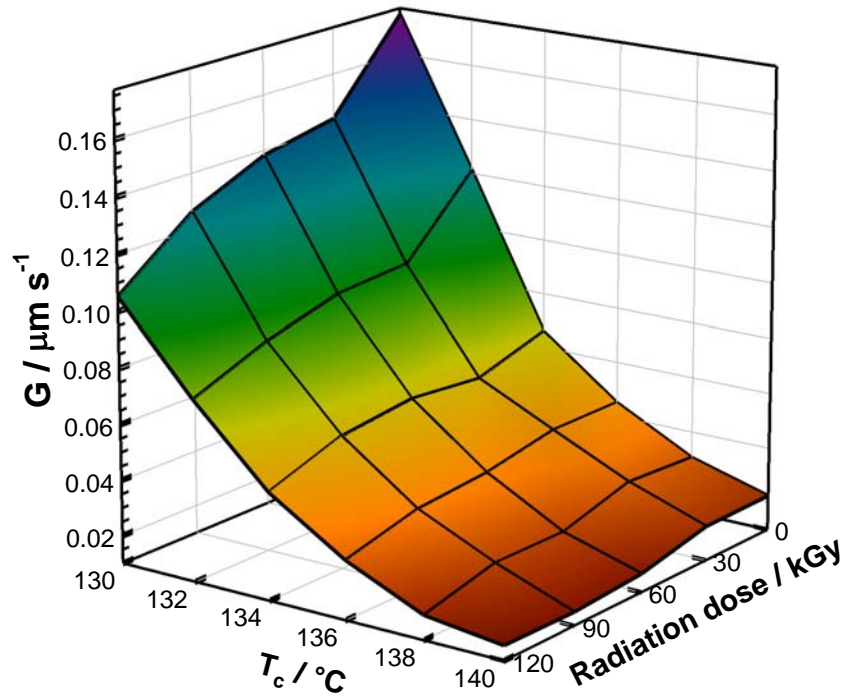
FIG 10. Growth of spherulites in time at 90kGy at various crystallization temperatures **(a)** 130°C, **(b)** 132°C, **(c)** 134°C, **(d)** 136°C, **(e)** 138°C and **(f)** 140°C for PP by hot-stage optical microscopy after 1 min pre-heating at 200°C (Number in upper left corner mean time of crystallization in min).

FIG 11. Spherulites growth rate as a function of crystallization temperature (T_c) and irradiation dose for PP from optical microscopy analysis.
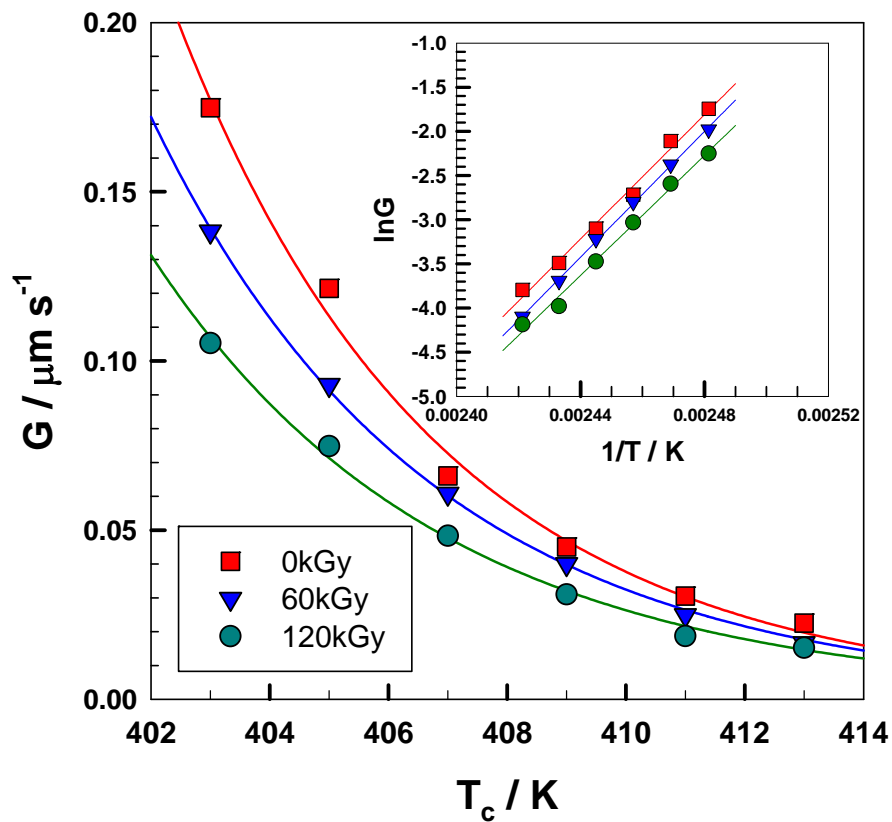
FIG 12. Spherulites growth rate (G) versus Crystallization temperatures (K) for PP at various irradiation doses (kGy) from optical analysis.
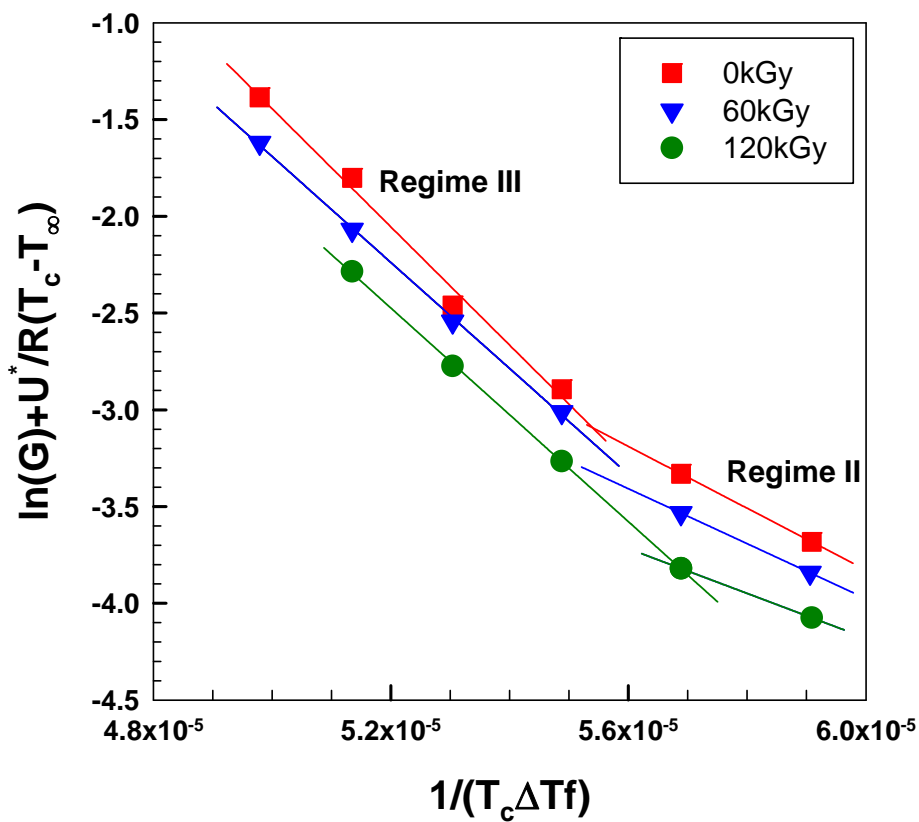
FIG 13. Hoffman-Lauritzen plots for PP at various irradiation doses from optical analysis.
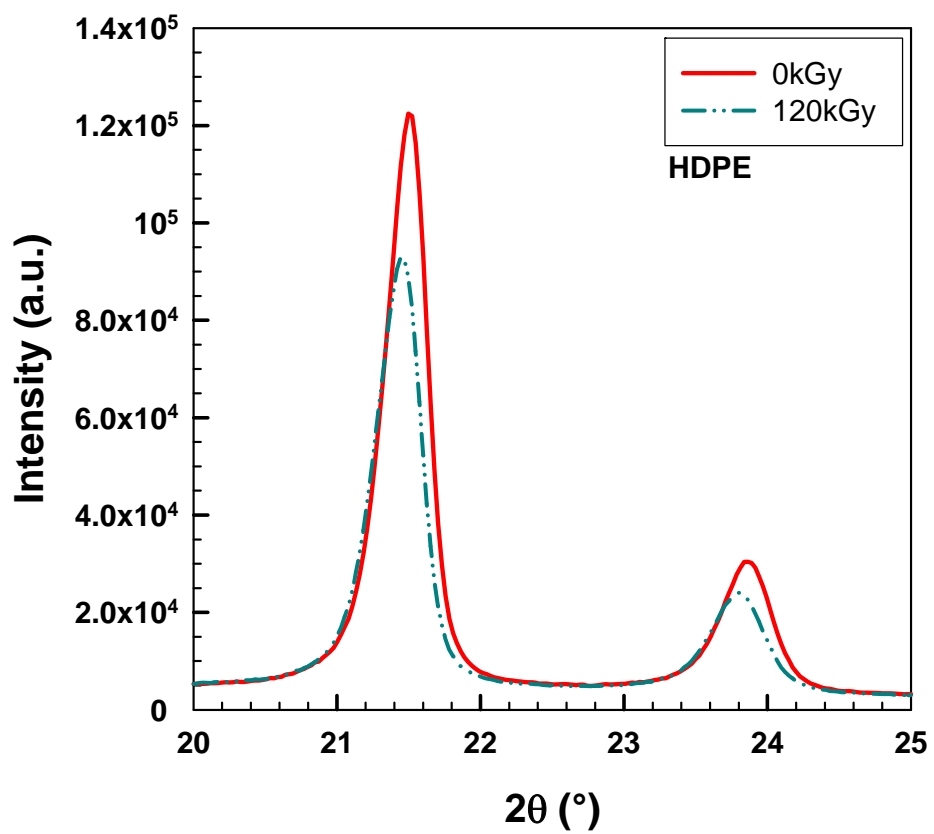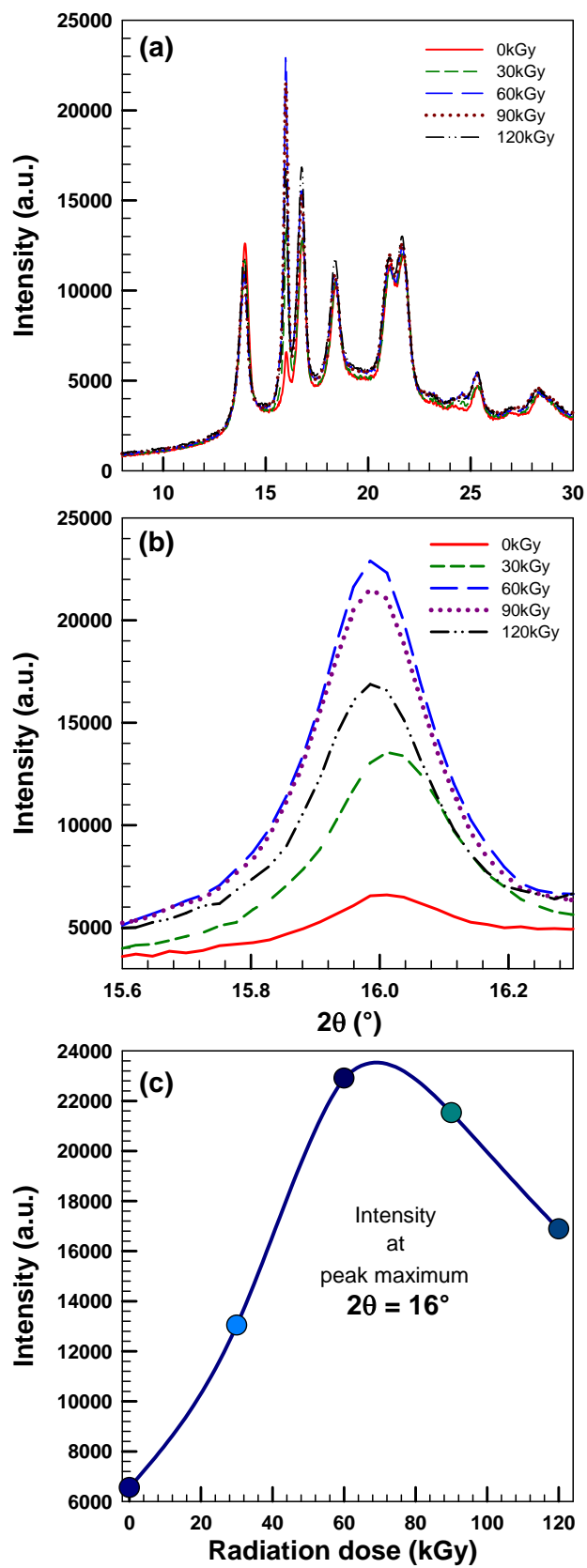
FIG 14. XRD analysis for HDPE

FIG 15. XRD analysis for PP